The Pennsylvania State University

The Graduate School

Department of Mechanical and Nuclear Engineering

EXPERIMENTAL ANALYSIS OF THE IMPACT OF FLOW GEOMETRIES FOR LAMINAR AND TURBULENT HEAT TRANSFER TO A GAS WITH TEMPERATURE DEPENDENT PROPERTIES

A Thesis in

Nuclear Engineering

by

Nicholas R. LeRose

Submitted in Partial Fulfillment
of the Requirements
for the Degree of

Master of Science

May 2008

The thesis of Nicholas LeRose was reviewed and approved* by the following:

Lawrence Hochreiter
Professor of Nuclear Engineering
Thesis Advisor

Jack Brenizer
Chair of Nuclear Engineering
Professor of Mechanical and Nuclear Engineering

Fan Bill Cheung
Professor of Mechanical and Nuclear Engineering

*Signatures are on file in the Graduate School

ABSTRACT

This work represents the second in a series of experiments and analysis for low Reynolds number laminar and transition range gas flows with variable properties. The objective of these experiments and analysis was to examine the flow geometry effects on low flow Reynolds numbers and it compliments the tube experiments by Kaizer [**1**] which were completed earlier.

This report documents the results of experimental and analytical investigations of laminar, transition, and turbulent flow heat transfer for Nitrogen gas flowing through a rectangular duct with an aspect ratio of 18.5 to one and a hydraulic diameter of 0.51 inches.

TABLE OF CONTENTS

LIST OF FIGURES

LIST OF TABLES

NOMENCLATURE

A = area, ft^2

Aspect Ratio = rectangular channel H/W ratio, (18.5)

C_p = specific heat, Btu/lbm-°F

D_h = hydraulic diameter, ft

g= gravitational acceleration, ft/s^2

Gr* = modified Grashof number = $\beta g \rho^2 D_h^4 q_w / \mu^2 k$, dimensionless

h = heat transfer coefficient, Btu/hr-ft^2-°F

H = channel height, (5.0")

k = thermal conductivity, Btu/hr-ft-°F

L = Heated Test Section Length, (4-ft)

l/d = dimensionless length into the test section, x/D_h

Nu_x = local Nusselt Number, $h_x D_h/k$, dimensionless

Pr = Prandtl Number, $\mu Cp / k$, dimensionless

q_w = wall heat flow, Btu/hr

$q"_w$ = wall heat flux, Btu/hr-ft^2

Ra* = modified Rayleigh number, Gr*Pr, dimensionless

Re = Reynolds Number, $\rho V D_h / \mu$

s = gap width, in.

T_{bulk} = local bulk mean temperature of the fluid, °F

T_{wall} = local wall temperature, °F

V = velocity of the fluid, ft/s

W = test section spacer width, (0.27”)

x = coordinate along the heated surface in the axial and flow direction

β = volumetric coefficient of thermal expansion, 1/T for an ideal gas

μ = dynamic viscosity, lbm/ft-s

ρ = density, lbm/ft^3

Chapter 1

Introduction and Background

1.1 Introduction

Understanding laminar and transition region convective heat transfer is important during postulated accident conditions for a Pressurized Water Reactor when the flow is in dispersed flow film boiling. In this situation, the steam is heated to high temperatures such that the local Reynolds number is in the laminar or transition region due to the temperature effects on the physical properties of the steam. Since the peak cladding temperature can occur in this heat transfer regime, accurate knowledge of the convective heat transfer coefficient, considering variable physical properties, under these conditions is needed.

An experimental and analytical program was initiated at The Pennsylvania State University to provide experimental data and analysis on different geometries, at high temperatures and at low Reynolds numbers using Nitrogen and Helium. A first report by Kaizer [**1**] examined the circular tube geometry over a range of Reynolds numbers and for variable fluid physical properties. This report documents the experimental and analytical studies performed in a rectangular geometry using Nitrogen over a range of Reynolds numbers between 100 and 10,000. The experiments were carried out at high wall temperatures such that the effects of variable fluid properties were present in the experimental results. Different heat transfer correlations and models are compared to the

experimental data and recommendations are made for proposed correlations for both laminar and turbulent flow.

1.2 Background

1.2.1 Variable Property Considerations for Low Reynolds Number Flow

Kaizer had performed a detailed literature review of low Reynolds number variable property heat transfer experiments, some of which will be repeated here. Most of these experiments were vertically oriented small diameter tubes, using gas as a working fluid, in which the tube walls were electrically heated. One of the key findings from this review was that all of these earlier experiments had significant heat losses, particularly at the top of the test section where the tube wall and the heated gas temperatures were at a maximum. Also, the heat to the fluid was determined in several of these experiments by separately measuring or characterizing the heat losses and measuring the total electrical power into the test section. The difference was assumed to be the heat going into the fluid and lead to several inaccuracies which Kaizer attempted to overcome in his experimental design.

The high gas temperatures used in these experiments resulted in variable fluid properties which would change along the length of the tube. As a result, the flow was never fully developed since the properties continued to change. Davenport [**2**] investigated this behavior of the continuing developing flow by adding a radial velocity component in his analytical investigation of his heated tube experiments. While the exact

value of the radial velocity component was unknown, Davenport made some reasonable assumptions on the magnitude of this component. Davenport's analytical results indicated that by accounting for the radial velocity, his friction factor was much larger and increased more rapidly with increasing wall-to-bulk temperature differences than similar results without the radial velocity component. He also found that his calculated Nusselt numbers were below the constant property value of 4.36 as the wall-to-bulk temperature difference increased.

These results are consistent with the experimental results of Kays and Nicoll [**3**] as seen in Figure **1-1**, however, there is significant scatter in their data as seen in the figure. As Kaizer pointed out, there are two possible reasons for the data scatter, the developing flow effects and the high heat losses.

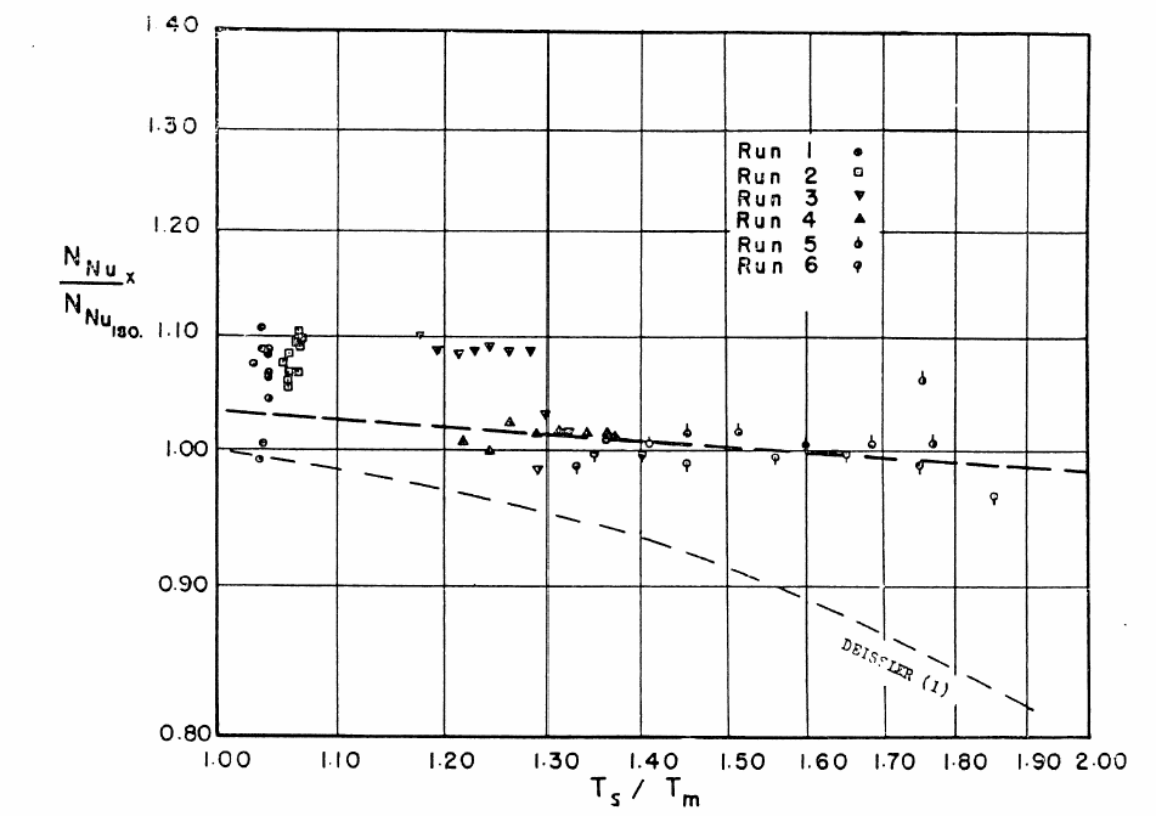

Figure **1-1**: Effect of temperature ratio on local Nusselt number for laminar flow heating in a circular tube, from Kays and Nicoll [**3**]

The effects of the heat losses are very significant since the highest heat losses are occurring just as the flow is becoming quasi-steady. The effect of the heat losses is to vary the rate of change of the bulk fluid temperature and hence its properties. The result of this is to prevent or at least complicate the definition of when the heat transfer is approaching a fully developed state.

In the rectangular geometry experiments performed in this report, the length of the test section was increased such that the flow could more easily approach a quasi-steady state and the effect of the end heat loss was minimized. Even though great care

was used to minimize the heat loss, it was still significant for the very low Reynolds number tests since the flow can not absorb a significant amount of heat.

The effect of variable fluid properties was also presented in 1966 by Worsoe-Schmidt [**4**] for a circular tube at high heating rates. Figure **1-2** displays his results which indicate that increasing the dimensionless heat flux causes a noticeable change in the development of the Nusselt number axially. This is because the fluid properties continue to change as the flow is heated such that the flow continues to develop. Figure **1-3** displays the friction factor development which shows a significant increase in the friction factor at higher heating rates where the effect of fluid property variation is more evident.

To help describe Figures **1-2** and **1-3**, the following definitions are presented: x^+ is a non-dimensional axial coordinate $x/\left(r_o \cdot N_{\mathrm{Re},o} \cdot N_{\mathrm{Pr},o}\right)$ where r_o is the tube radius, x is the distance along the tube, $N_{\mathrm{Re},o}$ is the inlet Reynolds number, and $N_{\mathrm{Pr},o}$ is the inlet Prandtl number. The variable q^+ is a non-dimensional heat flux given as $r_o \cdot q_w'' / \left(k_o \cdot T_o\right)$) where r_o is the tube radius, q_w'' is the heat flux at the tube wall, k_o is the thermal conductivity at x = 0, and T_o is the absolute temperature at x = 0. The variable $N_{Gr^*,o}$ is a modified Grashof number given as $8 \cdot g \cdot \rho_0^{\,2} \cdot r_o^{\,3} / \mu_o^{\,2}$ where g is the acceleration due to gravity, ρ_o is the density at x = 0, r_o is the tube radius, and μ_o is the viscosity at x = 0. The variable $N_{Re,o}$ is the Reynolds number at the inlet. The variable M_o is the Mach number at the inlet. When comparing this data with the current experiment, the r_o terms will be replaced with the hydraulic diameter divided by 2.

As x^+ increases in Figure **1-2** and Figure **1-3,** the flow is progressing along the tube further from the inlet and is in the process of reaching a fully developed state.

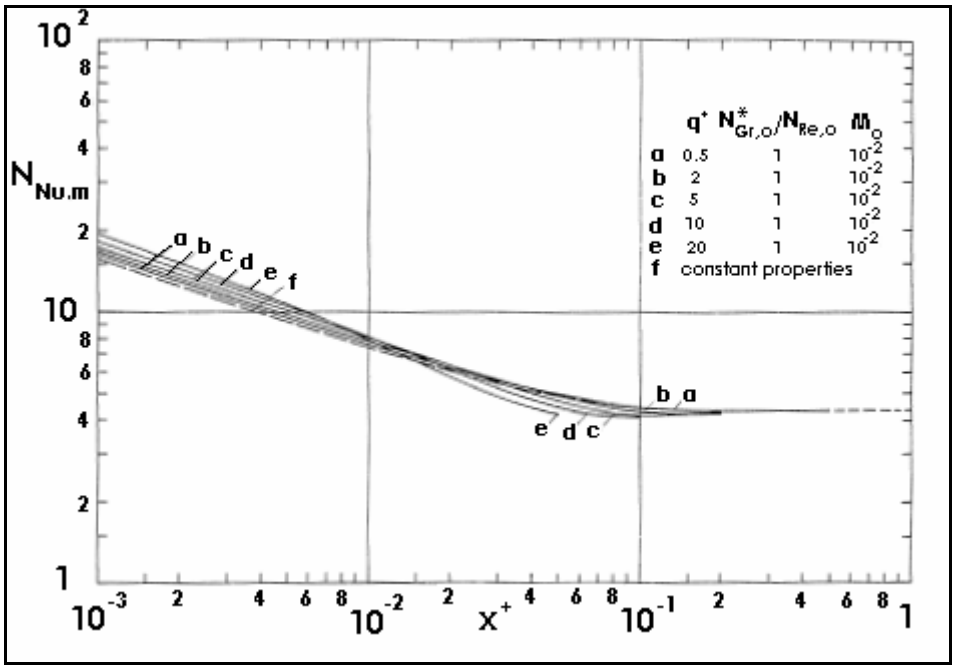

Figure **1-2**: Friction Factor and Temperature Ratio with respect to dimensionless axial distance and 5 dimensionless heat fluxes.

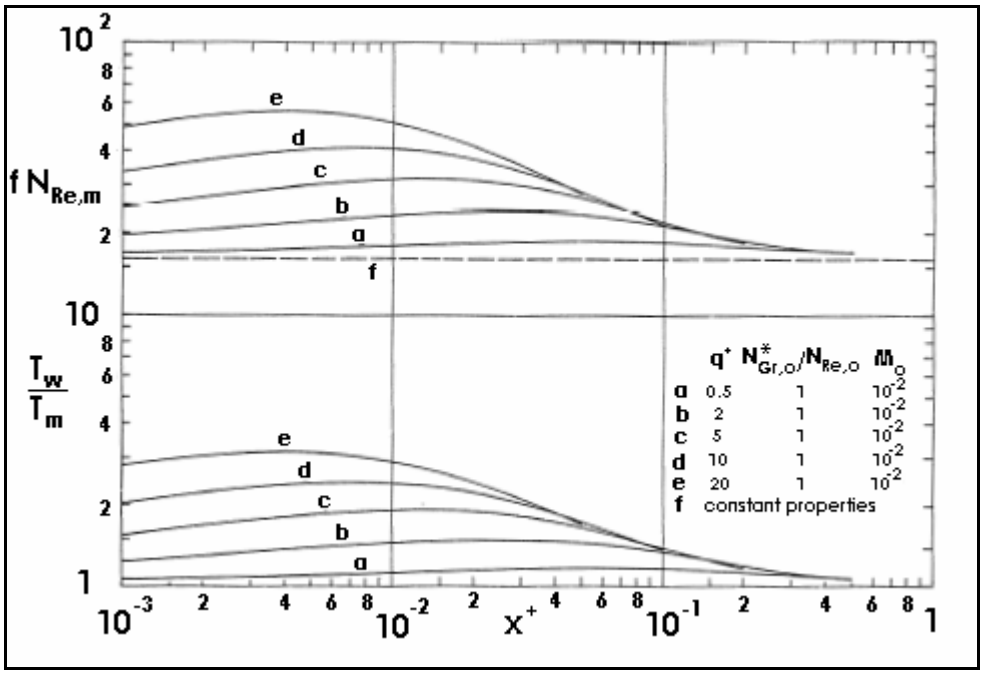

Figure **1-3**: Friction Factor and Temperature Ratio with respect to dimensionless axial distance and 5 dimensionless heat fluxes.

In Figure **1-3** the Nusselt number and friction factor are significantly higher than the constant property values at the tube entrance. However as the flow progresses down the tube they approach the constant property value.

In a similar fashion, Swearingen [**5**] combined an analytical investigation of laminar flow between parallel plates with an experimental investigation of laminar flow in a tube. His analytical investigation was an extension of Worsoe-Schmidt's analysis. He applied a similar finite difference technique to the case of parallel plates as well as an experimental investigation to confirm the work done by Worsoe-Schmidt. Swearingen's Nusselt number data for air experiments can be seen in Figure **1-4** and his data for helium experiments can be seen in Figure **1-5** . The experimental data is presented using dimensionless length and heat flux variables similar to Worsoe-Schmidt. Swearingen's

experimental data supports the Worsoe-Schmidt predictions on the behavior of Nusselt number with variable properties.

To help describe Figure **1-4** and Figure **1-5**, the following definitions are presented: x_m^+ is the dimensionless axial coordinate based on local conditions given as $x/D \cdot \mathrm{Pr}_m \cdot \mathrm{Re}_m$ where x is the local elevation, D is the inside tube diameter, Pr_m is the local Prandtl number, and Re_m is the local Reynolds numbers. The variable q^+ is a non-dimensional heat flux given as $q_w" \cdot r_o / (k_o \cdot T_o)$ where r_o is the inside tube radius, $q_w"$ is the axially constant heat flux at the tube wall, k_o is the thermal conductivity at x = 0, and T_o is the absolute temperature at x = 0. When comparing this data with the current experiment, the r_o terms will be replaced with the hydraulic diameter divided by 2.

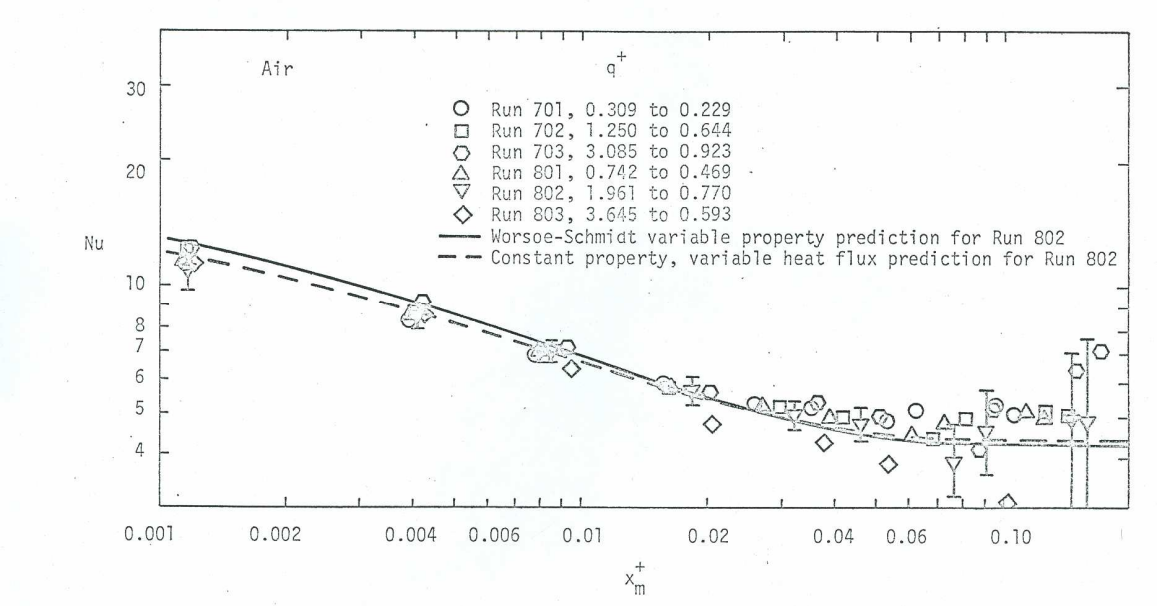

Figure **1-4**: Swearingen's Nusselt number axial development for Helium.

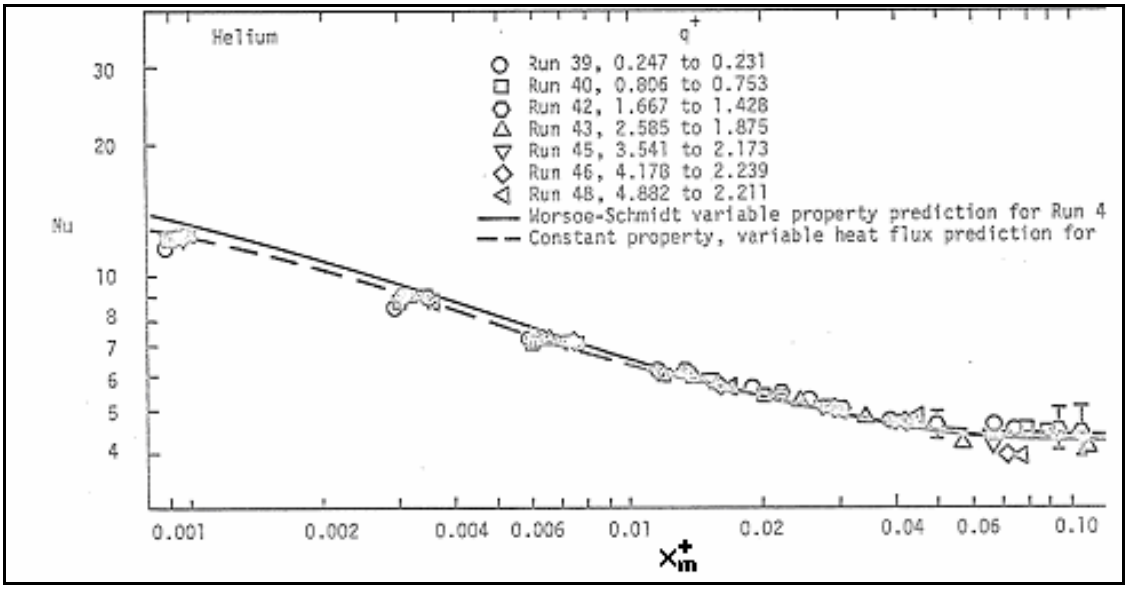

Figure **1-5**: Swearingen's Nusselt number axial development for Helium.

In Figure **1-4** and Figure **1-5** as $x+_m$ increases, the flow approaches a near developed state and the Nusselt number approaches a constant property value of 4.36. However, there is significant scatter.

This and other work has provided an understanding that when examining variable property situations, the variable properties result in a smaller Nusselt Number and a larger friction factor than the constant property case. Work from the present experiments, measures the convective heat transfer with variable properties to Reynolds numbers as low as 100.

Work from Mercer et al. [**6**] contained experiments on parallel plate geometries using a constant wall temperature in order to examine the Nusselt number development for variable properties. Their tests covered a range of Reynolds numbers between 300-1500. Equation **1.1** shows their correlation for Nusselt number as a function of x. The variable 's' in Equation Equation **1.1** is the gap distance between the plates.

$$Nu_M = 3.77 + \frac{0.066\left(\mathrm{Re}_d \,\mathrm{Pr}\cdot s/2x\right)^{1.2}}{1+0.1\cdot(\mathrm{Pr})^{0.87}\left(\mathrm{Re}_d\cdot s/2x\right)^{0.7}} \qquad (\mathbf{1.1})$$

It should be noted that Mercer's experiment was strictly a constant wall temperature problem, so the results can not be easily compared to the present nearly constant wall heat flux experiment.

1.2.2 Laminar Flow Literature

The difference between a rectangular channel and a tube geometry are evident in their respective friction factor and heat transfer correlations. This section will discuss

what the expectations are for the data in the current experiment, and also the differences between flow in the rectangular geometry and tube geometry.

The laminar friction factor for circular tube geometry can be described as 64/Re as found in White [**7**]. However, this relationship cannot be used for noncircular geometries. Figure **1-6** shows that for a rectangular geometry with the current height to width ratio of 0.054, the friction factor becomes approximately 89.5/Re. This polynomial fit was created using data from Table 6.4 in White [**7**].

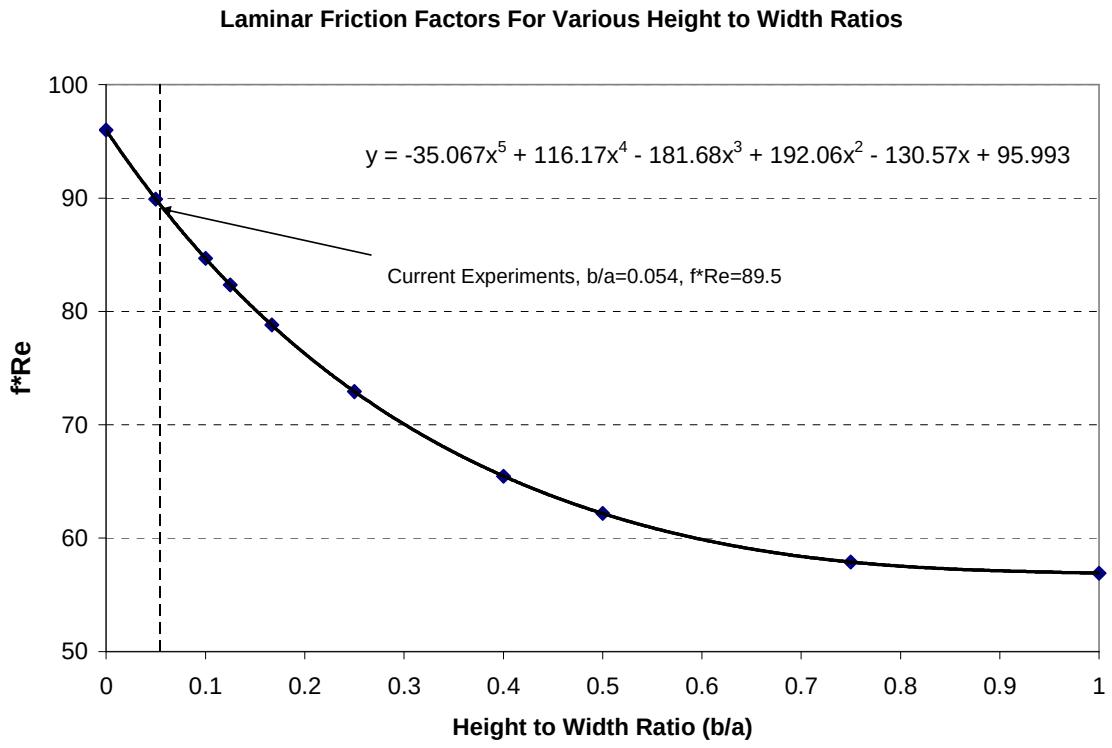

Figure **1-6**: Laminar Friction Factors based on Rectangular Height to Width Ratio

Data taken from Rohsenow [**8**] was used to form a correlation for fully developed constant property laminar Nusselt number as a function of height to width ratio for a rectangular channel. This data and correlation are given in Figure **1-7 .** From this correlation, the expected constant property Nusselt number was calculated to be 7.397 for a b/a ratio of 0.054, which is the height to width ratio for the present experiments. This value will be used to normalize the calculated Nusselt numbers from the present experiments.

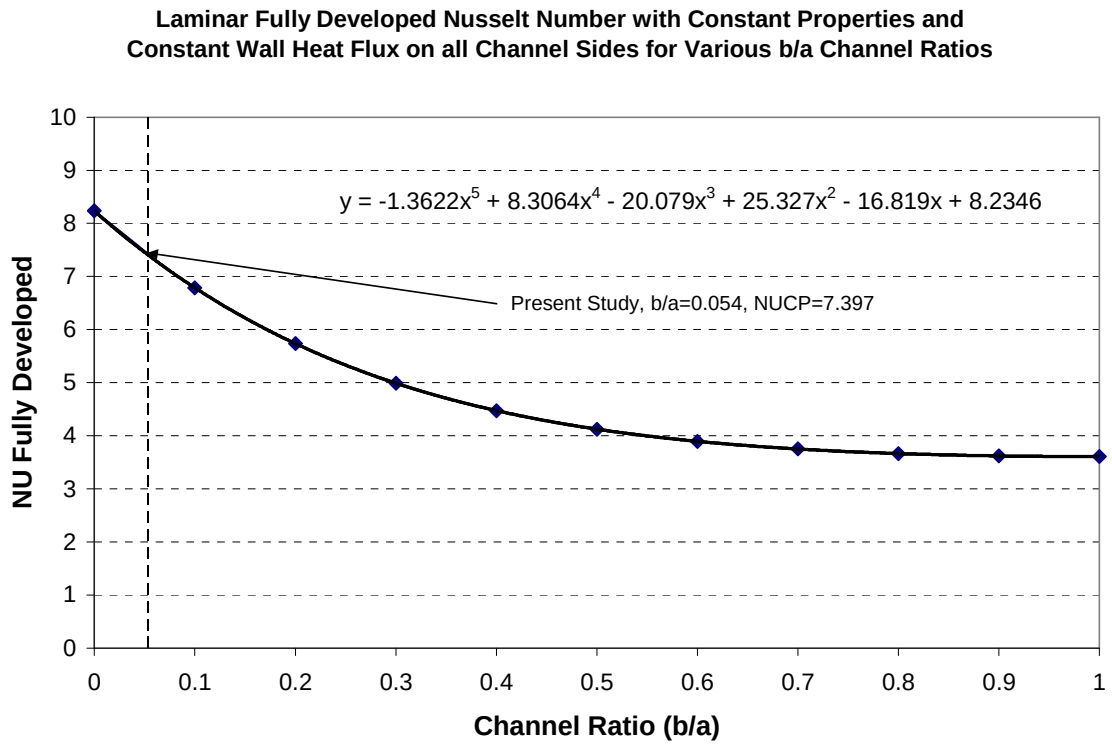

Figure **1-7**: Fully Developed Constant Property Laminar Nusselt Number for Different Channel Ratios.

In 1964, Hwang & Fan [**9**] conducted finite difference analysis to predict the Nusselt number in the entrance region of a constant wall temperature problem as well as a constant wall heat flux problem. However, constant fluid properties were assumed so the analysis cannot be compared directly to the present experiments at high heat flux. The boundary conditions used for the constant wall heat flux analysis included the following:

1) All fluid properties are constant.
2) The flow is laminar.
3) Both walls of the duct have the same uniform heat flux.
4) The thermal boundary layer thickness is zero at the entrance where x=0.
5) The thermal and velocity profiles develop simultaneously.

Nusselt data was taken from their paper and plotted against a dimensionless distance x' which is the L/d ratio divided by the Reynolds number. This data plot is given below in Figure **1-8 .** The Nusselt number approaches an asymptotic value of 8.22 which is expected for heated infinite parallel plates with constant properties.

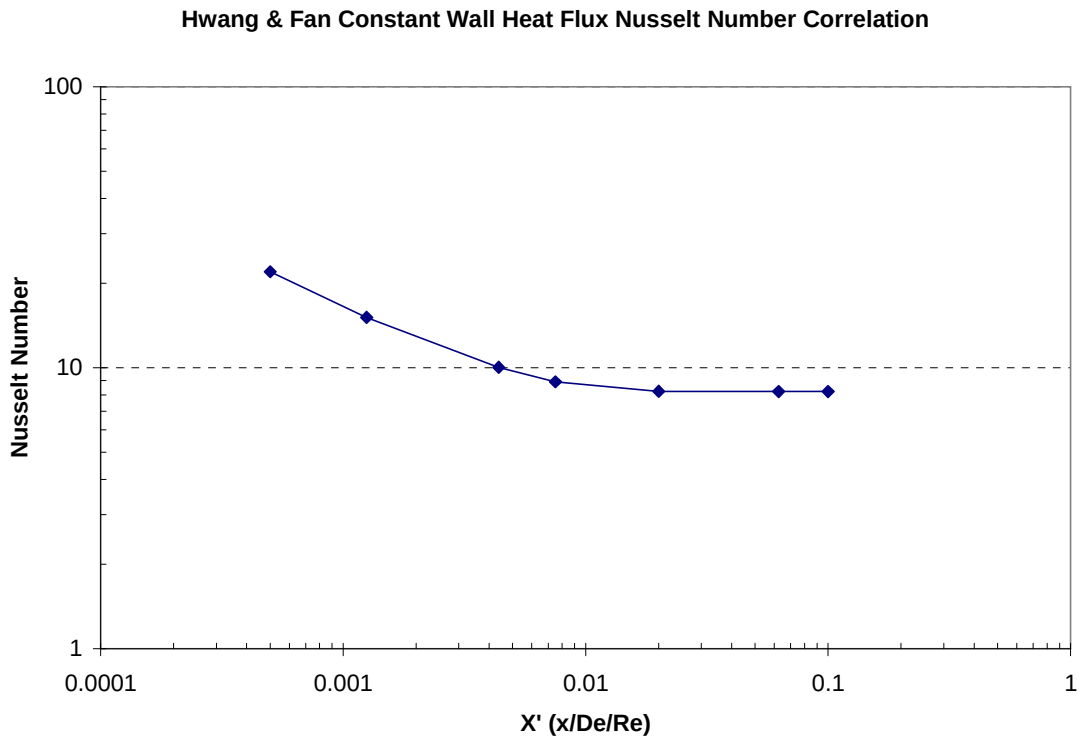

Figure **1-8**: Hwang and Fan Nusselt number development for a constant wall heat flux rectangular channel. Constant Fluid Properties Assumed.

In 2003 Wong [**10**] published an integral solution for the thermal entry length for a constant wall heat flux, rectangular geometry channel. His analysis had the following assumptions:

1) All fluid properties are constant.
2) The flow is laminar.
3) The viscous dissipation and the work of compression are both negligible.
4) Both walls of the duct have the same uniform heat flux.
5) The thermal boundary layer thickness is zero at the entrance where x=0.
6) The effects of heat transfer are found only within the thermal boundary layer. The fluid outside the thermal boundary layer will be unaffected by the heat transfer and have a uniform temperature T_{in} at the entrance where x=0.

He proposed that the Nusselt number for a fully developed hydrodynamic flow with a thermally developing region is given by Equation **1.2** as,

$$Nu_x = \frac{hd_h}{k} = \frac{2}{\left\{\frac{\xi}{3} - \frac{\xi^3}{10} + \frac{\xi^4}{48}\right\}} \qquad (\mathbf{1.2})$$

where $\xi = \left(\frac{80x/d_h}{Pe}\right)^{1/3}$, $d_h = 4d$, $Pe = \frac{U_m d_h}{\alpha}$, and $U_m = \frac{2}{3}U_c$.

This prediction of the Nusselt number development performs very well when the difference between the wall temperature and the bulk fluid temperature is small and when there is little property variation. However in the current experiment these assumptions are not always valid. For the high heating cases, the viscous and thermal boundary layers will continue to develop as the fluid properties change.

Heat transfer data presented by Kreith [**11**] contained laminar flows of ~700 Reynolds number, but when questioned, cautioned on its use since it was not taken under typical laboratory conditions and no uncertainty analysis had been performed on the data or experiment. Also, as will be discussed in Chapter 6, there is no published information on the experimental design and heat losses which are critical for these low Reynolds number experiments.

In 2002, Chin et. al. [**12**] performed a liquid crystal thermography technique to measure the convective heat transfer in asymmetrically heated narrow channels. This data matched well with the Tan & Charters [**13**] correlation, and was the first paper to mention buoyancy effects for laminar tests. Their laminar Nusselt results were 2-3 times

greater than the expected forced convection Nusselt numbers due to mixed convection effects.

Burmeister [**14**] explained that mixed convection flows can be described as a summation of the forced and natural convection Nusselt numbers as seen in Equation **1.3**. Where the exponent n=3 is suggested for the laminar and turbulent state as,

$$Nu_{combined}^{\ n} = Nu_{Forced}^{n} + Nu_{Natural}^{n} \qquad (\mathbf{1.3})$$

Buoyancy in the flow makes it difficult to analyze the effects of fluid property variation. This is because buoyancy is expected to increase the heat transfer while fluid property variation is expected to decrease the heat transfer.

1.2.3 Turbulent Flow Literature

In 1969, experimental turbulent data from Tan and Charters [**13**] suggested that for a 3:1 ratio rectangular channel, the turbulent Nusselt number was of the form of Dittus Boelter, but with a different leading constant. His turbulent correlation can be seen in Equation **(1.4)** as,

$$Nu_{fully,dev} = 0.018\,\mathrm{Re}^{0.8}\,\mathrm{Pr}^{0.4} \qquad (\mathbf{1.4})$$

In 1968, Forslund and Rosenhow [**19**] also modified the Dittus-Boelter correlation with their turbulent tube data. Their correlation was similar in form to the Tan and Charters correlation, but with a leading constant of 0.019 instead. Sparrow et. al. [**15**] compared his experimental asymmetric heating results to experimental symmetric heat transfer data provided by Novotny et. al. [**16**]. Both experimenters used a 5:1 aspect ratio rectangular

channel for their experiments. Their Nusselt data showed little difference between asymmetrical and symmetrical heating

Chapter 2

Experimental Apparatus

The experimental facility for the laminar flow heat transfer tests consisted of a gas supply, flow measurement and control manifold, inlet piping, test section, and exhaust piping. The test section was the main instrumentation piece which allowed for steady state measurement of lateral temperature profiles for a nearly constant wall heat flux over an axial length of 48 inches. It was machined from stainless steel 316 and heated using radiative ceramic fiber heaters. The following is a detailed description of each of the test facilities components including the gas supply, inlet manifold, test section, and exhaust system.

A schematic of the experimental apparatus can be seen in Figure **2.1**. Photographs of the experimental apparatus can be found in Appendix **A**. This once through design was made up of 4 stages: Gas Supply, Inlet Manifold, Test Section, and Exhaust System. The Gas Supply provided gas at a high pressure to the Inlet Piping. The Inlet Piping maintained a constant flow rate into the Test Section. The Test Section had two portions, a lower unheated portion, and an upper heated portion. The gas would enter the unheated portion where the velocity profile developed. The flow was then heated in the upper portion of the test section where the temperature profile developed the temperature measurements were taken. Exiting the heated portion, the gas flowed into the Exhaust System where it was cooled and exhausted into the atmosphere in a safe manner.

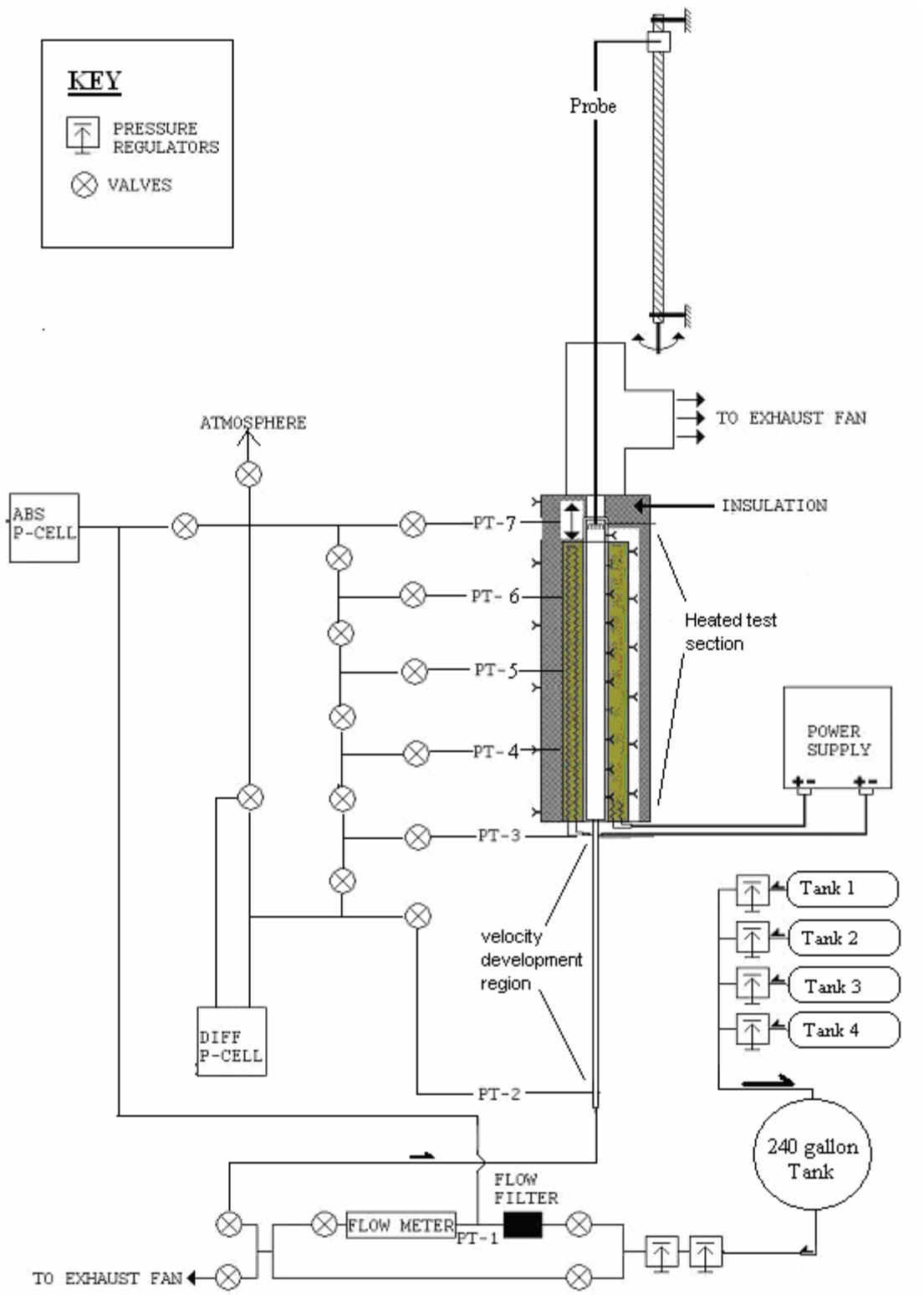

Figure **2.1**: Experimental apparatus diagram for the flat plate geometry

2.1 Gas Supply

The gas supply consisted of pressurized liquid nitrogen bottles, compressed helium and nitrogen bottles, a large pressure vessel, the gas manifold, and multiple single stage pressure regulator valves. Use of these components maintained a constant backpressure for the Inlet Piping for extended time periods. For lower Reynolds number experiments compressed nitrogen bottles were sufficient, however for turbulent Reynolds experiments, the use liquid nitrogen and the large pressure vessel were necessary to handle the larger flows. Helium was not used in the current experiments as it was in the tube experiments because Reynolds numbers below 100 were achievable with nitrogen.

The bottles of gas were connected to the gas manifold through a single stage pressure regulating valve. Each valve isolated the particular gas bottle from the other 3 connected to the manifold, allowing any bottle to be replaced without affecting the other 3 bottles. This first single stage pressure regulating valve allowed the testing to be done indefinitely by allowing gas bottles to be switched out, without upsetting the flow to the test section. The liquid nitrogen tank was connected to the large pressure vessel which acted as a gas capacitance as well as a heat exchanger to help vaporize the liquid nitrogen. This capacitance allowed for higher flows while maintaining constant pressure.

Each of these gas supply systems were connected to the Inlet Piping through two single-stage pressure regulators. These two single-stage regulators acted in series as a double-stage pressure regulator. This pairing helped provide a near constant back pressure that was needed during testing.

2.2 Gas Manifold

The gas manifold can be seen in Figure **2.2** . The gas manifold connected 4 pressurized gas bottles or 4 liquid nitrogen tanks together. At each of the 4 inlets to the manifold was a single stage pressure reducing valves. At the outlet of the gas manifold was another single stage pressure reducing valve. This set of valves helped to keep a constant flow and pressure to the inlet piping.

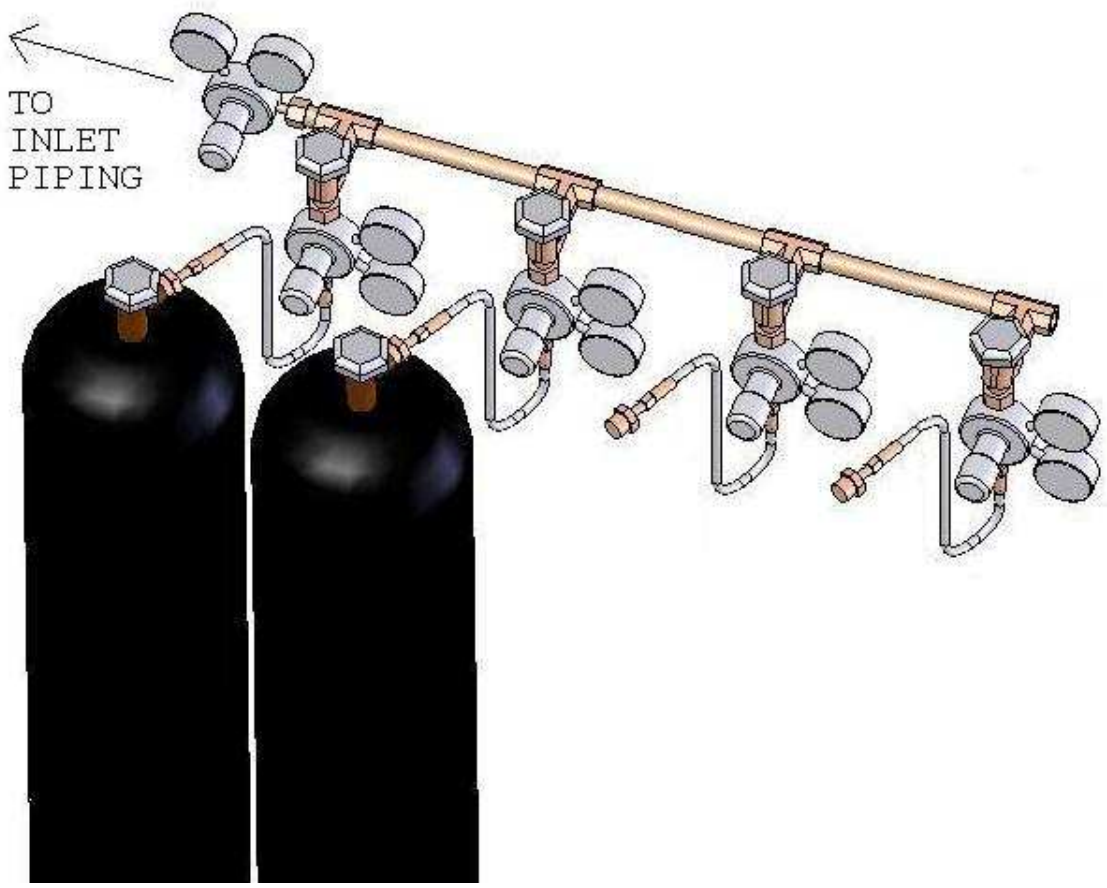

Figure **2.2**: Gas manifold visual

A total of 6 single stage pressure regulating valves were used to minimize any pressure perturbations due to the depressurization of the gas bottles. In normal practice, a single stage pressure regulator would output a constant pressure for a much higher inlet pressure. However, as the inlet pressure from the bottles decreased the output pressure generally increased until the bottle was almost empty and then it decreased. To compensate for this effect, a 2 stage pressure regulator was used. In this experiment, the combination of single stage pressure regulators acted as a 3 stage pressure regulator. Table **2.1** gives relevant pressure data for the pressure regulating valves.

Table **2.1**: Single Stage Pressure Reducer Data

	1st Stage	2nd Stage	3rd Stage
Number of Regulators	4	1	1
Inlet Pressure (psig)	2250 - 200	80	40
Inlet Location	Gas Bottles	Gas Manifold	2nd Stage Outlet
Outlet Pressure (psig)	80	40	20
Outlet Location	Gas Manifold	3rd Stage Inlet	Inlet Piping

2.3 Inlet Piping

A flow schematic of the Inlet Piping can be seen in Figure **2.3** . This design of inlet piping was recommended by the manufacturer of the flow meter, Flow Technology, for optimal flow measurements. Two flow paths were available, one path through the flow meter and one path that bypasses the flow meter.

In the flow meter flow path the gas first flows through the flow filter. Pressure Tap 1 was located at the exit of the flow filter followed by a 40 $^{L}/_{D}$ run of pipe, which was the upstream straightening section before the flow meter. Upon exiting the flow meter, the gas flowed through an 18 $^{L}/_{D}$ down stream straightening section before entering the flow control valve, CV-1, which regulated the flow rate. The Inlet thermocouple was placed in the flow at the outlet of the flow control valve. From this point, the gas could either flow into the test section or to the exhaust fan. If SV-2 was closed and SV-4 was opened, the flow would bypass the flow meter for high flow test section cooling or to flow gas immediately to the exhaust.

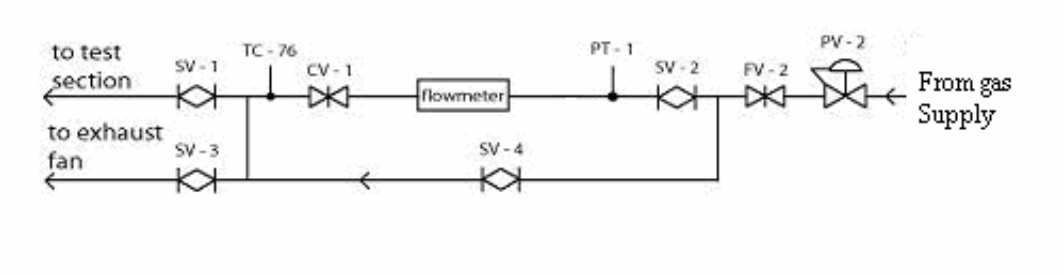

Figure **2.3**: Flow Schematic of the Inlet Piping

2.3.1 Flow Filters

The flow filters used were Swagelock 7 micron, 60 micron, and 440 micron inline filters recommended by Flow Technology. The finer filters were used in conjunction with the lower flow meters because they were more delicate. For the high Reynolds tests, the 440 micron filter was necessary to attain higher flows. The purpose of the filter was to protect the flow meter from any debris in the compressed gas.

2.3.2 Flow Meters

Three turbine meters from Flow Technology were used in this experiment to span the required Reynolds number range of 100 - 15000. Each flow meter was calibrated at 20 psia to account for the pressure drop through the test section. The volumetric flow rate of the smallest flow meter was 0.1 – 1.0 ACFM (Actual Cubic Feet per Minute). The volumetric flow rates of the middle and high range flow meters were 0.5 – 5.0 ACFM and 2.0-20 ACFM respectively. The high range flow-meter was recalibrated to higher pressures to obtain enough back pressure so that fully turbulent Reynolds numbers were attainable. These middle and high range flow meters were only calibrated with air. The statistics of the flow meters can be seen in Table **2.2**.

Table **2.2**: Flow Meter Statistics for Rectangular Geometry

	Flow Meter 1	**Flow Meter 2**	**Flow Meter 3**		
Calibration Pressure (psia)	20	20	20	30	50
Flow Rate (ft^3/min)	0.1 - 1.0	0.5 - 5.0	2.0 – 20.0		
Reynolds Number Range	60 - 600	300 – 3000	1200 - 12000	1800 -18000	3000-30000

2.3.3 Flow Control Valves

The original flow control valve was a ½” Swagelock needle valve. The maximum flow rate through the valve was listed as 5 CFM which was used for the lower Reynolds

number tests. This valve was removed and a ball valve was used to control flow for the high Reynolds number cases.

2.3.4 Inlet Thermocouple

The inlet thermocouple was placed down stream of the control valve before the exit of the inlet piping. There were initial concerns about low inlet temperatures from the expansion of the compressed gas. To raise the temperature of the gas, additional copper tubing was added between the gas manifold and inlet piping. Higher Reynolds number tests were more difficult to keep the inlet near room temperature due to the vaporization of liquid nitrogen. For this reason the range of inlet temperatures for tests was 40°F to 80°F. The inlet thermocouple was a type K ungrounded thermocouple with a 12 inch stainless steel sheath.

2.3.5 Bypass Flow

A bypass flow loop allowed maximum flow into the test section. The flow filter, Pressure Tap 1, flow meter, flow control valve, and inlet thermocouple were bypassed. The bypass was used for cooling down the test section. Even with the large flow rates, the cool down times ranged between 2 -3 hours.

2.4 Rectangular Geometry Test Section

The approach for the rectangular test section design much different than the circular test section design used in Kaizer's experiments, and using the knowledge gained from Kaizer's experiments, the rectangular geometry test section design was improved. The length was extended from 36" to 48" pushing the temperature plateau higher so that data collection in the first 60 L/D's (30") was more accurate. Kaizer [**1**] discusses this problem with temperature plateau and turnover for his test section and explained that making the test section longer would push the temperature plateau higher so that more accurate measurements of heat transfer and temperature development could be obtained over a larger L/D. The following list of parts describes the designed and built pieces for the rectangular test section. Figure **2-4** displays the test section assembly in an exploded view while Figure **2-5** displays the test section in a collapsed view.

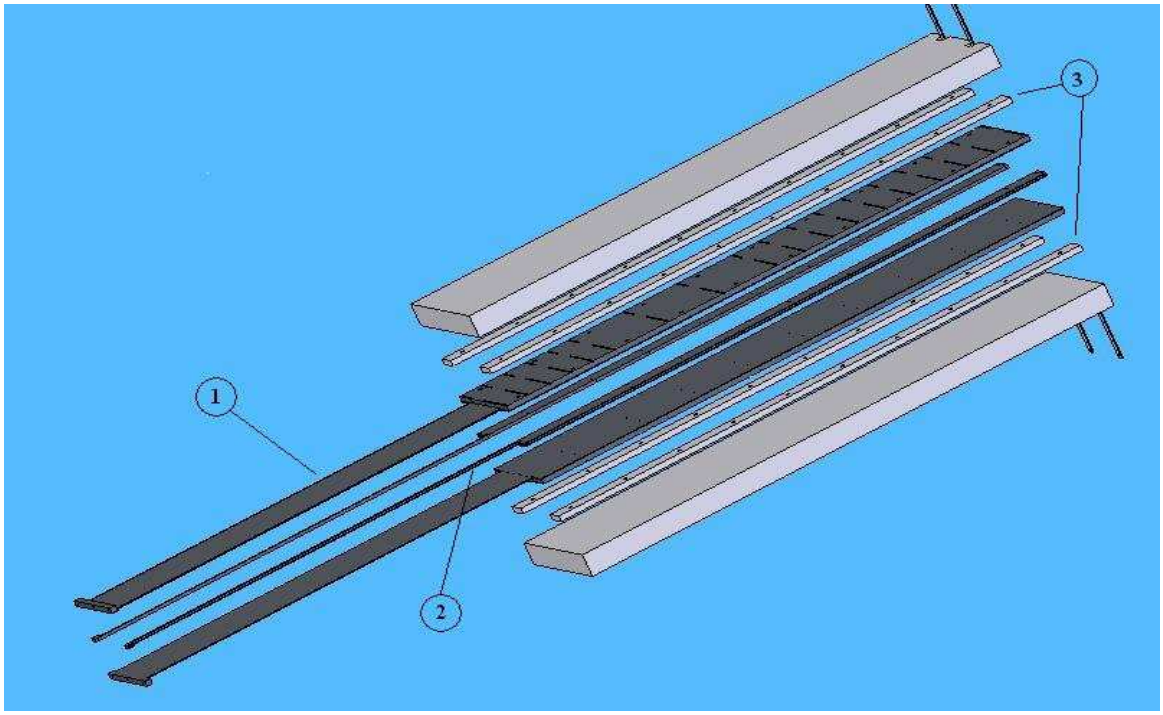

Figure **2-4**:Exploded view of the rectangular test section design

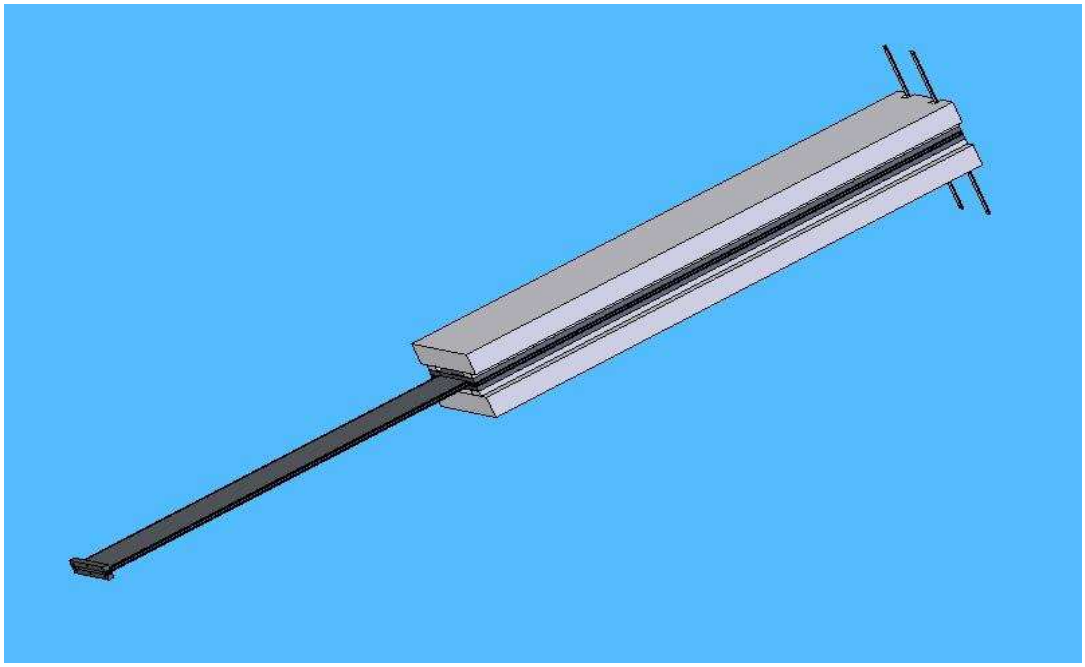

Figure **2-5**: Collapsed view of the rectangular test section design

1. Test Section Plate – A plate that makes up the wide wall of the test section. It contains two thin walled sections to reduce the heat losses from the heated sections. This plate is 12 inches longer than the previous circular tube design by Kaizer [**1**] to allow for extended L/D heated section data. Two test section plates will be welded with spacers between to form the complete channel.

2. Test Section Spacers – These spacers made up the side walls of the test section. They were machined using stainless steel 316. Two spacers were welded between the test section plates to form the flow channel.

3. Ceramic Heater Spacers – The heater spacers were made of a low conductivity ceramic material Aremcolox®. They separated the test section from the upper plenum to prevent any metal-to-metal contact. This prevented shorting out the exposed radiative heating elements.

2.4.1 Fluent Design Calculations

Prior to designing and building the current test section, it was necessary to calculate if the current ceramic fiber heaters could provide a uniform temperature distribution across the face of the heated channel. The boundary conditions used to solve the Fluent problem are outlined in Table **2-3**

Table **2-3**: Fluent Problem Boundary Conditions

Fluent Model Surface	**Condition or Method used for heat transfer calculation**
Insulation/Air Interface	Natural Convection heat transfer coefficient
Heaters	Power Input
Heater-Test Section Gap	2-D Radiation (calculated by Fluent)
Test Section Plate, facing the channel	Forced Convection heat transfer coefficient

Figure **2-6** displays the Fluent model used to estimate the temperature distribution that the ceramic heaters could provide for the current design. This diagram describes each of the 2-D components that were modeled. The meshing was rectangular with anywhere from 0.034-0.042 inch sides. This fine meshing scheme allowed for greater temperature resolution at the channel corners and channel spacers.

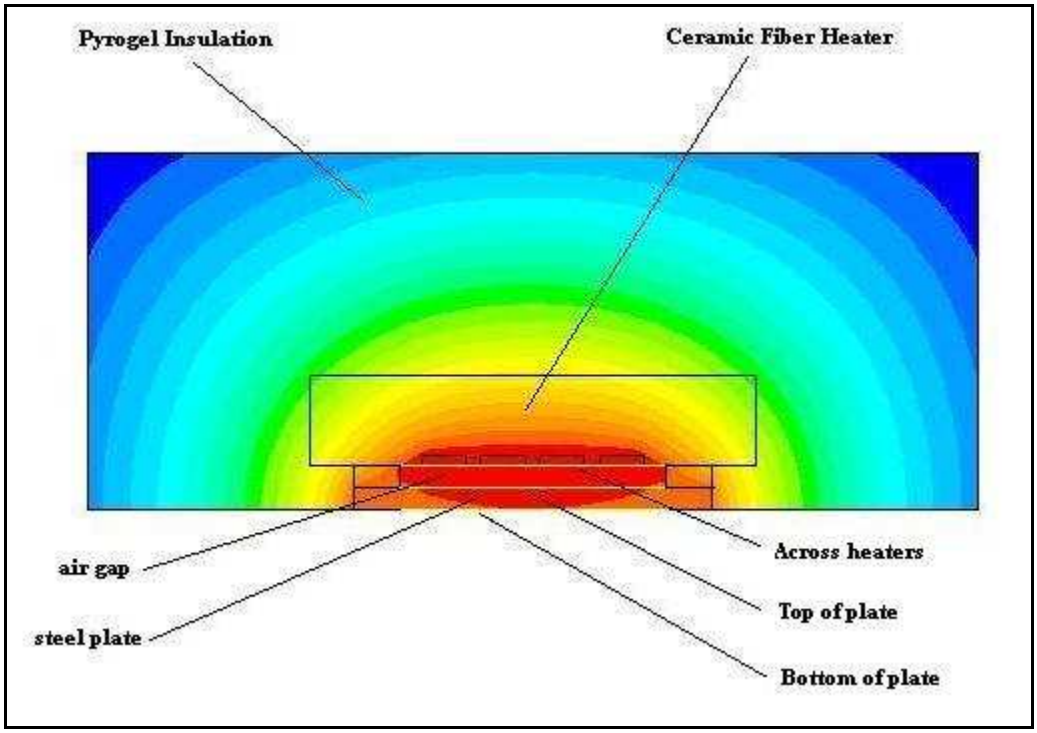

Figure **2-6**: Fluent model for temperature distribution calculations. Shown for modeling purposes only.

The ceramic fiber heaters provide radiant heat, which allowed the temperature profile to be more uniform at the channel wall. In Figure **2-6** the channel wall is labeled as 'Bottom of plate'. The air gap seen in Figure **2-6** gave a ½" of separation between the heater elements and the steel plate. This distance prevented the heaters from shorting out. Figures **2-7** and **2-8** give the lateral temperature profiles calculated by Fluent.

Comparing the heater element and the channel wall temperature profiles in Figure **2-7** shows the effectiveness of using radiative heaters to create a uniform temperature profile at the channel wall.

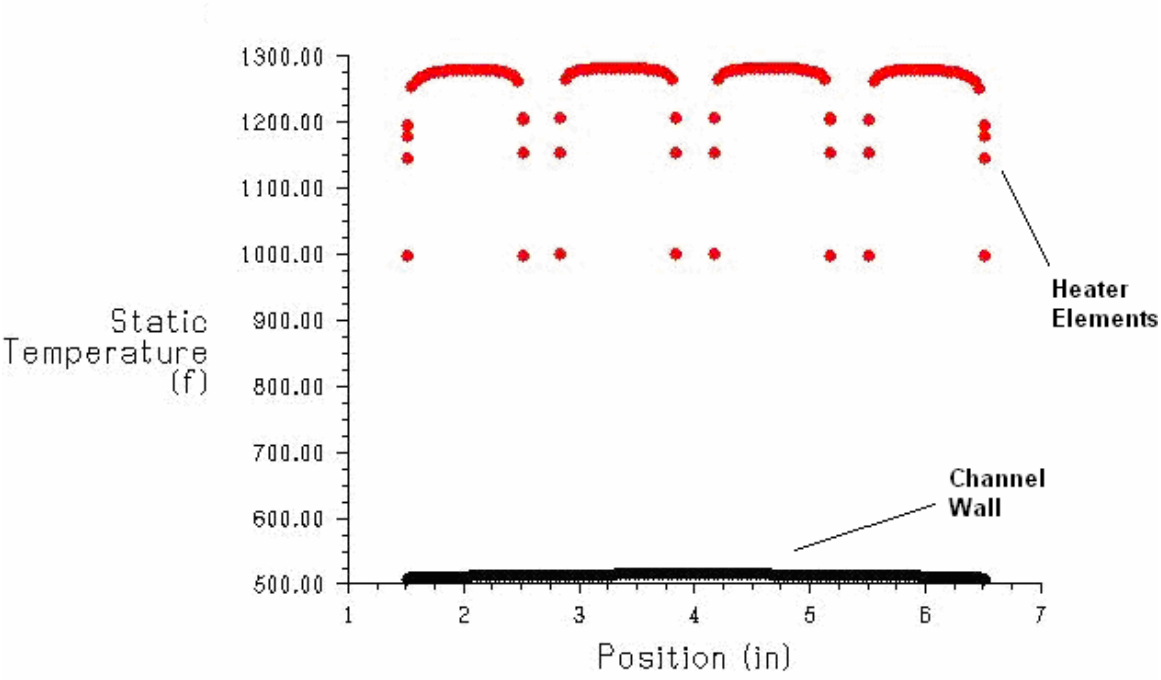

Figure **2-7**: Fluent temperature profiles at the heater elements and at the heated channel wall.

Figure **2-8** gives the exploded view of the Fluent calculated channel wall temperature profile, showing only a 6°F lateral temperature gradient.

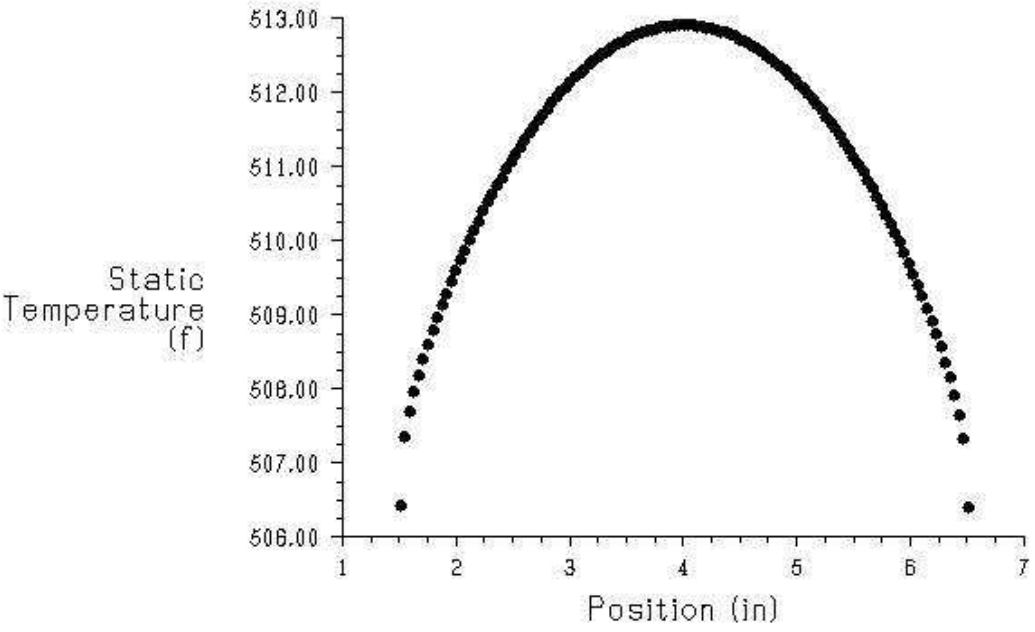

Figure **2-8**: Exploded view of the heated channel wall temperature profile.

2.4.2 Sealing

Sealing the rectangular test section was a concern during the design stages of these experiments. Initially the test section was to be bolted together and sealed with high temperature gaskets which may or may not have been successful. The current test section was sealed and fastened together with a temporary seam weld. This weld can be machined off if ever different sized plate spacers would be needed for future experiments. However, for the current experiments this channel spacer remained constant at 0.27”.

Figure **2-9** shows the machined lips that are welded together to form the seam welds.

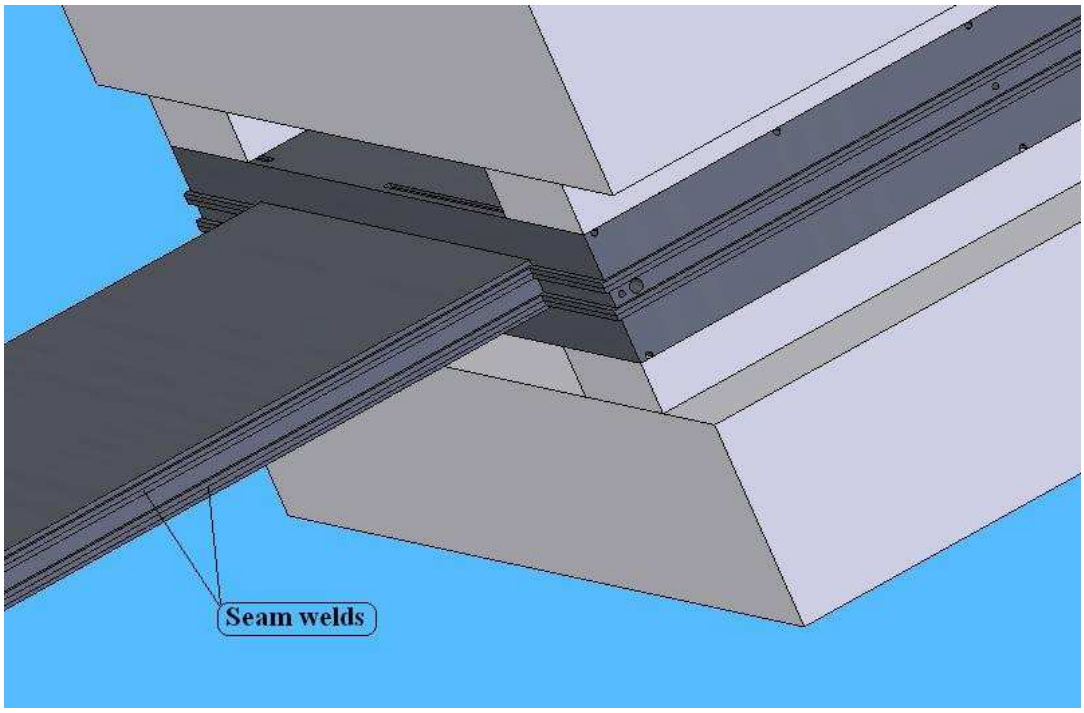

Figure **2-9**: Seam welds detail

2.4.3 Flow Straightener

A ceramic honeycomb insert from Applied Ceramics was used for the flow straightener. It contained 400 cells per square inch. The nominal hydraulic diameter was 0.043 inches, the open frontal area (hole vs cell) was 74%, and the geometric surface area was 826 ft^2/ft^3. To ensure the flow was fully straightened an L/D of 45 was used to straighten the flow. This resulted in the ceramic honeycomb being 2.0” in length.

2.5 Upper Plenum

Previous experiments had identified problems with heat loss from the top of the test section. To minimize such losses, the upper plenum was designed to keep conduction from the heated test section as low as possible. Therefore, the upper plenum had no direct metal contact with the test section.

The upper plenum was an aluminum 8 inch tee, generally used for residential duct work. A tee was chosen so that the gas from the test section could flow into the bottom leg of the tee, out the side leg of the tee, and the traversing thermocouple could enter the test section from the top leg of the tee. The gas exited the test section and expanded into the bottom leg of the tee, turned and flowed into the side leg of the tee, then flowed through duct work and into the exhaust fan where the heated gas was mixed with a much larger volume of gas from the room and was exhausted into the atmosphere.

2.6 Insulation

The ceramic fiber heaters themselves were insulated with approximately 2" of insulation but were further insulated with ½" of Pyrogel insulation and instrumented with thermocouples to allow for better heat loss control and measurement. The Pyrogel was from Aspen Aerogels and was used for insulating the sides of the test section. It had a nominal thermal conductivity of 0.15 Btu-in/hr-ft^2-°F which was used in the heat loss calculations. To further reduce heat losses, 4 inches of fiberglass insulation were also installed on the main wall surfaces outside the Pyrogel.

2.7 Supporting Assembly

The supporting assembly for the test section can be seen in Figure **2-10** . The test section rested on a large 1” thick stainless steel block with a layer of Pyrogel to reduce the heat transfer to the support. This stainless steel block was composed of two pieces held together by two keys so that the main support could be easily fit around the test section. The test section was instrumented with thermocouples near the support, so that heat loss data could be obtained.

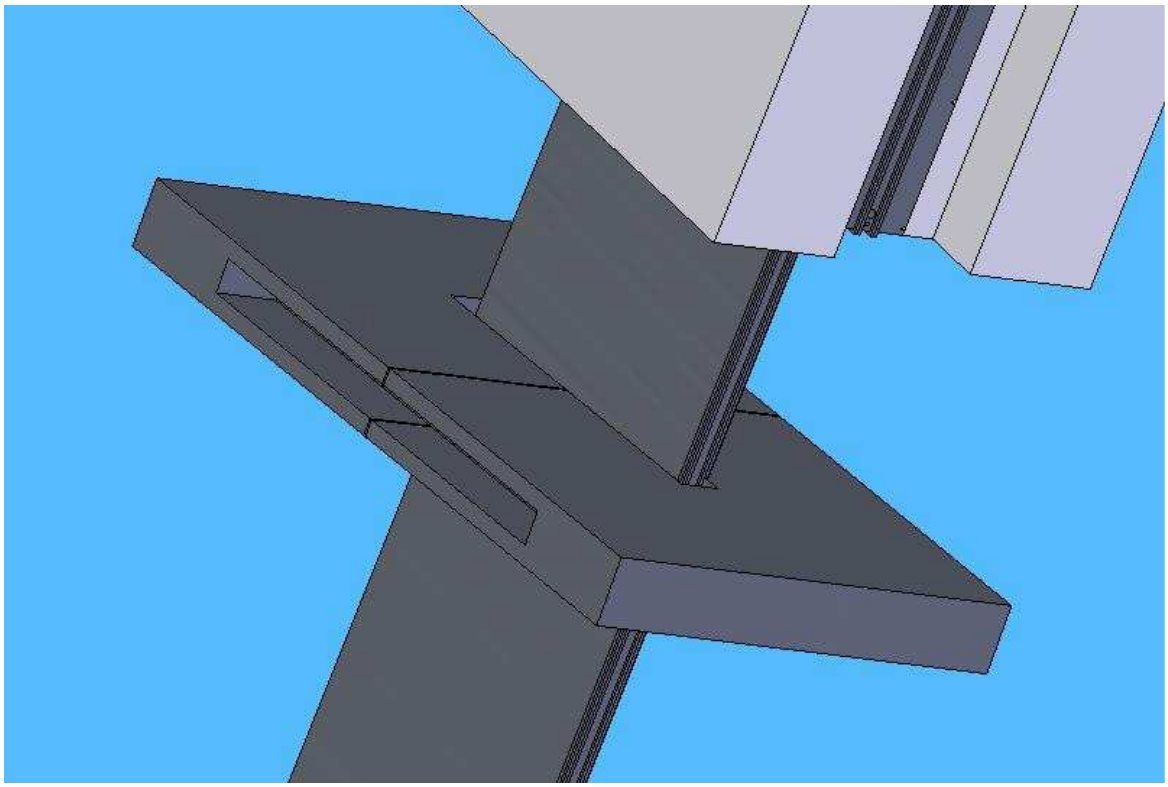

Figure **2-10**: Main support block detail

The main support block was bolted to the main frame of the experiment. This frame was build using steel uni-strut material from Kindorf. The Kindorf frame was then directly bolted to the cinder block wall to secure the experiment. Also attached to the

Kindorf frame were the lateral test section angle iron supports. To minimize heat loss, these lateral supports only contacted the insulation.

2.8 Traversing Fluid Thermocouple Probe Assembly

The traversing fluid thermocouple probe assembly can be seen in Figure **2-11**. The traversing probe assembly consisted of a large acme threaded rod (0.20”/revolution), traversing platform and scale. When the rod was rotated the platform would either move up or down. The platform had an indicator on the scale such that the exact location of the traversing thermocouples was known. There were two such probes with three thermocouples on each probe to measure the lateral fluid temperature profile at various axial positions.

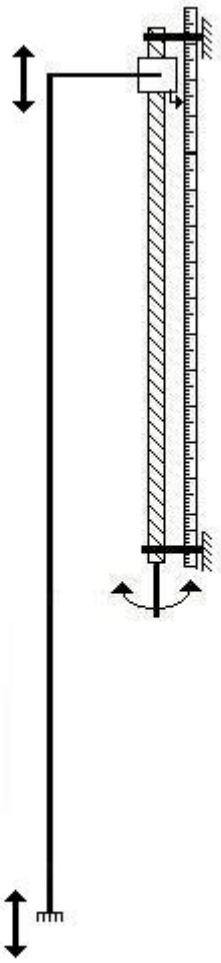

Figure **2-11**: Traversing Probe Assembly

2.9 Exhaust System

The exhaust system consisted of the exhaust duct and the exhaust fan. After the gas exited the upper plenum it ran through a 6” flexible duct to the exhaust fan. The fan mixed the heated gas with room air and exhausted the mixture into the atmosphere.

There is also a compressed air line running to the exhaust system to cool the exhaust further, however it was never necessary.

Chapter 3

Instrumentation and Measurements

3.1 Introduction

The instrumentation and measurements for this test was divided into one of the following four categories: temperature, pressure, flow, and power. Much of the experimental design centered on reducing the uncertainty in all these measurements. Often, the uncertainties in these measurements were based on the full scale value of each instrument. For this reason, flow and pressure were measured using different instruments that could cover only the desired range, thus minimizing uncertainty.

3.2 Temperature Measurements

The temperature measurements were made using three types of type K thermocouples. The thermocouple type depended on where the thermocouple was placed in the test section. There are also seven categories which describe the location of each thermocouple set. These include: center wall thermocouples, side wall thermocouples, channel spacer thermocouples, redundant wall thermocouples, insulation/heat-loss thermocouples, and safety thermocouples. To remain consistent, the axial locations of the thermocouples are described with respect to the beginning of the heated length.

All thermocouples were made using premium type K thermocouple wire, however not all thermocouples were of the same style. Three different styles of thermocouples

were used, simply called style 1, style 2, and style 3. All of the wire used in making the thermocouples came from the same premium grade lot. Figure **3-1** shows the axial locations of all the center and side wall thermocouples.

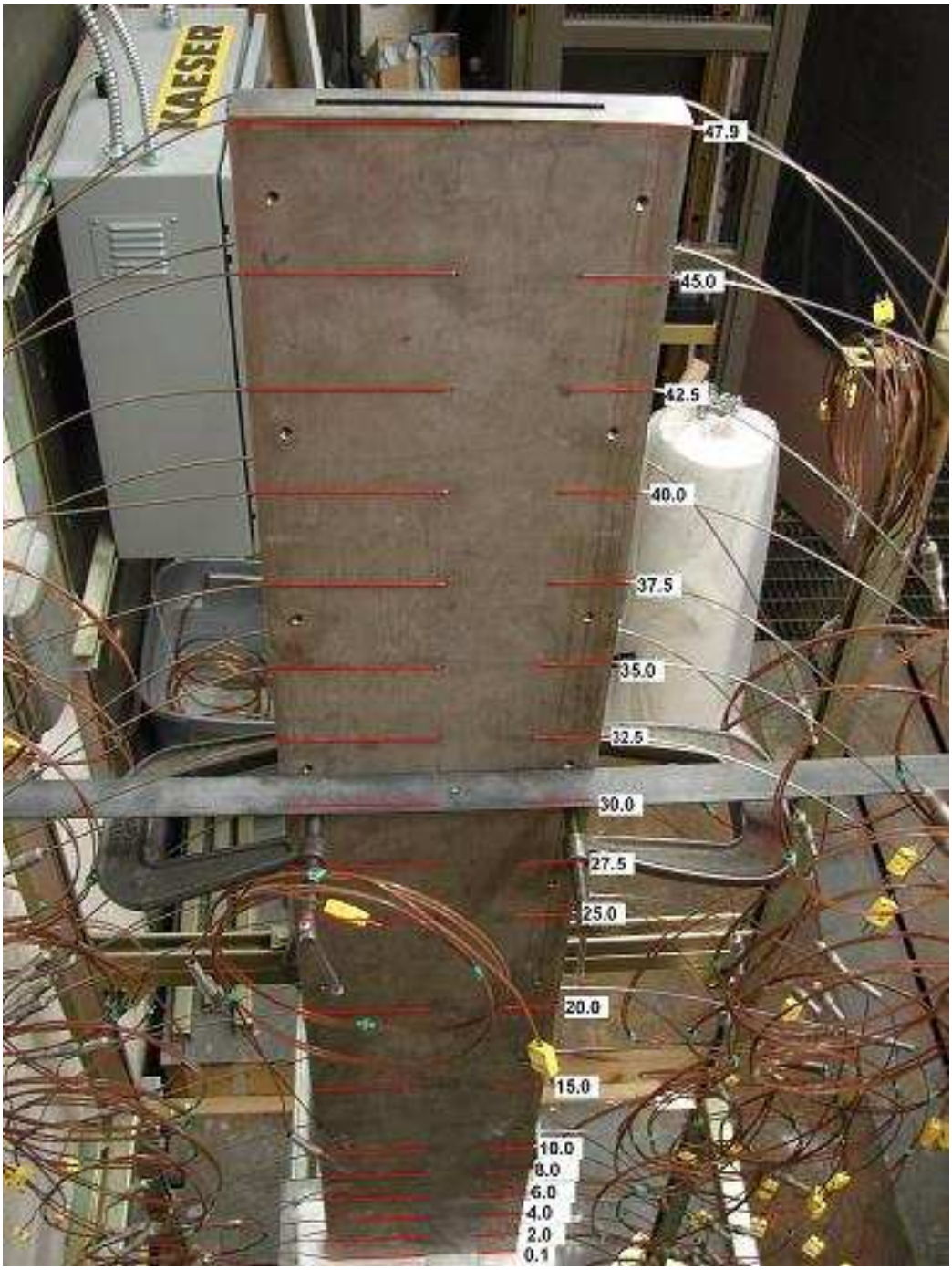

Figure **3-1**: Axial Thermocouple Layout for the Center and Side Wall Thermocouples

Figure **3-2** shows the lateral locations of the center wall, side wall, and channel spacer thermocouples. It also shows the piece used to center the thermocouple probe in the channel.

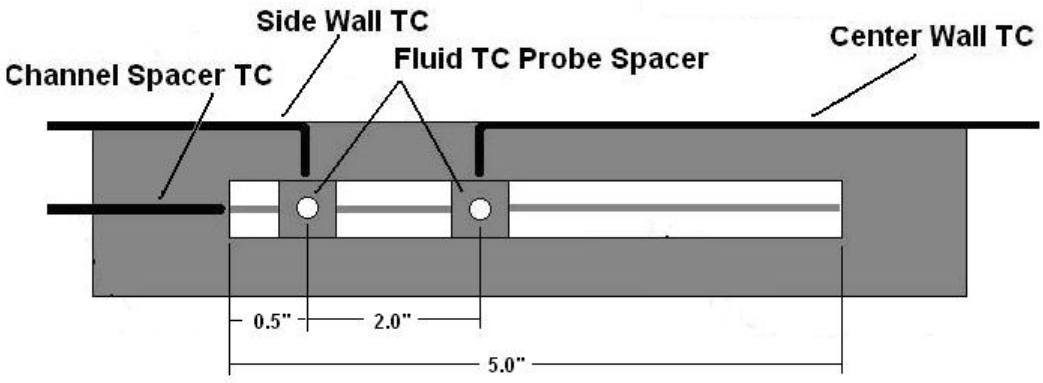

Figure **3-2**: Lateral Thermocouple Layout Showing the Thermocouple Probe Spacer Piece

3.2.1 Thermocouple Categories

3.2.1.1 Style 1 Thermocouple

Style 1 thermocouples were made by Delta M. They were Style T2 ungrounded premium grade type K thermocouple wire inside a 12 inch long inconel 600 sheath with 0.062 inch sheath diameter. Magnesium Oxide was used as the sheath insulation material and the lead insulation was Teflon. These thermocouples were used for the Center Wall, Side Wall, Channel Spacer, and Redundant wall thermocouples.

3.2.1.2 Style 2 Thermocouple

Style 2 thermocouples were hand welded from premium grade 24 gage type K thermocouple wire sheathed in Teflon. The wire was obtained from Delta M and the thermocouples were made at Penn State. These were used where a thermally insulated thermocouple was not necessary. These thermocouples were first welded together to form a small bimetallic sphere. Then they were either tack-welded to the unheated portion of the test section, or buried in the insulation. These thermocouples were mainly used for the insulation/heat-loss measurements and calculations.

3.2.1.3 Style 3 Thermocouple

Style 3 thermocouples were the traversing fluid thermocouples on the thermocouple probe made by Delta M. Premium type K thermocouple wire was used. The head of the probe was a 3 point rake spanning approximately 0.25 inches. The probe body was 60 inches long and $^{1}/_{8}$ inch in diameter. The thermocouples themselves were 0.0215 inches in diameter and sat approximately 0.25 inches from the probe body. Behind the rake is the probe spacer which is seen from above in Figure **3-2.** It was used to center the probe in the channel so that an accurate temperature profile measurement could be taken.

A close up of the head of the probe can be seen in Figure **3-3** . These thermocouples were used to measure the temperature profile of the flow inside the test section at various axial elevations.

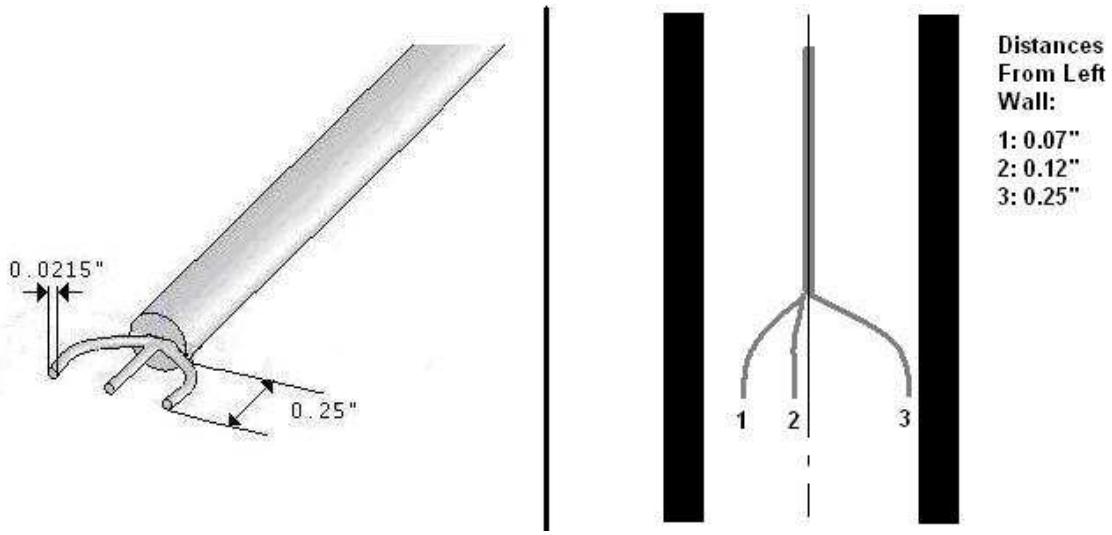

Figure **3-3**: Style 3 Thermocouple Close Up Showing the Lateral Probe Distances

3.2.2 Thermocouple Location Categories

3.2.2.1 Wall Thermocouples

The Wall Thermocouples consisted of 43 thermocouples in 3 sets: 17 center wall, 17 side wall, and 9 channel spacer thermocouples. These were all the style 1 thermocouples described prior, and were located axially as depicted in Figure **3-1** and laterally as depicted in Figure **3-2** above. These thermocouples were bent and pressed into the stainless steel test section and were on average 0.05 inches from the inside heated channel wall. The actual temperature difference between the true wall temperature and

that measured was found to be small, but the data reduction code accounts for this small temperature deviation based upon the calculated heat flow. Figure **3-4** displays a plot of the calculated difference in temperature between the measured and actual temperatures at the wall as a function of the wall heat flow.

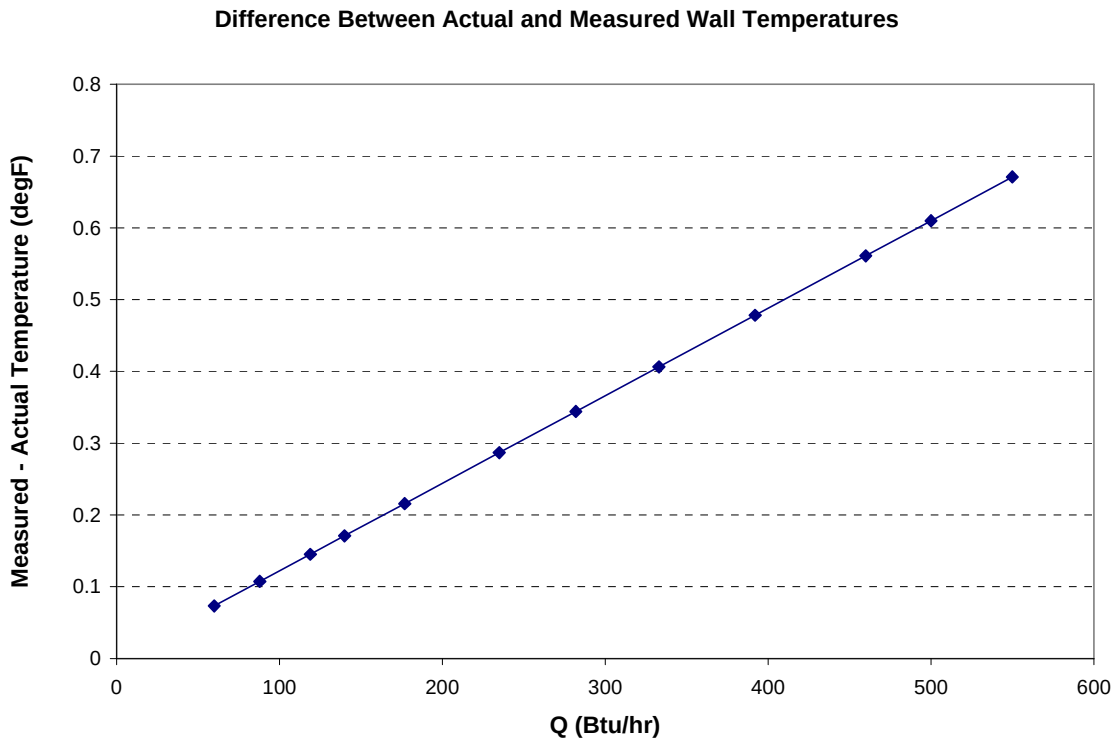

Figure **3-4**: : Temperature difference between measured and actual wall temperatures based on a 0.05" thermocouple to wall distance

3.2.2.2 Redundant Wall Thermocouples

The Redundant Wall Thermocouples (generally referred to as Redundant Thermocouples) consisted of 11 style 1 thermocouples located along the opposite side of the test section as the Wall Thermocouples. They were also bent and pressed into the

stainless steel test section in the positions seen in Figure **3-2** with the thermocouple tip 0.05 inches from the inside channel wall. The Redundant Thermocouples were placed in the test section should something happen to the Wall Thermocouples and to provide a double check for Wall Thermocouples. The axial locations of the redundant thermocouples can be found in Table **3-1** . These are also the same axial locations of the channel spacer thermocouples.

Table **3-1**: Redundant/Channel Spacer Thermocouple Information

Thermocouple Number	Location (with respect to heated section)
	(inches)
1	0.1
2	4
3	10
4	15
5	20
6	25
7	30
8	35
9	40
10	45
11	47.9

3.2.2.3 Insulation/Heat Loss Thermocouples

The Insulation thermocouples consisted of several style 2 thermocouples located on within the insulation as well as tacked to the test section in locations where heat loss measurement could be easily calculated. The heat losses and their respective thermocouples locations can be broken into 4 heat loss categories: bottom axial heat loss top axial heat loss, main wall lateral heat loss, and side wall lateral heat loss.

The bottom axial heat loss was measured in two ways. The first was to measure the difference in temperature between the top and bottom of the support plate. The second was to measure the axial temperature gradient of the thin walled section. The top axial heat loss was measured through a ¼" piece of Pyrogel insulation laid on the top of the test section and beneath the upper plenum. Thermocouples were placed on either side of this Pyrogel piece in order to get an axial temperature difference. The details of these thermocouple placements can be found in Figure **3.5**.

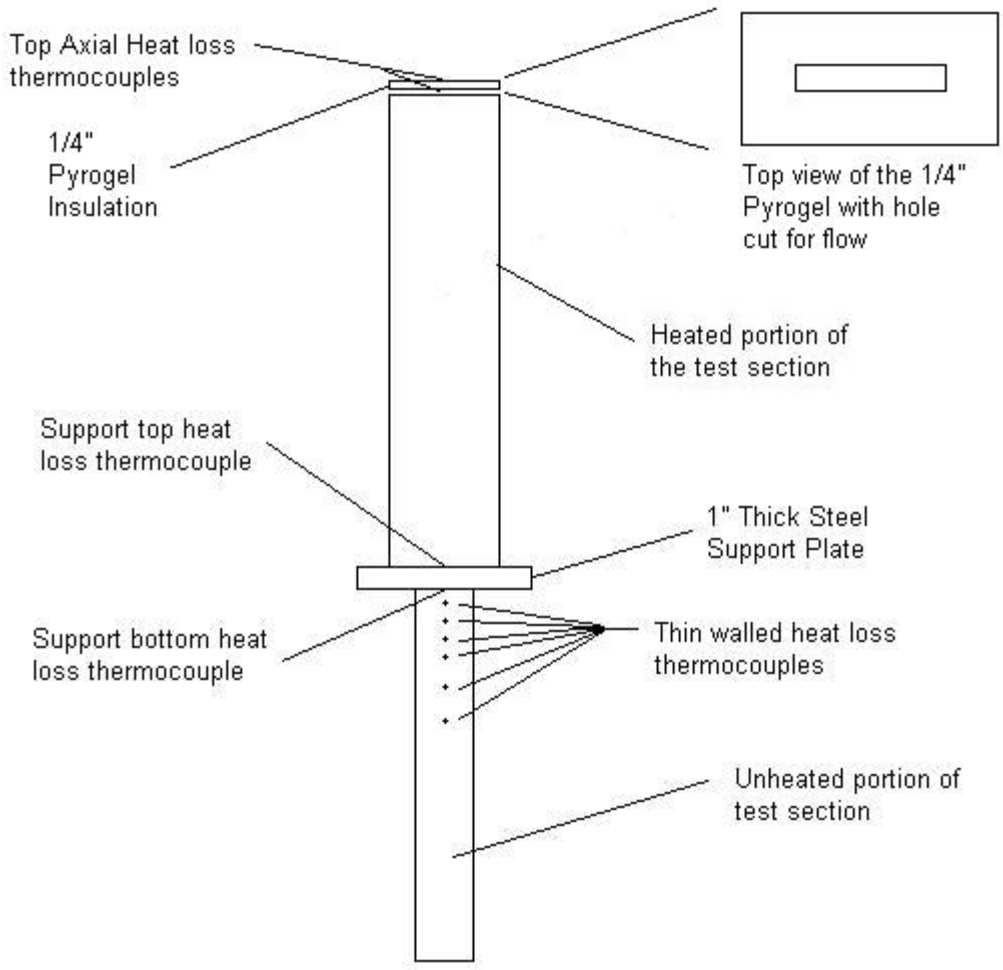

Figure **3.5**: Top and Bottom axial heat loss thermocouples. The thin walled heat loss thermocouples are at -2",-4",-6",-8",-12", and -16" with respect to the entrance of the heated length.

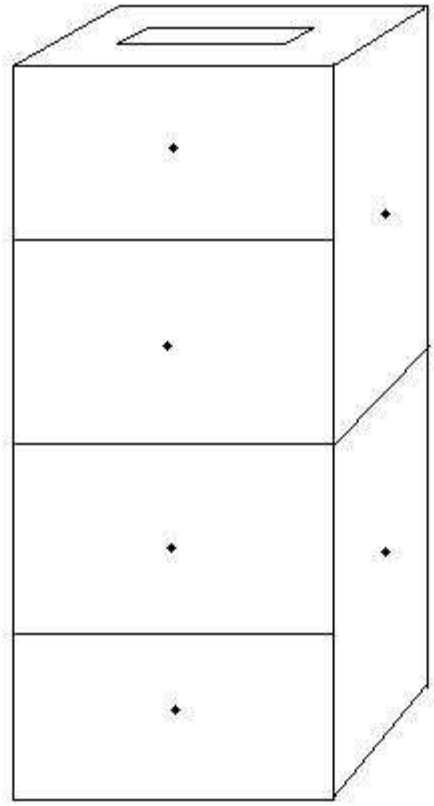

Figure **3.6**: Lateral heat loss noding and placement of thermocouple sets. Main Wall has 4 nodes and TC sets at 10",20", 30" and 40". Side Wall has 2 nodes with TC sets at 10" and 30".

The main wall lateral heat loss and the side wall lateral heat loss were both measured using temperature differences across a ¼" Pyrogel sheet. The total lateral area was broken into separate pieces to help account for the axial dependence on lateral heat loss. Figure **3.6** depicts the noding scheme to measure the lateral heat loss as well as shows the locations of the thermocouple sets to measure the delta temperature across the ¼" Pyrogel at those locations.

3.2.2.4 Inlet/Outlet Safety Thermocouples

To measure the inlet temperature of the fluid, a thermocouple was placed in the inlet piping directly after the flow-meter. This temperature was an inlet condition to help calculate the energy balance in the data reduction program. The exit temperature from the heated test section was measured using the traversing thermocouple probe fully retracted to the test section exit. The exiting exhaust temperature was measured at the exhaust fan for safety reasons. This is because of the close proximity of a pedestrian walkway at the exhaust fan exit. Another thermocouple was placed inside the power box to ensure safe operating temperatures for that unit.

3.3 Pressure Measurements

The pressure measurements were made using absolute and differential pressure cells from Rosemount. The absolute pressure tap was located prior to the inlet of the flow-meter so that an accurate flow measurement could be taken relative to the inlet pressure. The differential pressure measurements were able to be taken across 6 different pressure taps. In the heated length there was a tap at the inlet and then at every 12” increment of the heated length.

Figure **3.7** depicts the absolute and differential pressure tap layout.

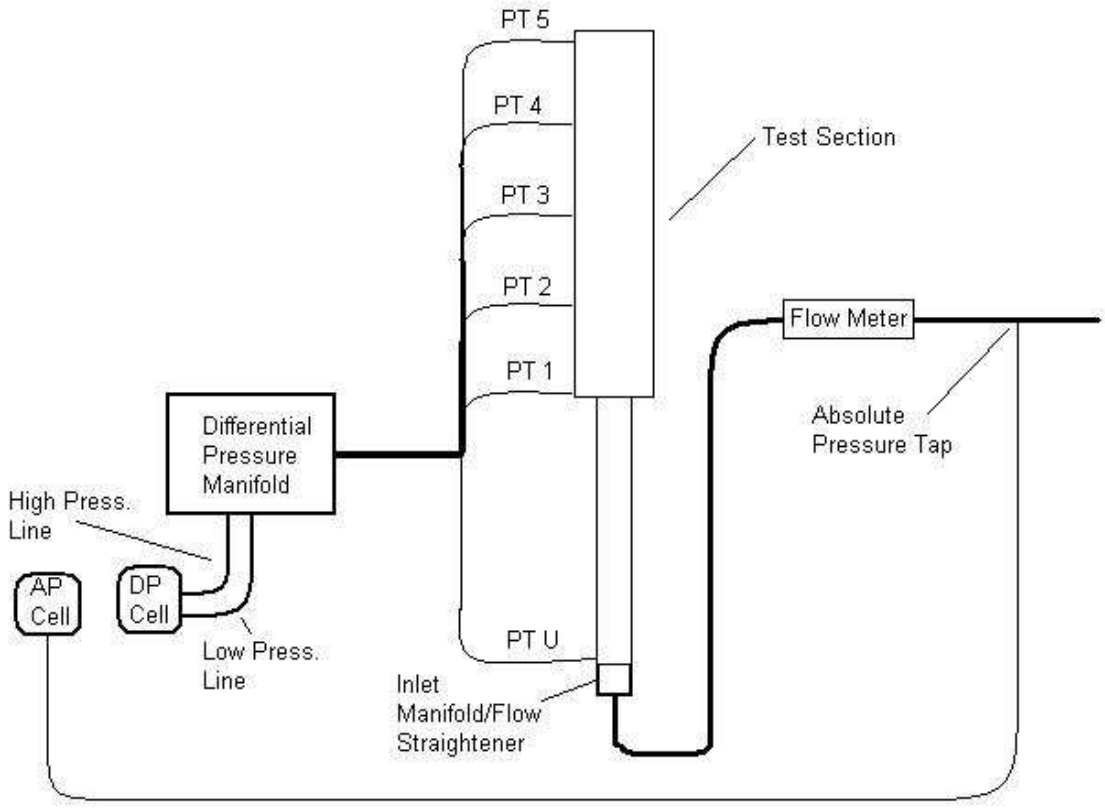

Figure **3.7**: Pressure Tap Layout

3.3.1 Absolute Pressure Measurements

The absolute pressure measurements were taken at the absolute pressure tap seen in Figure **3.7** above. The signal was received by an absolute pressure transducer by Rosemount. This pressure transducer's range was between 0-30 psia. A second absolute pressure transducer was needed for the high Reynolds number experiments due to the

higher back pressure required to drive higher flows. It was capable of reading pressures from 0-150psia but was calibrated to measure between 0-80psia.

3.3.2 Differential Pressure Measurements

Differential pressure measurements were taken between Pressure Taps U & 1, 1 & 2, 2 & 3, 3 & 4, and U & 4 as depicted in Figure **3.7** above. Pressure tap 5 was ignored because of interference with the traversing probe at that elevation. A differential pressure transducer from Rosemount was used to span the range of the pressure drops. The differential pressure transducer was originally ranged between 0-25 inches of water but was sent back to Rosemount and re-ranged to span 0 – 1.67 inches of water due to the low pressure drops in the rectangular test section.

3.4 Flow Measurements

The flow measurements were made using turbine flow meters from Flow Technology. Three flow meters were needed to cover the Reynolds number range of the experiment. The meters used were labeled FT 2-8, FT 6-8, and FT-12. Because turbine flow meters are sensitive to both temperature and pressure, the inlet flow temperature and pressure were measured. The inlet pressure was maintained between 20.00 and 20.1 psia and the inlet temperature was fairly constant at around 70°F. However the pressure in the test section was always near an atmospheric pressure of 14.1 psia for the test site elevation of 1200 feet above sea level. This meant that the actual CFM in the test section

was different than what the flow meter measured. The calculation for a meter pressure of 20 psia as was performed using a simplified form of ideal gas law is seen in Equation **3.1** as,

$$ActualCFM = \frac{P_{inlet}}{P_{calibration}} * MeterCFM$$
$$ActualCFM = \frac{20.0}{14.1} * MeterCFM \quad (\mathbf{3.1})$$

3.4.1 Low Range Flow Meter (FT 2-8)

The FT 2-8 was the smaller of the two flow meters. It was calibrated for air at 20.0 psia. The Air calibration was used for the Nitrogen runs. The normal range of the flow meter was between 0.1 – 1.0 ACFM. This allowed for nitrogen to cover the Reynolds number range approximately between 60 – 600.

3.4.2 Mid Range Flow Meter (FT 6-8)

The FT6-8 was the mid range flow meter. It was calibrated using Air at 20.0 psia. The Air calibration was used for the Nitrogen runs. The normal range of the flow meter was between 0.5 – 5.0 ACFM. This allowed for nitrogen to cover the Reynolds number range approximately between 300 – 3000.

3.4.3 High Range Flow Meter (FT 12)

The FT 12 was the larger of the two flow meters. It was calibrated using Air at 20.0, 30.0, and 50.0 psia. The Air calibration was used for the Nitrogen runs. The normal range of the flow meter was between 2.0 – 20.0 ACFM. This allowed for nitrogen to cover the Reynolds number range between 1,200 – 12,000 at 20psia, 1,800 – 18,000 at 30psia, and 3,000 - 30,000 at 50psia.

3.5 Power Measurements

The power measurements were made using watt transducers from NK Technologies. One watt transducer was needed to cover the Power range of this experiment. The maximum wattage of the transducer (the maximum wattage the transducer can measure) was a jumper selectable input on the transducer. The available powers were 2880 watts, 3840 watts, and 6000 watts. Of the 3 available powers, only the larger 2 powers were used in the current experiments.

3.6 Instrumentation Uncertainties

As was previously discussed in this chapter, the instrumentation was chosen specifically to reduce the overall uncertainty of all the measurements, in order to obtain limited uncertainty in the final heat transfer correlations. All uncertainty information and calculations are found in Appendix **F**.

Chapter 4

Data Reduction

4.1 Steady State Data

An initial steady state was obtained once the maximum change in temperature of the wall thermocouples was less than 2 degrees Fahrenheit in a 15 minute time period. This was also assuming that pressure, power and flow to the system were held constant while approaching steady state. The traversing thermocouple probe was held in the top 3 inches of the test section while the system approached steady state to achieve accurate and steady wall temperature readings as well as unobstructed pressure drop measurements. The traversing thermocouple probe was then inserted and was used to acquire fluid temperature profiles at various axial locations. Its presence did affect the local pressure and had a small affect on the local wall temperatures because of its mass and flow restriction locally.

4.1.1 Steady State with Probe Withdrawn

The steady state data for most measurements were found with the probe withdrawn from the heated section. This was because the presence of the probe not only affected the pressure drop due to the decrease in flow area, but its mass acted as a heat sink which had a small affect on the local wall temperatures. For these reasons, the

steady state wall temperatures and pressure drops were taken while the probe was withdrawn as far as possible without removing it completely from the test section.

Once the test section had reached steady state and prior to the probe being inserted, the pressure drop measurements were taken. The pressure drop was measured between each of the 5 differential pressure taps, and also between pressure taps 1 and 4 to obtain a total pressure drop for the heated length. Pressure tap 5 was ignored because it was obstructed when probe was withdrawn to its maximum height. During each pressure drop measurement, the test section was held at a steady state for at least 30 seconds. Since 6 pressure drop measurements were taken, the test section was at steady state for 180 seconds. Over this 180 second window, all wall temperature and heat loss temperature measurements were also averaged to obtain their steady state values.

4.1.2 Steady State with Probe Inserted

The steady state value of the flow rate, power to the test section, and probe thermocouple temperatures were obtained with the probe inserted into the test section. More specifically, they were found at each axial probe location. The probe was moved to a specific elevation and given time to reach steady state. A graphical output on the data acquisition system allowed the user to observe the probe temperatures and decide when to begin the 30 second data acquisition. Also averaged over this period were the flow rate and the power to the test section. The number of data points that were averaged was equal to the number of axial steps the probe took.

For each axial set of wall thermocouples, a bulk temperature measurement was taken in between or at the node center between the two axial wall thermocouple locations. This was done such that an energy balance could be performed axially. The axial wall thermocouple locations where data was taken are (45, 42.5, 40, 37.5, 35, 32.5, 30, 25, 20, 15, 10, 8, 6, 4, 2, 0.1) therefore the axial bulk temperature measurements were taken at the node centers or (43.75, 41.25, 39.75, 36.25, 33.75, 31.25, 27.5, 22.5, 17.5, 12.5, 9, 7, 5, 3, 1.05). These bulk temperature measurements were eventually mated to their respective wall temperature. However, since the wall temperatures were measured at different axial locations than the bulk temperatures (node end vs. node center), the wall temperatures were axially spline fit to match the axial location of the bulk temperature measurement. The axially fit wall temperatures were used to mate a wall temperature to a bulk temperature profile for the purpose of adding the wall temperature to the local lateral temperature profile.

A second set of wall temperature measurements was taken after all other measurements were taken. This was done to ensure the experiment was at a true steady state for the entire testing period. Table **4-1** gives data from the best and worst case steady state data sets. The best case is the test where the wall temperatures changed the least over the course of the experiment and vice versa. The table shows the deviation between the wall temperatures prior and post testing, as well as the deviation with respect to time.

Table **4-1**: Steady State Pre and Post Test Temperature Data

	Run 922, Inlet Re = 8000				Length = 2998 seconds			
Axial Location	**Pre-Test Center Wall**	**Pre-Test Side Wall**	**Post-Test Center Wall**	**Post-Test Side Wall**	**Center Deviation**	**Side Deviation**	**Center DegF/15min**	**Side DegF/15min**
1.05	195.7	210.3	194.6	209.2	1.1	1.1	0.33	0.34
3	248.3	260.5	246.9	259.0	1.4	1.5	0.42	0.45
5	297.5	309.2	295.8	307.3	1.7	1.9	0.52	0.56
7	337.9	350.3	336.0	348.3	1.9	2.0	0.56	0.61
9	375.3	386.6	373.5	384.6	1.9	2.0	0.56	0.60
12.5	423.4	433.4	421.5	431.5	1.9	1.9	0.57	0.57
17.5	469.8	483.8	467.7	481.7	2.1	2.2	0.63	0.65
22.5	524.0	537.3	521.5	534.5	2.5	2.9	0.74	0.86
27.5	572.3	586.8	569.4	583.2	2.8	3.5	0.85	1.05
31.25	602.5	619.2	599.1	615.0	3.4	4.2	1.02	1.27
33.75	620.2	635.0	616.2	630.1	4.0	4.9	1.20	1.47
36.25	635.2	648.0	630.8	642.7	4.4	5.4	1.32	1.62
38.75	647.4	659.8	643.0	654.5	4.3	5.4	1.30	1.61
41.25	654.5	665.4	651.0	660.8	3.5	4.6	1.07	1.38
43.75	650.3	660.7	648.1	657.4	2.2	3.3	0.66	0.99
	Run 921, Inlet Re = 6600				**Length = 2314 seconds**			
Axial Location	**Pre-Test Center Wall**	**Pre-Test Side Wall**	**Post-Test Center Wall**	**Post-Test Side Wall**	**Center Deviation**	**Side Deviation**	**Center DegF/15min**	**Side DegF/15min**
1.05	198.4	212.2	194.9	208.8	3.5	3.4	1.36	1.32
3	248.7	260.0	243.4	254.9	5.3	5.0	2.05	1.96
5	297.9	308.1	290.5	301.1	7.4	7.0	2.87	2.72
7	339.8	350.4	330.9	341.8	8.9	8.5	3.45	3.33
9	378.5	388.0	368.8	378.5	9.7	9.5	3.79	3.71
12.5	429.1	437.4	418.0	426.6	11.1	10.8	4.31	4.21
17.5	478.4	490.5	466.6	478.7	11.8	11.8	4.59	4.58
22.5	533.1	544.4	521.8	532.5	11.3	11.9	4.40	4.62
27.5	581.5	593.8	570.7	582.0	10.8	11.8	4.20	4.59
31.25	612.4	626.6	600.7	614.2	11.7	12.4	4.53	4.83
33.75	630.5	643.0	617.3	629.5	13.3	13.5	5.17	5.25
36.25	645.7	656.2	631.1	641.9	14.6	14.3	5.70	5.56
38.75	657.3	667.3	643.1	653.5	14.2	13.8	5.51	5.37
41.25	662.5	671.3	651.2	659.7	11.3	11.6	4.41	4.53
43.75	655.7	664.4	650.0	657.0	5.7	7.4	2.22	2.89

4.2 Data Analysis

The data analysis used many steps to obtain the fluid heat transfer parameters from the raw test data. The first step was to reduce the initial output file to a more manageable size. This was done by looking for steady state data markers that were embedded into the file every time a data point was taken. The data markers were numbered specifically to identify what data was of interest when the data point was taken. For the bulk temperature measurements, this marker identified what axial location the probe was at when that data was taken.

The data was sampled/logged at one data point per second. The logged data was then averaged for 30 seconds prior to the point at which the experimenter flagged the measurement. This reduced the size of the data matrix from several thousand rows of data to a single 30 second time averaged row for every data marker. For most tests there was a data marker for each of the different pressure drop measurements and a data marker for each axial bulk temperature measurement.

Obtaining the bulk temperature required radial profiles of temperature, density, specific heat, and velocity. The temperature profiles were measured using the traversing probe. Radial density and specific heat were found using NIST tables for nitrogen at 14psia and correlating to a specific temperature. Fluent was used to solve for the velocity profiles using a 2 dimensional model. For more information see Section **4.2.5.**

Once the radial velocity profile was calculated, the bulk temperature could be calculated at a specific axial elevation from Equation **4.1** , given as

$$T_{bulk} = \frac{\int_0^W u(x) \cdot Cp(x) \cdot \rho(x) \cdot T(x) dx}{\int_0^W u(x) \cdot Cp(x) \cdot \rho(x) dx} \quad (\mathbf{4.1})$$

with the profiles for velocity, specific heat, density, and temperature all known at that specific elevation.

Once the bulk temperature was known, other axial properties such as the average thermal conductivity and average specific heat could be found and used to obtain the heat flux calculated from Equation **4.2**, given in differential form as,

$$q'' = \frac{\dot{m} \cdot Cp}{(2L + 2W)} \frac{dT_{bulk}}{dz} \quad (\mathbf{4.2})$$

where the heat flux is assumed to be uniform on all sides of the channel. The heat transfer coefficient calculated from Equation **4.3** given as,

$$h = \frac{q''}{\Delta T_{wall-bulk}} \quad (\mathbf{4.3})$$

the Nusselt number calculated from Equation **4.4** given as,

$$Nu = \frac{h \cdot D_h}{k} \quad (\mathbf{4.4})$$

and the Reynolds number calculated from Equation **4.5** given as,

$$\mathrm{Re} = \frac{\dot{m} \cdot D_h}{\mu \cdot A_{flow}} \quad (\mathbf{4.5})$$

4.2.1 Reflecting the Probe Thermocouple Temperatures

The traversing probe had a 3 point thermocouple rake at its head therefore 3 radial temperature measurements were made at various axial elevations within the fluid. Because of the symmetry of the flow area, the 3 radial points could be reflected to produce a 6 radial point temperature profile which can be seen in Figure **4.1**.

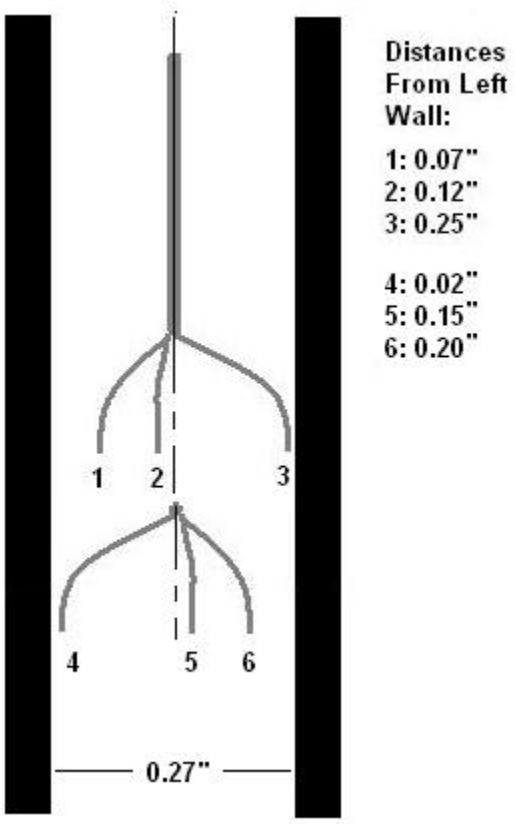

Figure **4.1**: Reflecting the Probe Thermocouples

4.2.2 Adding the Wall Temperatures to the Lateral Temperature Profile

For each axial fluid temperature measurement, the wall temperature from the Center and Side Wall Thermocouples was also added to the lateral temperature profile. The center and side probe temperatures were matched to the corresponding center and side wall temperatures. Now the fluid temperature profile was known at eight lateral locations for each axial location. It should be noted that the steady state temperatures for the Wall Thermocouples were obtained at the beginning of each test run when the pressure drop measurements were being taken. Therefore, even though that wall temperature is used in the lateral temperature profile, it was not the wall temperature when the probe was physically there. This was because as the probe moved to a specific elevation the wall temperature at that elevation would decrease and the wall temperatures near that elevation would also decrease. The temperature reading from the Redundant Thermocouples did not appear in the lateral temperature profile because the Redundant Thermocouples were only used as a check of the Wall Thermocouples.

4.2.3 Obtaining Lateral Profiles of the Fluid Properties

To obtain the temperature dependent fluid properties (density, specific heat, and viscosity) the 8 point lateral temperature profile was used along with tables from NIST. The pressure was assumed to be constant at 14 psia. The gas property values at each point in the lateral temperature profile were found by interpolating the NIST tables with the given lateral temperature profiles. This allowed for calculation of the gas properties at each of the eight lateral nodes and at each of the 16 axial nodes.

4.2.4 Using Spline Interpolation to Fit the Lateral Profiles

Calculating the bulk temperature required integrating continuous functions of the temperature, density, specific heat, lateral distance, and velocity; however, the temperature measurements resulted in point values at each node end for the temperature and gas properties, not continuous function. Converting these node values into continuous functions was completed by using a spline interpolation function in MatLab. This function fits a cubic spline between each of the known node values and then calculates the values for the splines at user defined points. This allows the user to specify a much finer node scheme so that an accurate numerical integration could be performed to find the bulk temperature. Using this method, the original 8 lateral node points were fit so that 28 lateral points at each axial location were known. Cubic spline interpolation was used to refine the lateral temperature profiles because:

1) The spline fit would go through each data point. This is not true for low order polynomial fits.
2) The first derivative of the fit would be continuous.
3) The slope of the spline fit at the walls could be forced to be linear, better approximating reality. (The slope was found using the wall temperature and the temperature from the probe thermocouple closest to the wall)
4) The slope at the center of each profile would be 0.

4.2.5 Obtaining the Lateral Velocity Profiles

FLUENT computational fluid dynamics code version 5/6 was used to create individual velocity profiles for each test. A two-dimensional model was used with an unheated and heated portion. This model was used to obtain velocity profiles for each of flows and powers necessary for all of the tests. Each of the velocity profiles was broken into 28 lateral points to match the noding scheme of the temperature and fluid property lateral profiles. These profiles were written to a data file for each case which was read by the MatLab data reduction program.

A mesh sizing study was completed to ensure fine enough meshing was used to calculate the lateral velocity profiles correctly. The lateral mesh for the fluid was increased from 10 to 20 and finally to 27 lateral mesh nodes. It was found that the error in the integrated velocity profiles between the 20 and 27 node cases was on the order of 1% therefore the 28 lateral node scheme was considered a good approximation.

The k-epsilon turbulent model was used for the turbulent cases above a Reynolds number of 2300 while the laminar flow model was used for cases below a Reynolds number of 2300. Figure **4-2** gives confidence that the FLUENT models are capable of accurately modeling turbulent and laminar flow when compared to the traduational $1/7^{th}$ and parabolic normalized profiles.

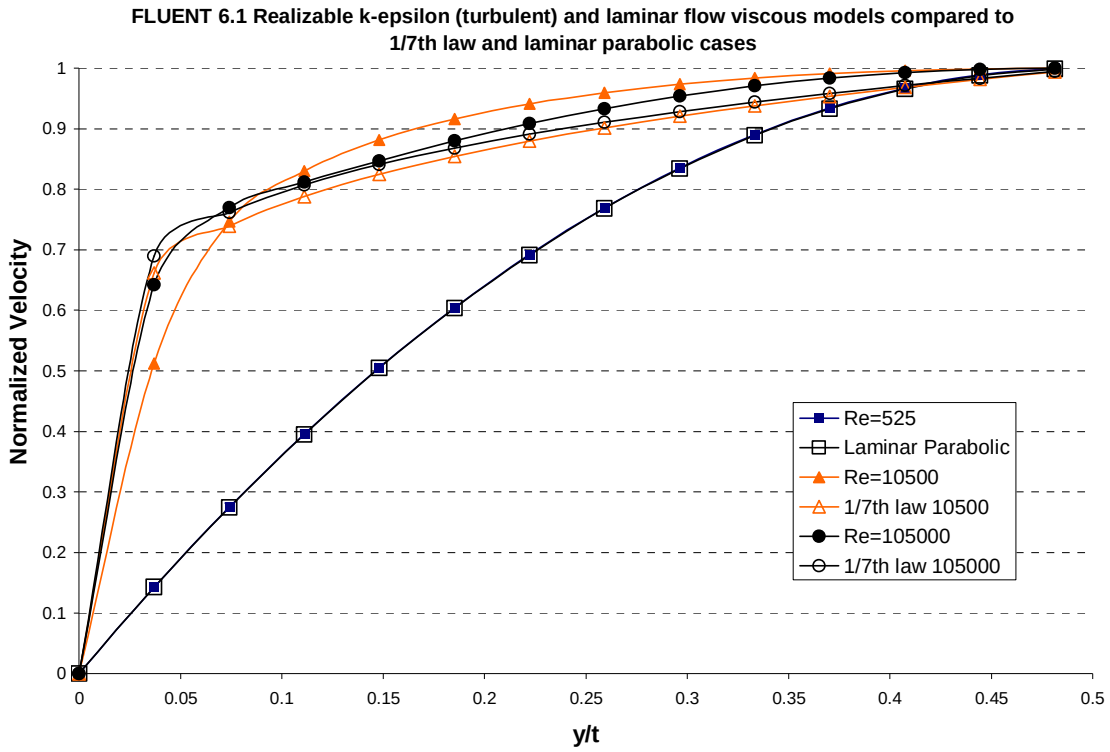

Figure **4-2**: Fluent Normalized Velocity Profile Study. The x-axis represents the normalized channel thickness.

The FLUENT model accounted for variable fluid properties with respect to temperature. The default Fluent polynomial fits for the fluid properties were used in solving each case. A run was considered converged when each of the model parameters (Viscous, Continuity, Energy, Momentum) had residuals smaller than $1x10^{-5}$.

Prior to entering the heated length of 48 inches, the flow was allowed to develop in a thin walled 36 inch unheated length. This thin wall was used only as a means to bound the fluid flow as it developed. The outside walls of the model were considered adiabatic so all of the heat would transfer to the fluid. For a given flow condition, the power to the heaters would be adjusted until the desired fluid exit temperatures were

achieved. A set of velocity profiles was then generated for each axial node and then written to file.

4.2.6 Solving for the Bulk Temperature

Using the lateral profiles of velocity, density, specific heat with constant pressure, and the measured temperature profiles, an axial bulk temperature was calculated for the center and side probes using Equation **4.2**. The data reduction program used a rectangular numerical integration scheme to integrate each of the parameters over the 28 lateral nodes.

4.2.7 Calculating the Heat Transfer Parameters of Interest

Heat transfer parameters were calculated at each axial node using the actual data from each experiment. The only fits used in the calculation of the heat transfer parameters are the spline fits used to refine the lateral nodes in the temperature profiles. Axial values for fluid density, viscosity, thermal conductivity, and Cp were found by spline interpolating between a NIST fluid property data table. These were based on the bulk fluid temperature at 14psi at each axial node. This table can be found in Appendix **F**.

The process for calculating the heat transfer parameters began by using the predefined axial nodes which were based on the location of the wall thermocouples. The 48 inch heated length was broken up into 16 axial nodes. The axial node size was

variable, based on the spacing of the wall thermocouples. The surface area used for heat transfer in each node was calculated from Equation **4.6**, given as

$$Area_{node} = 2(L+W)\cdot H_{node} \quad (\mathbf{4.6})$$

The length and width were preset at 5.0" and 0.27" respectively, and the height of each node was dependent on the node.

Nodal average values for the fluid parameters were necessary to obtain the heat transfer coefficient. This was done by interpolating the NIST fluid data tables. These parameters were dependent on the bulk temperatures at the node center, therefore each of the parameters was found axially at the node center. Using this method, the node center values for the wall temperatures, specific heat at constant pressure, fluid conductivity, and fluid viscosity were found.

The bulk temperature difference was found by subtracting the bulk temperature at the bottom of the node from the bulk temperature at the top as seen in Equation **4.7**, given as,

$$\Delta T_{bulk} = T_{bulk,top} - T_{bulk,bottom} \quad (\mathbf{4.7})$$

The wall to bulk temperature difference was found by subtracting the bulk temperature at the node center from the wall temperature at the node center as seen in Equation **4.8** , given as,

$$\Delta T_{wall-bulk} = T_{wall,node} - T_{bulk,node} \quad (\mathbf{4.8})$$

With the necessary variables obtained, the heat flux was calculated from Equation **4.9** , given as,

$$q''(x) = \frac{\dot{m} \cdot C_p(x) \cdot \Delta T_{bulk}}{A(x)} \quad (\mathbf{4.9})$$

where Cp(x) is based on the bulk temperature at node x, and A(x) is based on the length of node x multiplied by the perimeter of the flow channel. The heat transfer coefficient was calculated from Equation **4.10** given as,

$$h(x) = \frac{q''(x)}{\Delta T(x)_{wall-bulk}} \quad (\mathbf{4.10})$$

where $\Delta T(x)_{wall\text{-}bulk}$ is the bulk temperature difference at node x. Finally, the Nusselt number was calculated from Equation **4.11** given as,

$$Nu(x) = \frac{h(x) \cdot D_h}{k(x)} \quad (\mathbf{4.11})$$

where k(x) is the fluid conductivity at node x based on the bulk temperature at node x.

4.3 Other Data Reduction

4.3.1 Friction Factors

Both the friction factor and local Reynolds number were required for the pressure drop analysis (which was done separately from the above analysis). However, the pressure drop due to acceleration had to be subtracted from the total measured pressure drop to provide the pressure drop due to friction alone. The pressure drop due to acceleration was calculated from Equation **4.12** given as,

$$\Delta P_{Acceleration} = \left(\frac{\dot{m}}{A_{flow}}\right)^2 \left(\left(\frac{1}{\rho_{out}}\right)^2 - \left(\frac{1}{\rho_{in}}\right)^2\right) \frac{\bar{\rho}}{2 \cdot g_c} \qquad \textbf{(4.12)}$$

Using these two equations, the pressure drop due to friction alone was calculated from Equation **4.13** given as,

$$\Delta P_{Friction} = \Delta P_{Total} - \Delta P_{Acceleration} \qquad \textbf{(4.13)}$$

The general form of the Moody friction factor was calculated from Equation **4.14** given as,

$$f_{Moody} = \frac{2 \cdot \Delta P_{Friction} \cdot D_h \cdot g_c}{\rho \cdot u^2 \cdot L} \qquad \textbf{(4.14)}$$

This Moody friction factor can also be put into terms of mass flow rate as in Equation **4.15** given as,

$$f_{Moody} = \frac{2 \cdot \Delta P_{friction} \cdot D_h \cdot \rho \cdot g_c \cdot A^2{}_{flow}}{\dot{m}^2 \cdot L} \qquad \textbf{(4.15)}$$

The local Reynolds number expressed in terms of the mass flow rate is given in Equation **4.16** as,

$$\mathrm{Re}(x) = \frac{\dot{m} \cdot D_h}{\mu(x) \cdot A_{flow}} \qquad \textbf{(4.16)}$$

where $\mu(x)$ is the viscosity of the fluid at node x based on the bulk temperature at node x. The flow area was a constant (0.27” by 5.0”) for all of the experiments. An axial averaged density and viscosity was needed to solve for the friction factor and Reynolds number. It was decided that the test section should be divided up into the heated and unheated regions based on the locations of the pressure taps. The heated region

contained pressure drop data from 0.1-12, 12-24, 24-36, and 36-47.9 inches. The data from 36-47.9 inches was not used due to the thermocouple probe interfering with the flow in that region while the data was being collected. This meant there were only 3 axial nodes for heated pressure drop data with node centers at 6.05, 18, and 30 inches. The average density and viscosity for the nodes were found by using the bulk temperature at the pressure drop node center locations. Once the average density and viscosities were evaluated, the Moody friction factors and Reynolds numbers were obtained. The length $'L'$ in Equation **4.15** is the distance between the pressure taps of interest.

Chapter 5

Experimental Results

5.1 Introduction

The results for laminar and turbulent heat transfer in a rectangular channel with an aspect ratio of 18.5:1 are presented. The data was taken from over 30 tests ranging in Reynolds numbers from 100 to 10,000. Two methods are given to calculate heat losses, showing that decoupling the heat losses from the heat transfer problem is the most accurate method. Also, laminar and turbulent friction factor results are compared to the expected correlations and relationships. The laminar and turbulent Nusselt number data is also presented and discussed.

5.2 Heat Loss Closure

Heat loss calculations were performed to provide an energy closure for the experiments and to calculate the percentage of total energy lost to the environment. The method used in the current experiments directly measures the heat added to the fluid by measuring the bulk fluid temperature profile at specified axial locations. Previous experimental methods have relied on using a heat balance between the power input and the calculated heat loss to obtain the energy deposited into the fluid as a difference. This section outlines the discrepancies between the two methods, and shows results from both methods.

An energy balance was performed on each of the current tests to determine the difference between a heat loss balance method and a nodal energy addition method. The heat loss balance method calculates the heat addition to the fluid using Equation **5.1**, as

$$\dot{Q}_{fluid} = \dot{Q}_{heaters} - \dot{Q}_{heatloss} \qquad (\mathbf{5.1})$$

This method works well when the heat losses are small and can be characterized very well using data from the heat loss thermocouples embedded in the insulation. Heat loss thermocouples for the current experiment were positioned as given previously in Figure **3.5**, however calculating the heat added to the fluid by subtracting the measured heat loss can be very inaccurate, especially at low Reynolds numbers. A much more accurate method is to directly measure the heat addition to the fluid by measuring the axial bulk fluid temperature, T_{bulk}, change. This method is described in Equation **5.2** , as,

$$\dot{Q}_{fluid} = \dot{m} c_{p,x} \int_0^L \frac{dT_{bulk}}{dx} dx \qquad (\mathbf{5.2})$$

The heat loss can then be calculated by subtracting the fluid heat gain from the power input to the heaters using Equation **5.3** , as

$$\dot{Q}_{heatloss} = \dot{Q}_{heaters} - \dot{Q}_{fluid} \qquad (\mathbf{5.3})$$

Table **5-1** gives the calculated heat balance data from tests 903-930. Some of the tests are omitted due to flow-meter malfunctions during testing.

Table **5-1**: Comparison of two methods for calculating the heat added to the fluid, measuring the heat loss (1), and measuring the bulk temperature directly (2)

Test #	Exit Temp. (deg F)	Inlet Re	Heater Power (W)	Measured Heat Loss (W)	Estimated Energy Addition (W)	% Heat Loss	Estimated Heat Loss (W)	Measured Energy Addition (W)	% Heat Loss
903	500	2766.2	1246.2	286.1	960.1	23	509.5	736.7	40.9
904	500	3525.8	1525.6	314.1	1211.5	20.6	532.2	993.4	34.9
905	500	4033.2	1786.5	324.2	1462.2	18.1	623.2	1163.3	34.9
906	500	4528.6	1809.4	328.5	1480.9	18.2	595.1	1214.3	32.9
907	500	3048.5	1361.8	296.6	1065.2	21.8	511.8	850	37.6
908	500	2526	1195	290.1	905	24.3	483.8	711.3	40.5
909	500	2003.3	1080.5	270.6	809.9	25	482.8	597.7	44.7
910	500	1990.6	1010.3	241.5	768.7	23.9	436.4	573.9	43.2
911	500	1692.3	885.6	235.9	649.7	26.6	369.6	516.1	41.7
912	500	1401.9	789	209.2	579.7	26.5	365.5	423.4	46.3
913	500	1099.4	686.8	187.2	499.6	27.3	353	333.8	51.4
914	500	831.7	522.4	182.6	339.8	34.9	259.8	262.7	49.7
915	500	620.7	456.1	163.9	292.3	35.9	261.4	194.7	57.3
916	500	426.8	408.6	141.9	266.7	34.7	272.8	135.8	66.8
921	500	6724.8	2429.2	365	2064.2	15	690.5	1738.7	28.4
922	500	7995	2834.4	151.9	2682.5	5.4	779.4	2055.1	27.5
923	500	10369	3637	449	3188	12.3	1058.6	2578.4	29.1
924	500	10622	3651.4	460	3191.4	12.6	990.6	2660.7	27.1
928	300	1111.9	320	136.3	183.6	42.6	139.2	180.8	43.5
929	300	1694	496.4	169.8	326.6	34.2	214	282.4	43.1
930	300	2591.6	691.3	208.7	482.6	30.2	269.5	421.7	39
917	700	1084.7	945	241.9	703.1	25.6	465.5	479.5	49.3
918	700	1660.6	1295.4	283.2	1012.2	21.9	575.5	719.9	44.4
919	700	2541.2	1693.5	442.2	1251.3	26.1	634.3	1059.1	37.5

The total heat loss increased as the Reynolds number increased, but heat loss as a percentage of total heater power actually decreased as the Reynolds number increased. The increase in heat loss was due to the higher heater temperatures needed to drive the fluid exit temperatures to high values at the higher flow rates. The decrease in heat loss percentage at higher flow-rates was due to the fluid acting as a larger heat sink as the

Reynolds number increased. Figure **5-1** displays the heat loss percentage as a function of Reynolds number. Although the heat losses were significant, the energy added to the fluid was still able to be calculated very accurately due to the decoupling of the heat loss in the energy balance. With accurate axial wall and bulk temperature data, the energy addition to the fluid, as well as the heat transfer parameters could be calculated very accurately at each axial node.

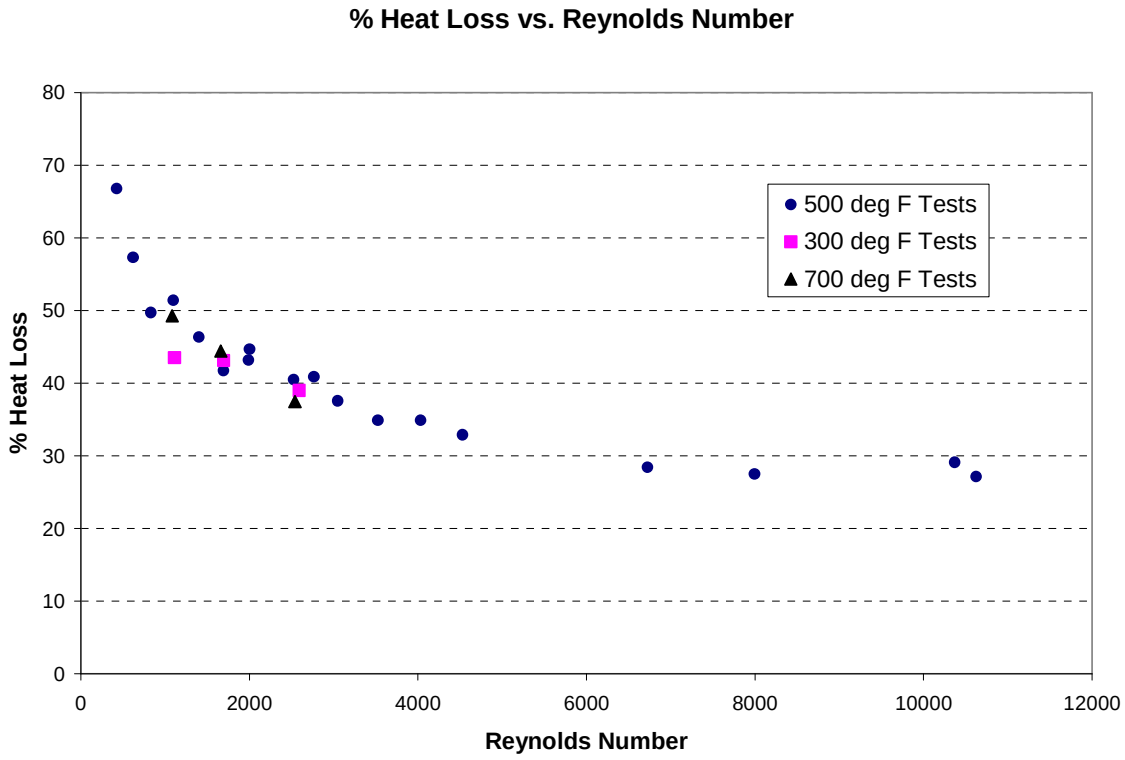

Figure **5-1**: Heat Loss Percentage for Different Reynolds Numbers, Nodal Energy Addition Method

5.3 Friction Factor Results

The laminar fully developed friction factor matched well with the expected 89.5/Re value seen derived from [**7**] as seen in Section **1.2.2**. The data also matched well with friction factor data taken in 1937 by Washington and Marks [**17**] for a 20:1 aspect ratio rectangular channel. The heated data matched well for the laminar and turbulent cases, but only when accounting was made for the acceleration pressure drop and the reference leg density difference.

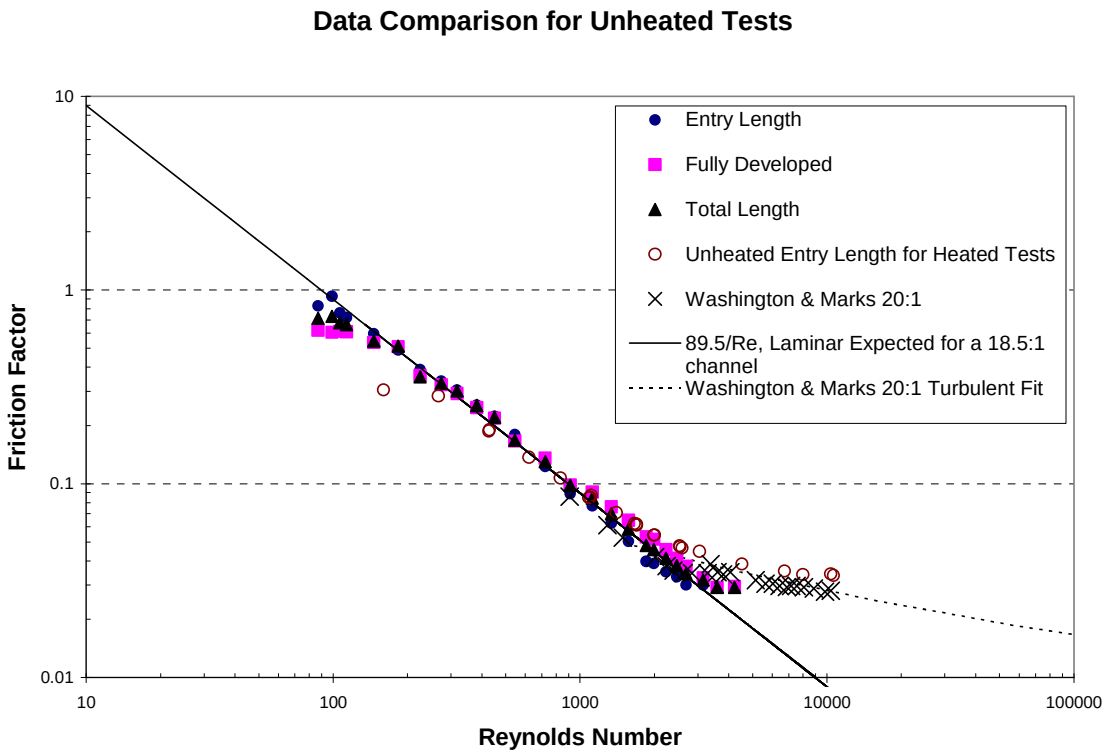

Figure **5-2**: Friction Factor Results for Unheated Tests

Figure **5-2** shows the friction factor data for all the unheated tests, as well as data from the unheated entry length in the heated tests. The data is compared to 20:1 aspect

ratio rectangular geometry friction data taken from Washington and Marks. The laminar data falls directly over the 89.5/Re line which is expected for laminar flow through a rectangular channel of aspect ratio 18.5:1.

Figure **5-3** shows the friction factor results for the heated tests. A differential pressure adjustment was made for pressure drop calculations in the heated length due to the large density change. This discrepancy between the density of the flow and the density in the differential pressure lines caused the gravity head term in the energy balance to be significant for the heated tests.

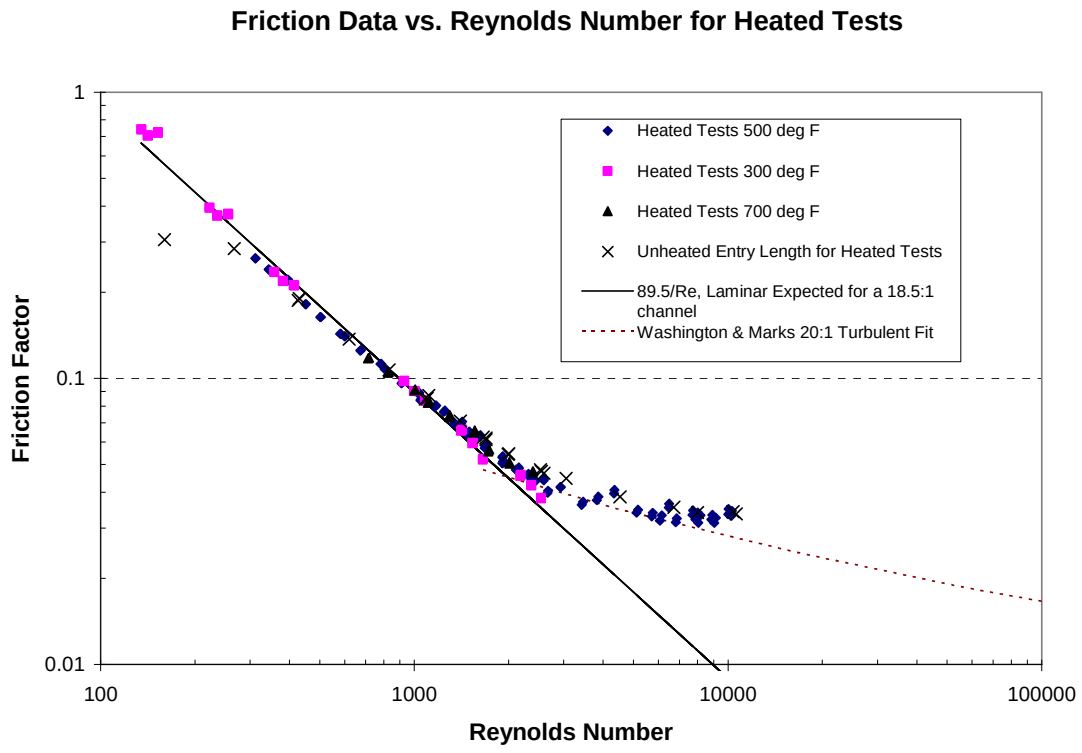

Figure **5-3:** Friction Factor Results for Heated Tests

The gravitational head was subject of much confusion because initially it was assumed negligible. However, for the very low Reynolds number tests, negative pressure drops were observed. This implied that the gravitational head for these cases was actually larger than the frictional head. To account for this gravitational head, Equation **5.4** was used. This pressure head accounts for the density difference between the fluid in the test section at a given height, and the cold reference leg fluid to which the differential pressure lines were connected.

$$\Delta P_{head} = \frac{g}{g_c}(\rho_z - \rho_{cold-line})\Delta Z \qquad (\mathbf{5.4})$$

Using Equation **5.4** for the gravitational head pressure and Equation **4.12** for the acceleration pressure drop; the frictional pressure drop can be attained using Equation **5.5** as,

$$P_{friction} = \Delta P_{measured} - P_{acceleration} + P_{head} \qquad (\mathbf{5.5})$$

A heated, zero flow test was run to confirm that the calculated pressure head matched the measured pressure head. A glass thermometer was attached to the differential pressure cell cold lines so that the cold line density was known. The fluid temperature was then measured at the axial centerline between the high and low pressure signals to attain ρ_z. Table **5-2** displays the results from this hot, zero flow test.

Table **5-2**: Density Change Gravity Head Data for a Zero Flow Test

	deg F		lbm/ft^3		inches water			
Axial Location	**T cold line**	**Fluid T**	**rho cold**	**rho hot**	**delta P measured**	**delta P calculated**	**Difference from Measured**	**% Difference from Measured**
30"	72.2	506	0.06971	0.038369	-0.0053	-0.00602	0.00072	13.7
18"	72.2	449	0.06971	0.040777	-0.00495	-0.00556	0.00061	12.3
6"	72.2	345	0.06971	0.046049	-0.0038	-0.00451	0.00075	18.7

This test proved that the density difference between the cold reference leg fluid and the hot fluid in the test section had a measurable and significant affect on the pressure drop data, especially for tests where the fictional pressure drop was on the order of the gravity head pressure difference.

5.4 Lateral Temperature Profiles

The actual thermocouple probe temperature measurements are presented in this section so that the development of the lateral temperature profiles can be observed. Laminar and turbulent cases are presented in order to bound the test matrix. The laminar run 916 and the turbulent run 924 are presented below.

Figure **5-4** gives the temperature profiles for turbulent run 924. These temperature profiles were plotted at five axial locations which cover a majority of the heated length.

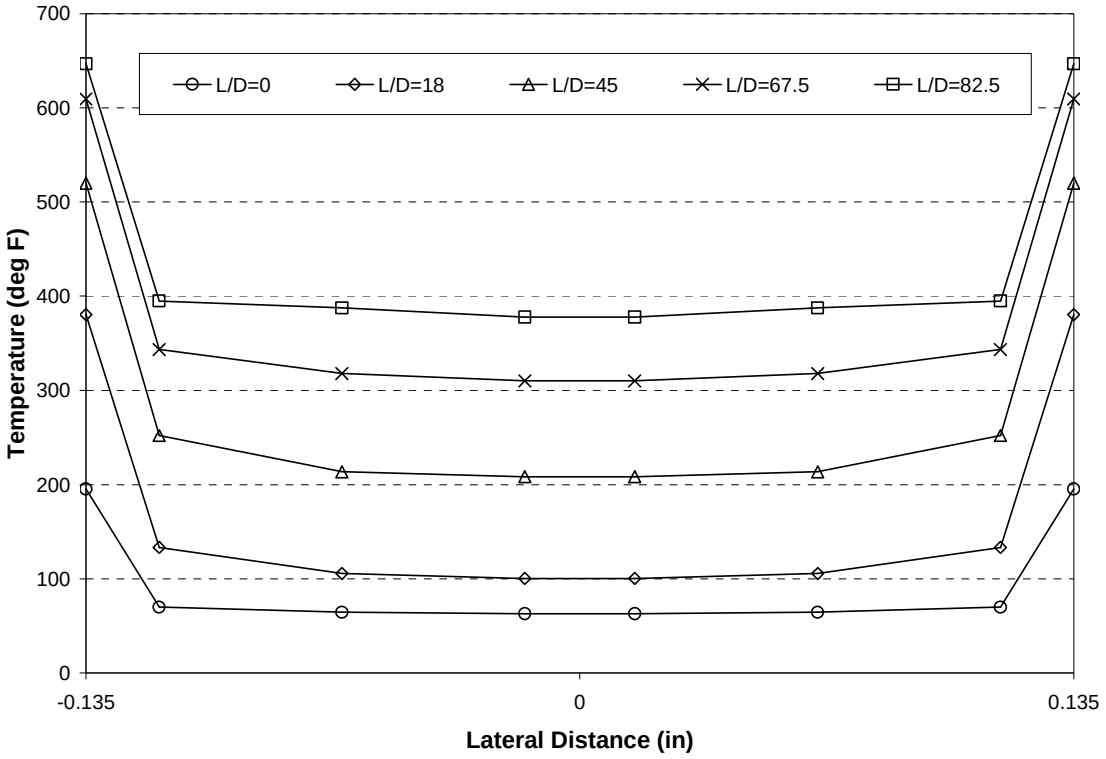

Figure **5-4**: Run 924, Turbulent temperature profiles at selected axial locations

Figure **5-5** gives the temperature profiles for laminar run 916. These temperature profiles were also plotted at the same five axial locations as the figure above. The lines drawn through the true data points are linear interpolations which help display the development of the temperature profiles axially.

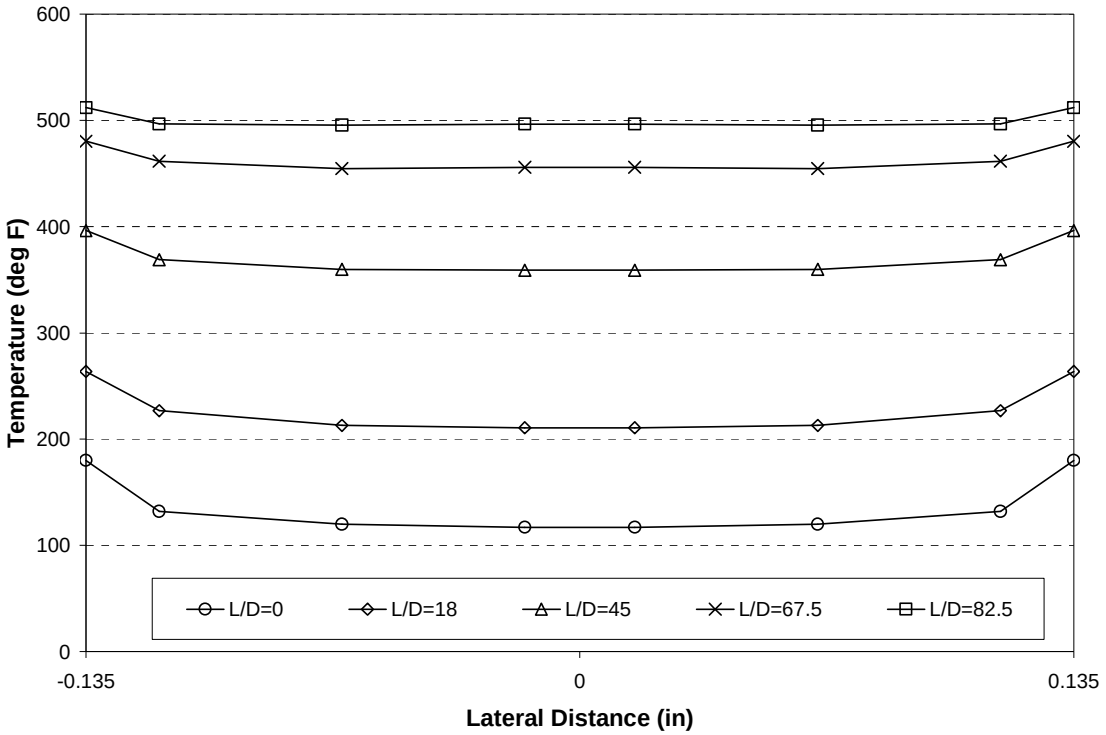

Figure **5-5**: Run 916, Laminar temperature profiles at selected axial locations

5.5 Laminar Heat Transfer Results

Laminar heat transfer data were taken down to a Reynolds number of approximately 100. The axial heat transfer development, as well as the fully developed Nusselt number was calculated for each test run. The data shows correlation to other data

sets for laminar heat transfer. The possibility of mixed convection was also analyzed showing that the buoyancy effects were negligible over the entire test range.

5.5.1 Laminar Axial Development

The entry length for constant property laminar flow heat transfer is given by Burmeister [**14**] as Equation **5.6**.

$$\frac{L_{e,laminar}}{D} \cong 0.05\,\mathrm{Re} \qquad (\mathbf{5.6})$$

This would mean in the lower range of Reynolds numbers, the entry length is extremely short relative to the axial node length of 2 inches which was used in the experiment. The axial development may also have been affected by the non-uniformity of the axial heat flux caused by axial heat losses at the entrance and exit of the heated length.

The Nusselt numbers were compared to the laminar fully developed Nusselt number for constant fluid properties (Nu_{cp}). The laminar Nu_{cp} for a rectangular channel of aspect ratio 18.5 is given as 7.394 from the correlation in Section **1.2.2** derived from data in the Heat Transfer Handbook [**8**].

Figure **5-6** shows the laminar axial development of the Nusselt number as a function of length to diameter ratio for 3 tests with an exit temperature of 500°F. The Data from the 1100 and 2000 Reynolds number tests agrees well with the expected laminar Nu_{cp} value of 7.394, while the data with an inlet Reynolds number of 400 is above the expected value. It is also interesting to note the lack of a heat transfer entry length in the data. This may be due to the short ~2 inch expected entry length described above. It also may have been due to the axial non uniformity of the heat flux, especially in the entrance length due to axial heat losses, as well as variable fluid properties.

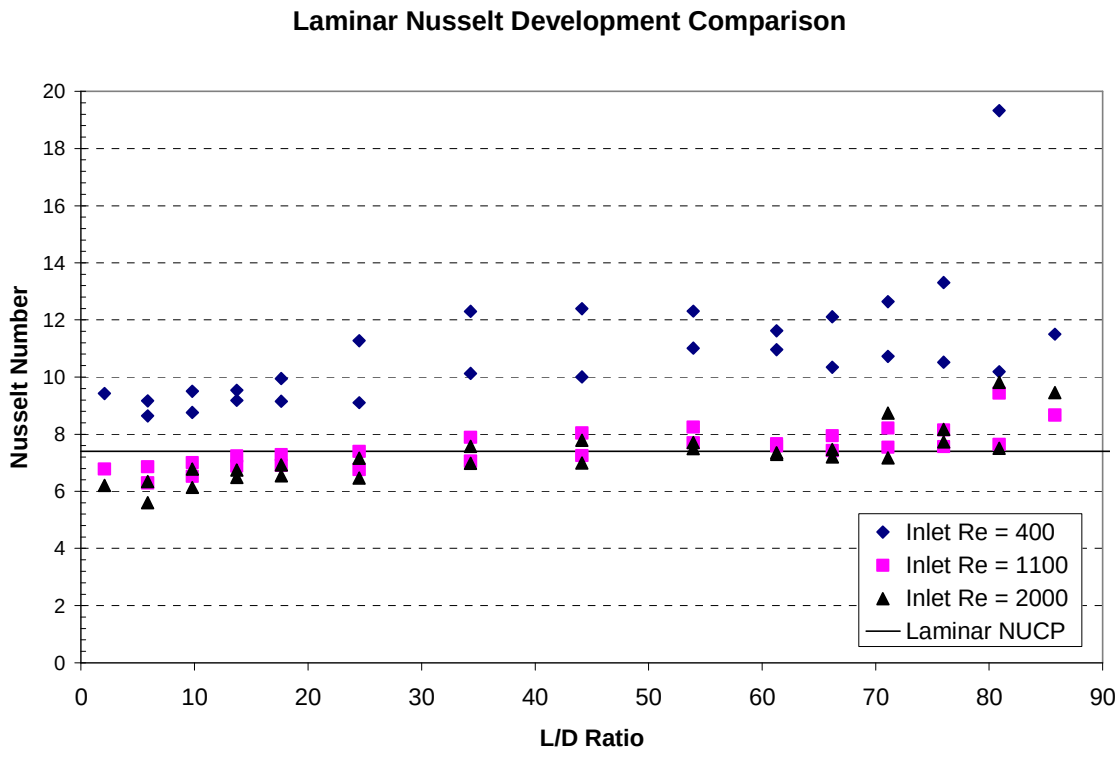

Figure **5-6**: Laminar Nusselt Development for an Exit Temperature of 500°F

Figure **5-7** shows the laminar Nusselt Development for an inlet Reynolds number of 1700 and 3 separate exit temperatures.

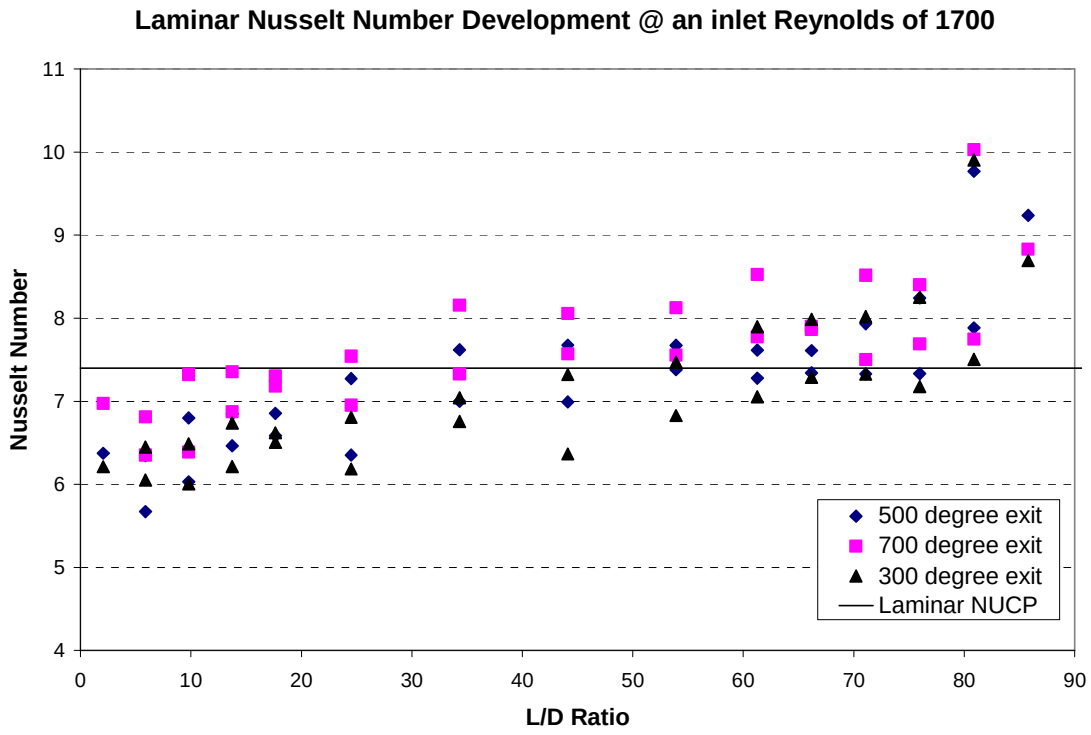

Figure **5-7**: Laminar Nusselt Development for an inlet Reynolds of 1700

Observing both Figure **5-6** and Figure **5-7,** there is an unexpected increase in the Nusselt number for the inlet Reynolds case of 400 in Figure **5-6** this was first thought to be attributed to mixed convection affects, however later in this chapter, this hypothesis was proven to be incorrect based on Grashof number calculations. The discrepancy is likely due to the bulk temperature difference approaching zero for the low Reynolds number cases, especially towards the top of the test section where axial heat losses depressed the wall temperatures with respect to the bulk temperature.

Figure **5-8** gives a comparison between the laminar data seen in Swearingen [**5**], and laminar data for tests 911, 912, and 913 from the current experiments. Table **5-3** gives the conditions that the Swearingen and current experiments were taken at for comparison.

The x^+ value in all the Swearingen plots represents a dimensionless variable that gets larger as the flow becomes more fully developed and toward the end of the test section. This x^+ value is also influenced by the Reynolds number and Pr number in the denominator. A larger Reynolds or Pr number would decrease the x^+ value relative to the actual x/D ratio.

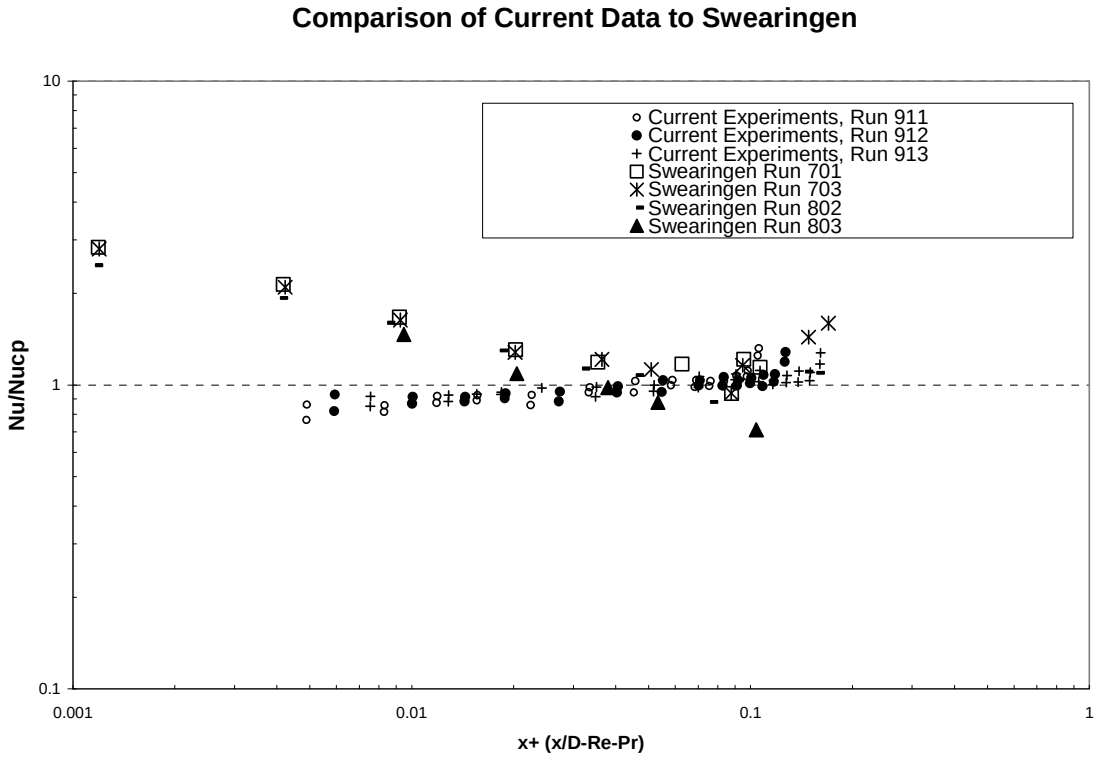

Figure **5-8**: Laminar Nusselt Comparison to Swearingen Data, 500°F Fluid Exit Temperatures

Table **5-3**: Conditions for Comparison with Swearingen Data

Swearingen	**Inlet Re**	**Exit T (℉)**
701	1470	226
703	1442	877
802	1477	706
803	1458	990
Current		
911	1700	500
912	1400	500
913	1100	500
917	1100	700
918	1700	700
928	1100	300
929	1700	300

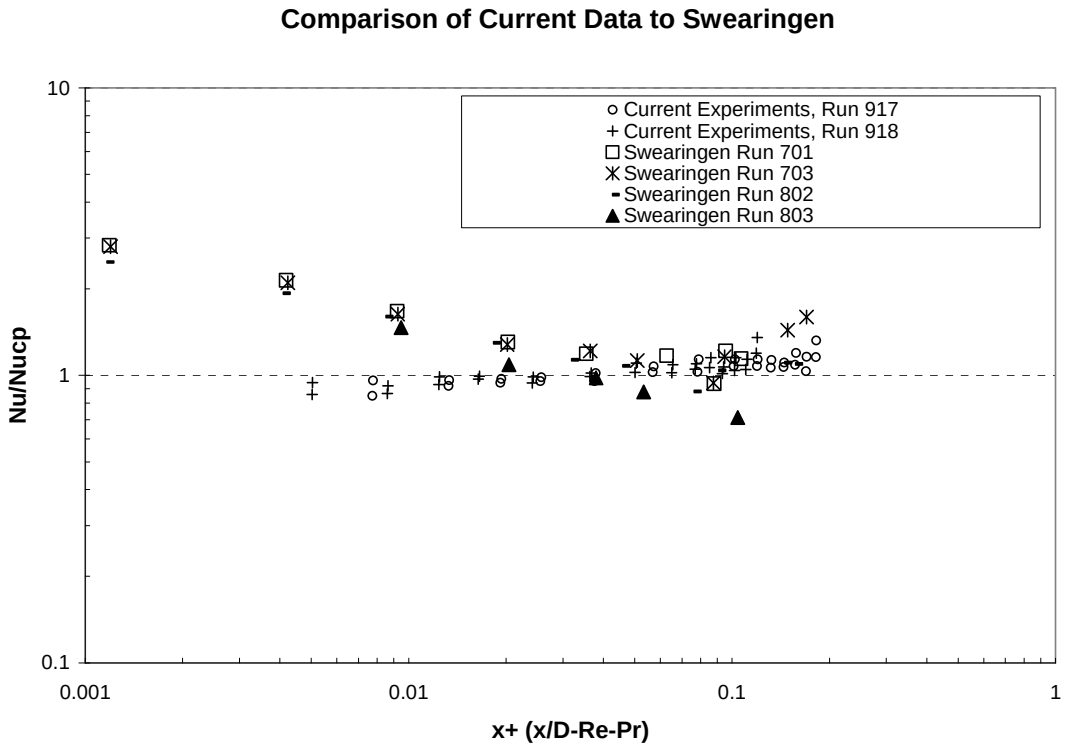

Figure **5-9**: Laminar Nusselt Comparison to Swearingen Data, 700°F Fluid Exit Temperatures

The Nusselt number data had to be normalized to the laminar Nu_{cp} for comparisons between the two geometries. Figure **5-9** gives the same Swearingen data, but compared with runs 917 and 918 which were run at higher exit temperatures. The discrepancy in the data is likely due to the depression of the Nusselt number in the entry length of the heated portion of the test section.

Figure **5-10** gives another comparison to the Swearingen data but with tests 928 and 929 which were run at lower exit temperatures. It is interesting that the Swearingen data has conflicting trends at larger values of x+. He explains this behavior in his uncertainty section as mainly due to the diminishing of the wall to bulk temperature difference, especially at low Reynolds numbers at axial locations in the fully developed regions.

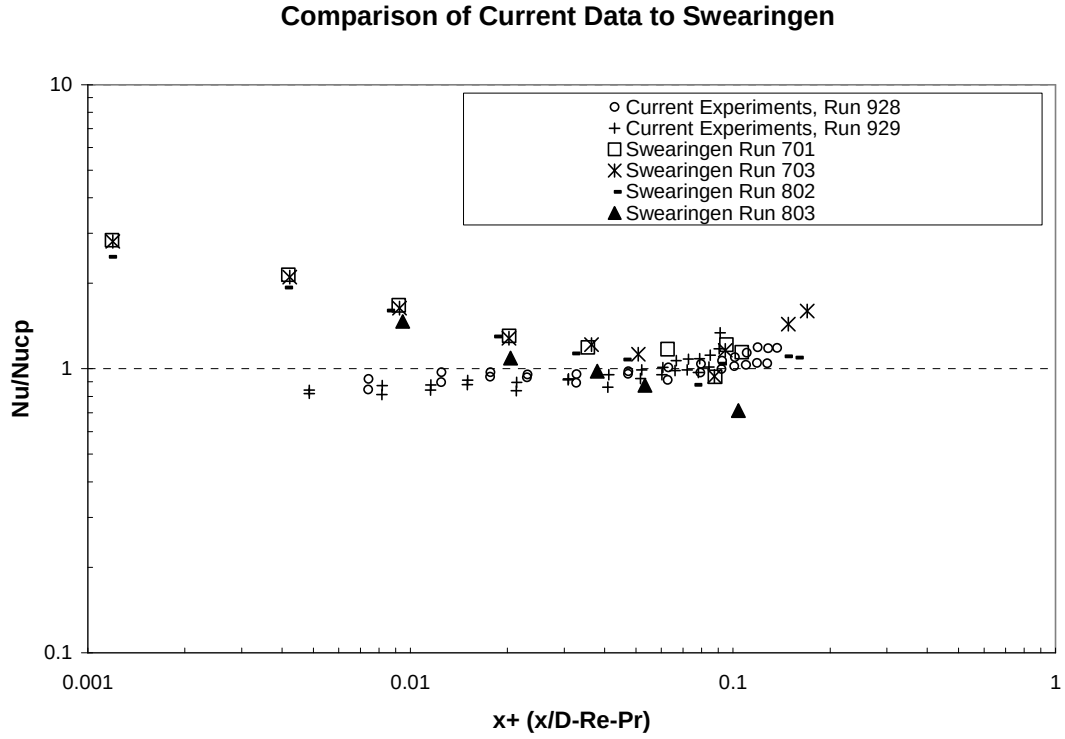

Figure **5-10**: Laminar Nusselt Comparison to Swearingen Data, 300°F Fluid Exit Temperatures

Figure **5-11** shows the axial Reynolds number development for 3 tests with an inlet Reynolds number of 1700. As expected, the Reynolds number is more affected in the higher heat flux cases, due to increased fluid property variation. Two data points are marked for each L/D location because the bulk fluid temperature profile was taken at two different lateral locations for each axial step.

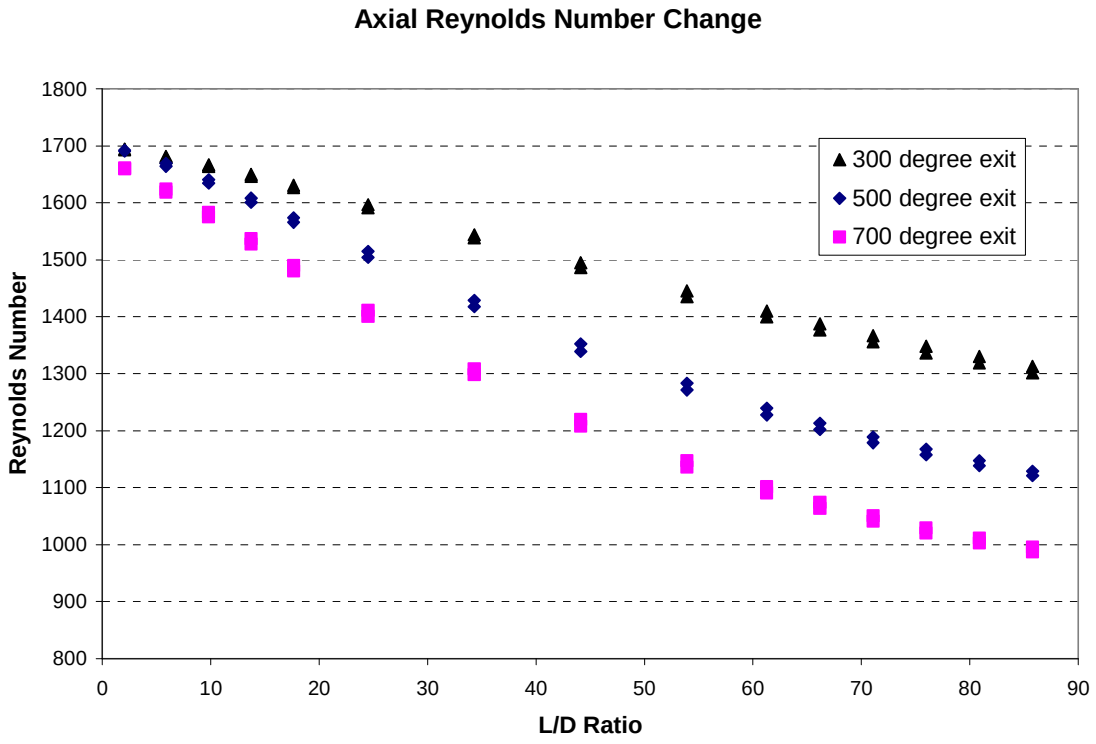

Figure **5-11**: Axial Reynolds Number Variation

Figure **5-12** and Figure **5-13** depict the axial development of the differential bulk gradient. This parameter is helpful in determining the axial location where a constant wall heat flux condition exists, i.e. when the bulk temperature gradient is zero.

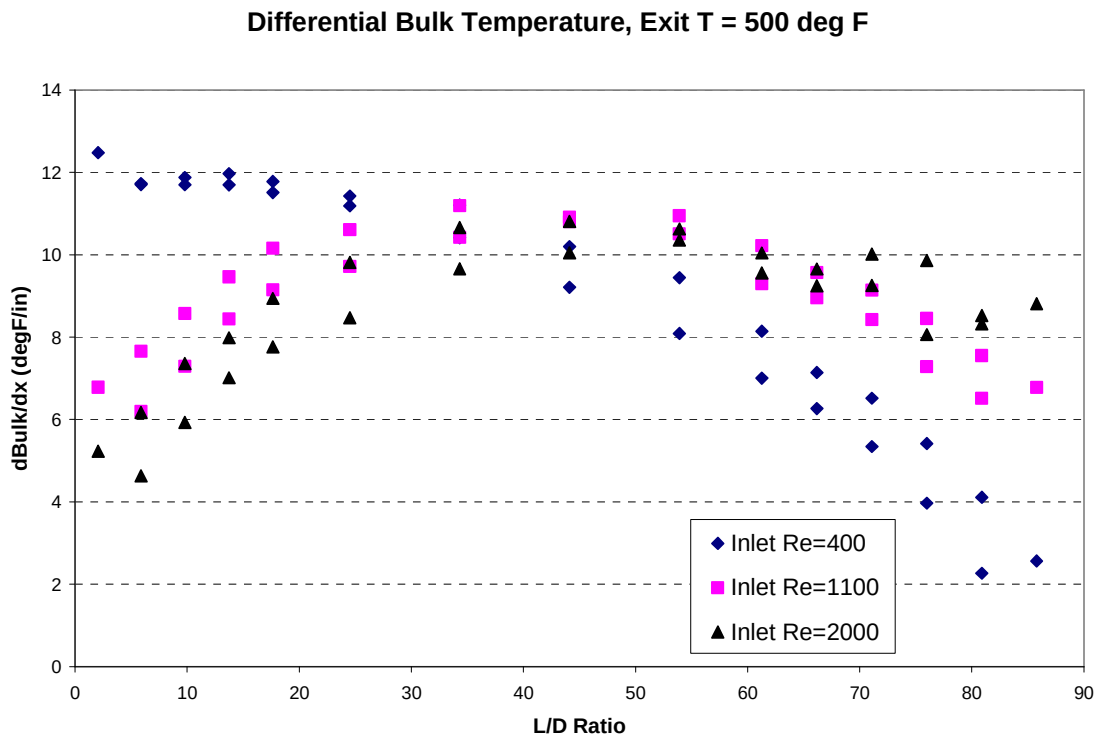

Figure **5-12**: Axial change in the bulk temperature, for 3 laminar cases

An interesting behavior to note is the Reynolds number dependence on the axial position of constant wall heat flux. The higher the Reynolds number, the further the constant wall heat flux condition moved up the test section. The decrease in dBulk/dx at the entrance and exit to the heated test section can only be explained by axial heat losses. However, for the most part, the heat flux was nearly constant for L/D locations between 30-60, which is also the locations where the Nusselt numbers were assumed fully developed. In

the Kaizer [**1**] thesis, the fully developed region was much shorter due to a shorter test section and higher heat losses.

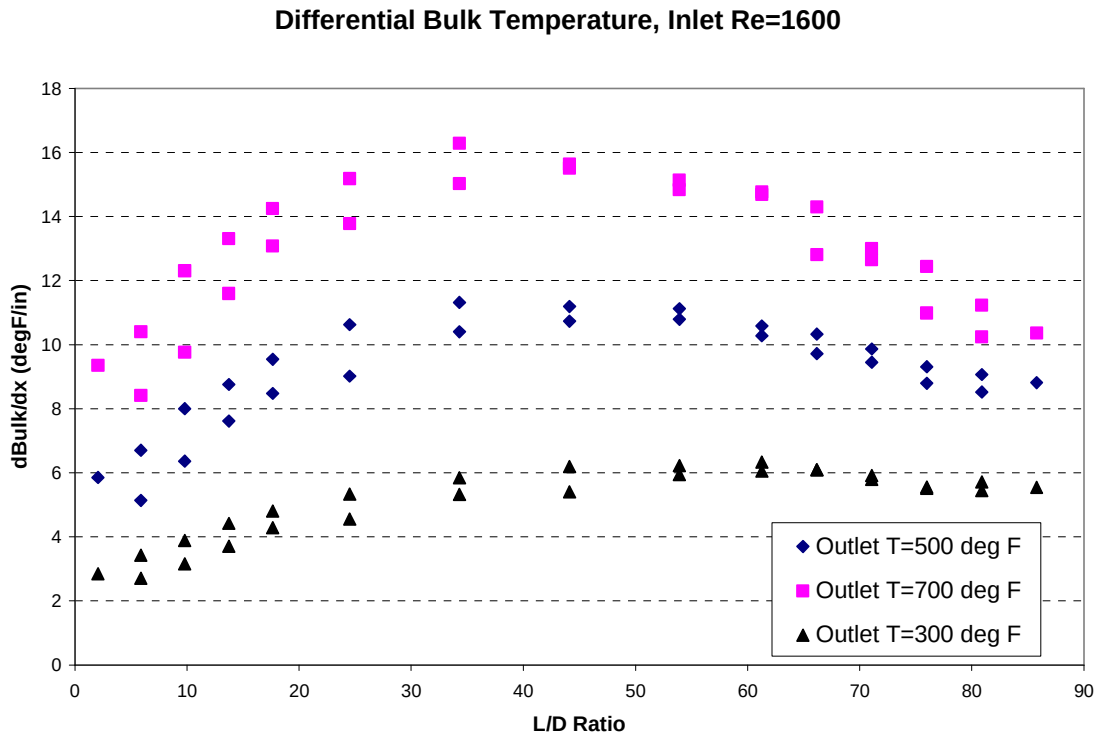

Figure **5-13**: Temperature Dependence on Axial change in the bulk temperature, for laminar case.

5.5.2 Fully Developed Laminar Results

The fully developed point for the Nusselt number in the laminar flow regime was difficult to pinpoint. This was due to the axial property variation of the fluid, the possibility of mixed convection, as well as the non-uniformity of the heat flux axially. Therefore, fully developed data points were chosen considering both the location of the

most constant wall heat flux and the consistency of the Nusselt number axially. This point was usually between 30-60 L/D's for the laminar cases.

Figure **5-14** shows the laminar fully developed Nusselt Data compared to the laminar fully developed constant property Nusselt number (Nu_{cp}). This fully developed value of 7.397 is for a rectangular channel with an aspect ratio of 18.5 as discussed in Chapter **1**.

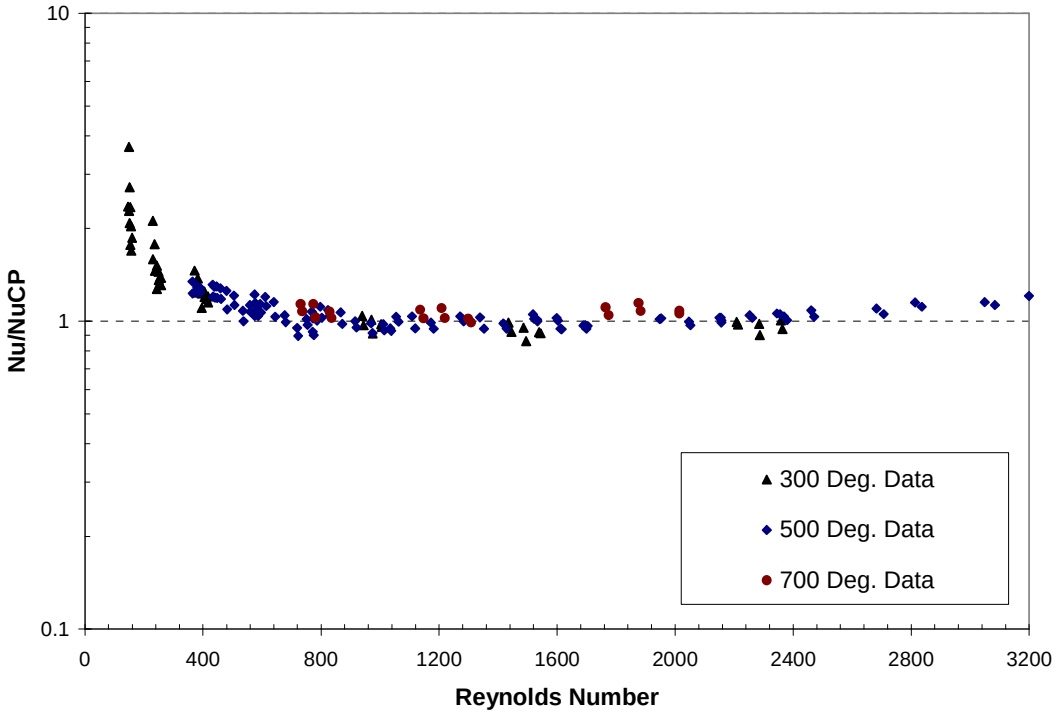

Figure **5-14**: Fully Developed Laminar Flow Results

The fully developed data for the rectangular tests were chosen at the 3 or 4 most fully developed axial locations for each test. The data matched well with the expected laminar Nu_{cp} value, although the trend as the Reynolds number decreased was opposite that was seen in the Kaizer [**1**], Wibulswas [**18**] , and Kreith [**11**] data at low Reynolds

numbers. In the present data, the Nusselt number ratio increased above unity as the Reynolds number decreased to very low values.

The trend with respect to fluid exit temperature was unexpected but very slight. The higher exit temperature cases resulted in a larger laminar fully developed Nusselt number than the medium and low temperature cases. It would be expected that the laminar fully developed Nusselt number would decrease with increasing heat flux because of the larger impact of fluid property variation. However, for the 18.5:1 rectangular channel data, this trend was not observed.

As seen in Figure **5-14**, as the Reynolds number decreases the ratio of Nu/Nucp trends above unity. The cause for this behavior is believed to be the diminishing difference between the wall temperature and the bulk fluid temperature. The uncertainty analysis performed in Appendix **F.3** addresses this temperature difference and its impact on the calculated heat transfer coefficient and Nusselt number. Using the uncertainty analysis, data points in which the watt-to-bulk temperature difference is within the uncertainty at a 95^{th} percentile level have been eliminated from the data shown in Figure **5-14**. Therefore, unless there are other uncertainties, which can not be quantified such as variable property effects or continuing developing flow behavior, the data trends shown in Figure **5-14** should be regarded as “real”.

Figure **5-15** gives the laminar fully developed results compared to the fully developed results from the 0.5" diameter tube tests by Kaizer [**1**]. Examining Kaizer's [**1**] data indicates that in his experiments, the heat transfer and flow are not as fully developed as in the present tests since his test section was not as long, there were excessive axial heat losses at the top of the test section, and the fluid properties were changing. Therefore, it is not clear if Kaizer's observed Nusselt number represents the correct trend.

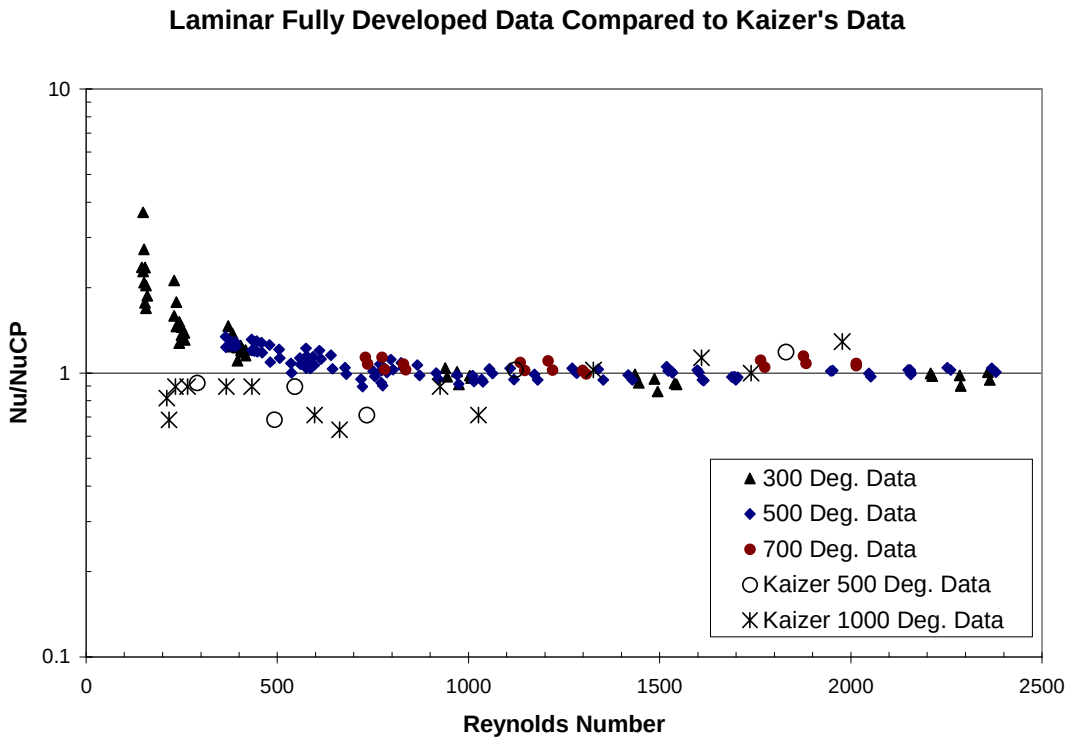

Figure **5-15**: Fully Developed Laminar Flow Results Compared to Kaizer [**1**]

Figure **5-16** gives the laminar fully developed data compared with Davenport's [**2**] tube data. His laminar Nusselt data also shows very little dependence on the Reynolds number. Davenport also reported significant heat losses as the Reynolds number decreased. In his experiment, he attempted to characterize the heat losses with adiabatic tests and then would subtract the heat losses from the total power to the test section. Both the current experiments and Kaizer's [**1**] experiments indicated that the heat losses are non-linear and are much more pronounced at the top of the test section, where the temperatures are the highest, and where the heat transfer is becoming fully developed. The heat loss problem becomes more severe as the Reynolds number decreases.

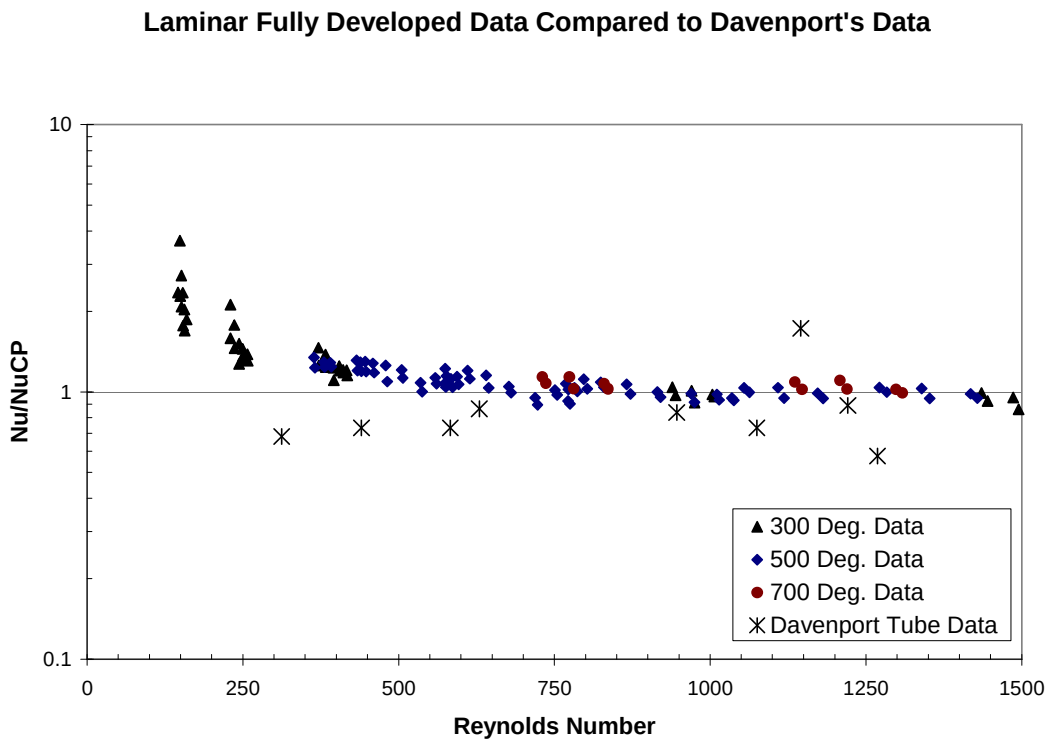

Figure **5-16**: Fully Developed Laminar Flow Results Compared to Davenport data

Figure **5-17** and Figure **5-18** give the laminar fully developed data compared to Wibulswas [**18**] and Kreith [**11**] respectively. These two comparisons show a dependence on the Laminar fully developed Nusselt number with respect to Reynolds number. It is difficult to comment on the Kreith results since there are no details on his tests, the axial heat losses, whether fully developed flow was achieved and how the heat transfer was calculated from the experiments. Therefore, it is not clear what confidence can be placed in this data relative to the other experiments reported here.

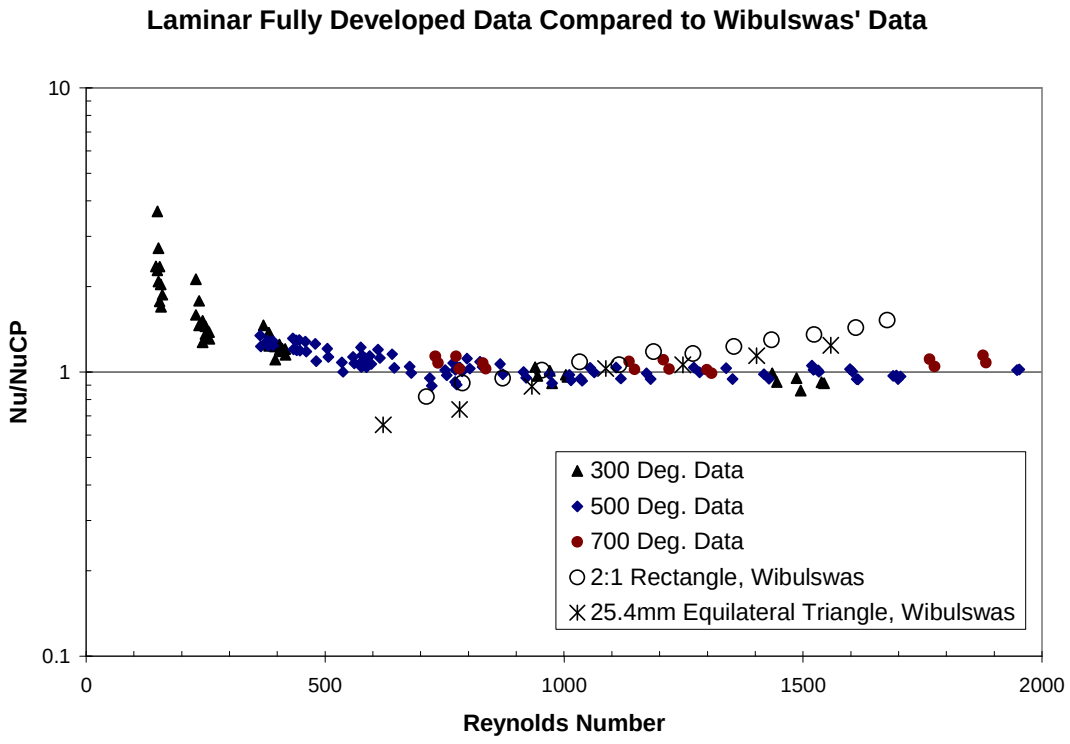

Figure **5-17**: Fully Developed Laminar Flow Results compared to Wibulswas data

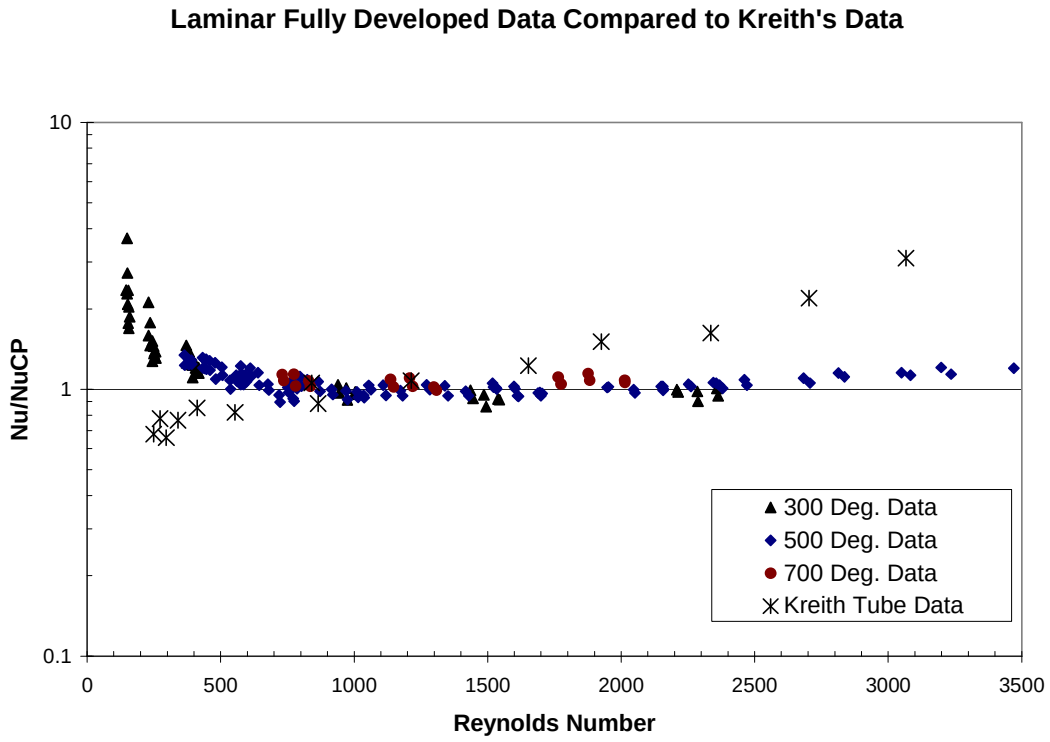

Figure **5-18**: Fully Developed Laminar Flow Results Compared to Kreith data

5.5.3 Buoyancy Considerations

It was suspected that buoyant forces may be disrupting the forced convection flow in the lower Reynolds number cases. To determine the amount of buoyancy in the flow, a modified Grashof number was used which relies on the heat flux to play the role of the temperature difference, seen in Equation **5.6** as,

$$Gr^* = \frac{\beta g \rho^2 D_h^4 q_w}{\mu^2 k} \qquad \textbf{5.6}$$

The ratio of Gr^*/Re^2 as seen in Chapter 10 of Burmeister [**14**] determines the importance of natural and forced convection in a given flow. If the ratio is less than 1.0, then forced convection is dominant, and if the ratio is greater than 1.0, then natural convection is dominant.

The relationship between forced and natural convection has also been described by Metais and Eckert as adapted by Chin [**12**] in the form of a flow regime map which relates the modified Grashof number to the forced convection Reynolds number. A replica of this flow regime map has been constructed with the data from several of the current experiments, and can be seen in Figure **5-19**.

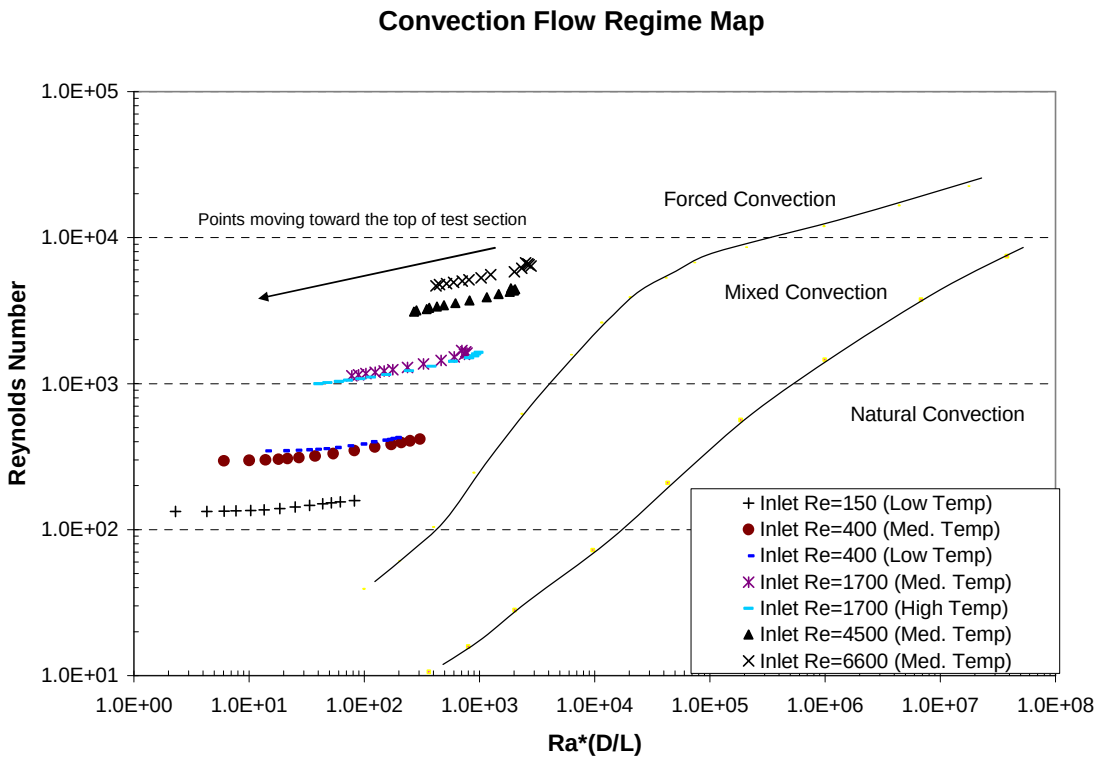

Figure **5-19**: Adaptation of the Metais and Eckert flow regime map with selected tests

The data from the map shows that mixed convection was not large enough to be important for any of the cases. Especially important is that the significance of mixed convection diminished as the fluid became fully thermally developed. This is shown by the arrow in Figure **5-19** which gives the direction of data points moving toward the top of the test section. The non significance of mixed convection was further demonstrated when calculating Gr^*/Re^2 for the suspect lower Reynolds number cases. A plot of this Grashof ratio as a function of Reynolds number for the selected low Reynolds number tests is given in Figure **5-20** .

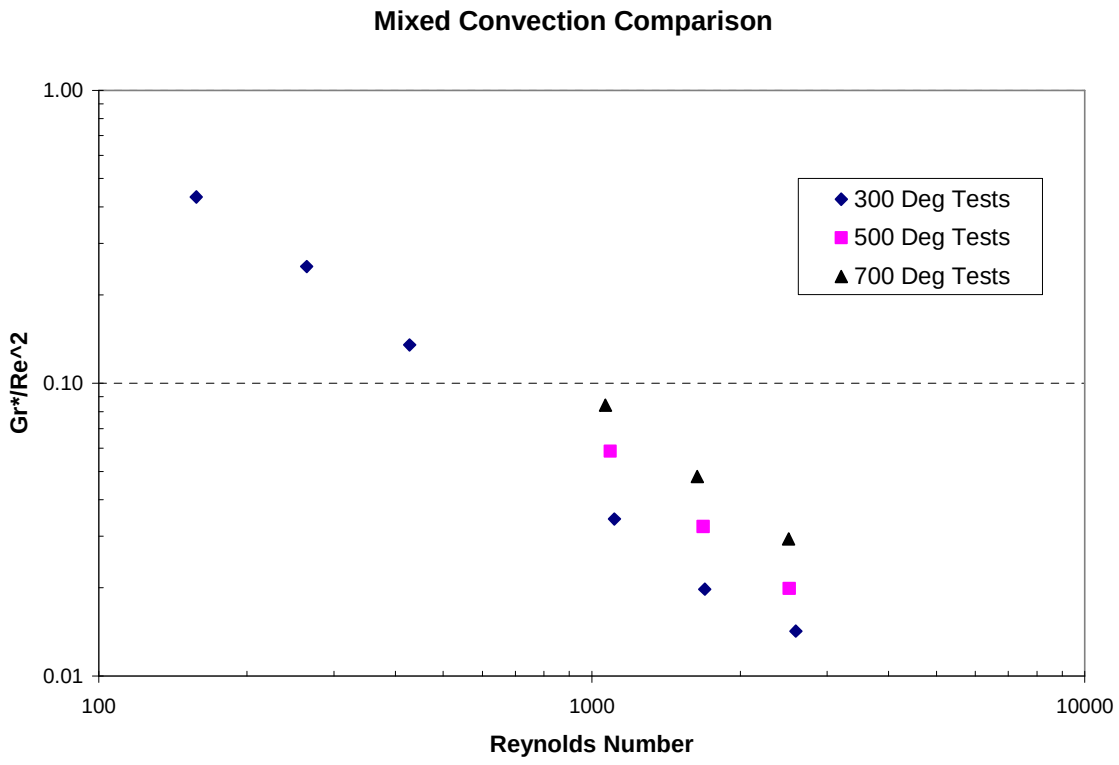

Figure **5-20**: Comparison of the Gr^*/Re^2 Ratio for low Reynolds number tests for data points at the entrance to the heated length

The data points seen in Figure **5-20** are only taken from the first axial node in the heated entrance length which always provided the largest Grashof ratio. This implies that the largest buoyant were found at the entrance to the heated length, and always diminished as the flow became more fully thermally developed. These Grashof number comparisons indicate that the buoyancy is not important and there is no mixed convection for the suspect runs.

5.6 Turbulent Heat Transfer Results

Turbulent heat transfer data were taken up to a Reynolds number of about 10,000. These tests were run in order to compare the current data to the many turbulent heat transfer data and correlations that exist for internal flow. The channel geometry seemed to have little effect on the fully turbulent data with respect to Nusselt number. The transition to turbulence happened close to a Reynolds number of 2300 as expected, which was also seen in the turbulent friction factor data earlier in the chapter. This section gives the turbulent heat transfer data for the current experiments and also compares it to other experimental turbulent heat transfer data.

5.6.1 Turbulent Axial Development

Figure **5-21** depicts the axial development of the Nusselt number as a function of L/D ratio. The expected axial development of the heat transfer was however hindered by the not quite constant heat flux into the fluid, especially in the first 40 L/D's.

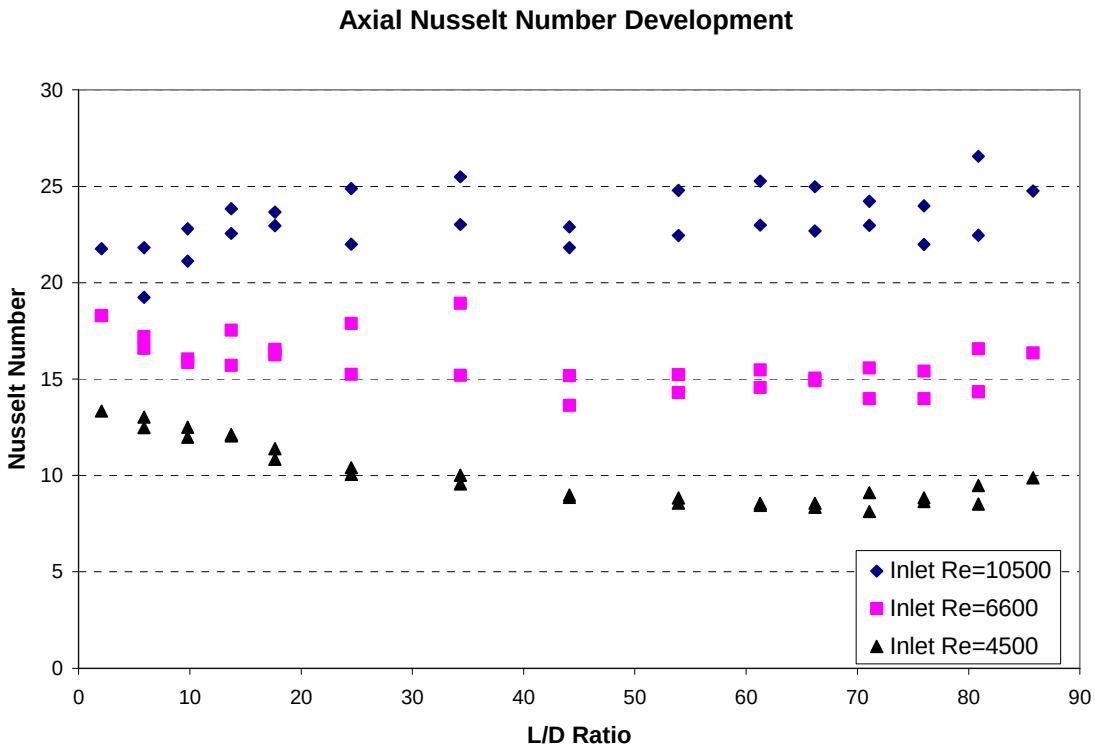

Figure **5-21**: Axial Nusselt Number Development for 3 Turbulent Cases

The heat flux, which is dependent on dT_b/dx, can be seen in Figure **5-22** which gives this relationship with respect to x. After an L/D of approximately 40, the heat flux and Nusselt numbers are nearly constant, therefore the Nusselt numbers can be assumed fully developed once past this point. Again, there are two data points per each L/D location because two lateral bulk temperature profiles were taken at each axial step.

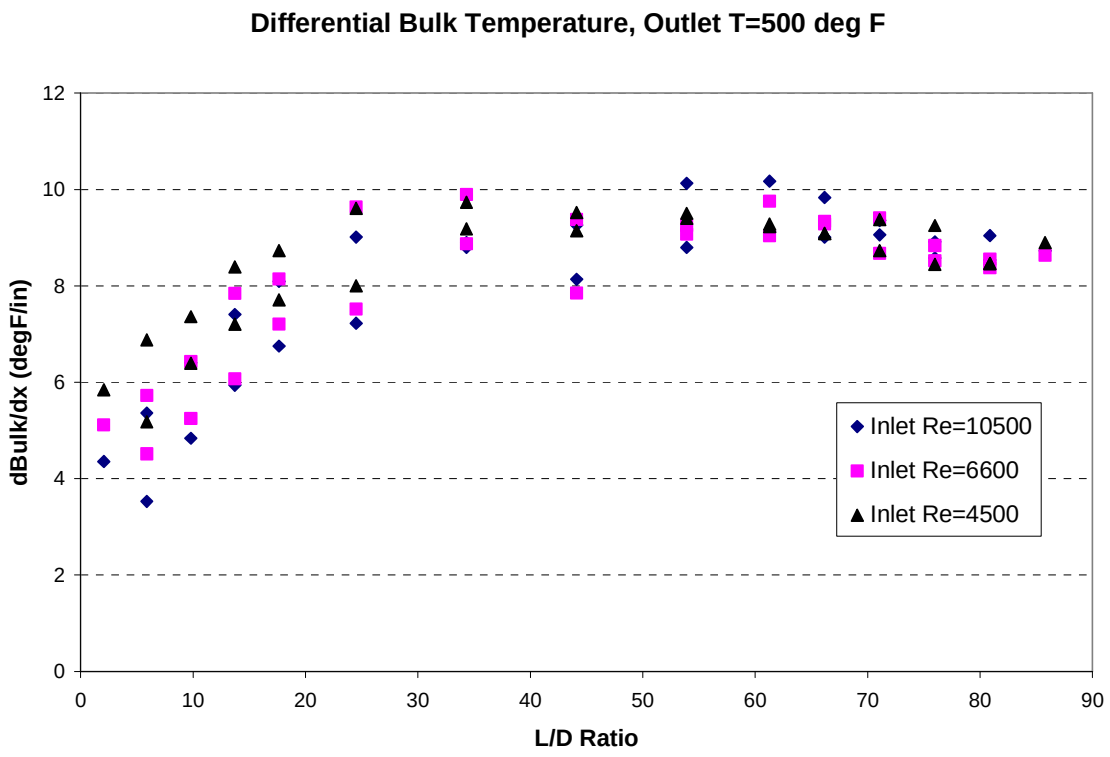

Figure **5-22**: Axial change in the bulk temperature, for 3 turbulent cases

5.6.2 Turbulent Fully Developed Results

The fully developed turbulent data is given in Figure **5-23** and consists of data taken between an L/D of 40 to 80. As Figure **5-23** indicates, the Dittus-Boelter correlation clearly over estimates the heat transfer for the current channel geometry.

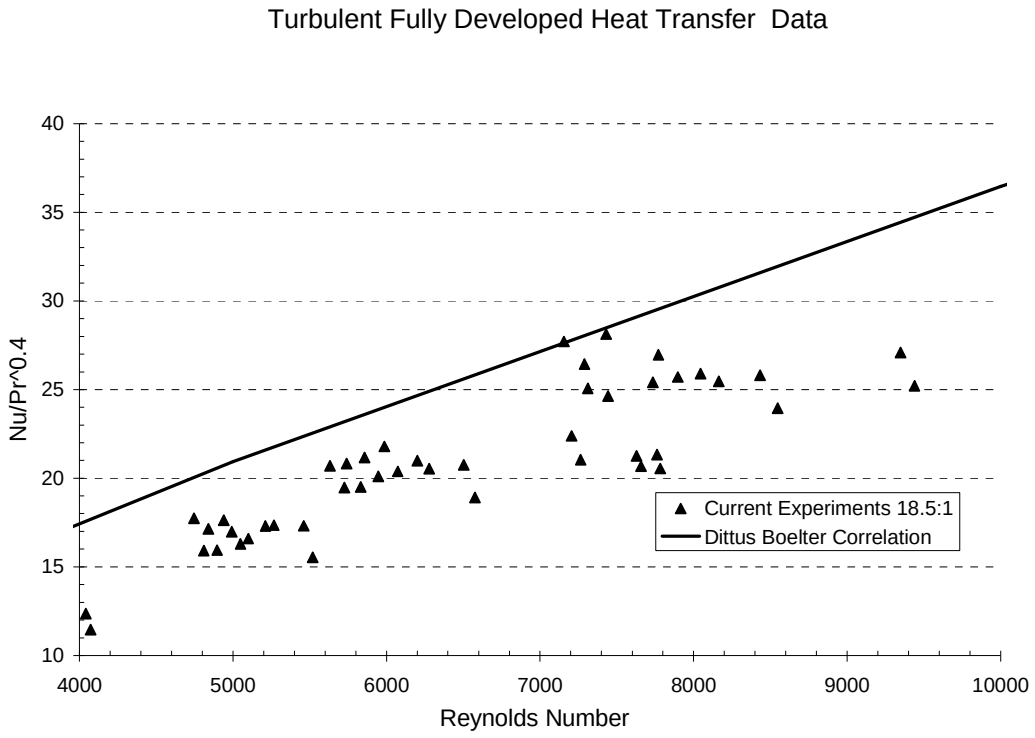

Figure **5-23**: Turbulent Fully Developed Heat Transfer Data

Figure **5-24** shows the current data compared to turbulent fully developed tube heat transfer data from Forslund and Rohsenhow [**19**] along with the turbulent heat transfer tube data taken at The Pennsylvania State University by Kaizer [**1**]. As Figure **5-24** indicates, there is good comparison between the present channel data and the tube data by Kaizer for the turbulent region. The present data also agrees with the Forslund-Rohsenow data trends, although the Forshund-Rohsenow data is at higher Reynolds numbers. All the experimental data lie below the predictions from the Dittus-Boelter correlation.

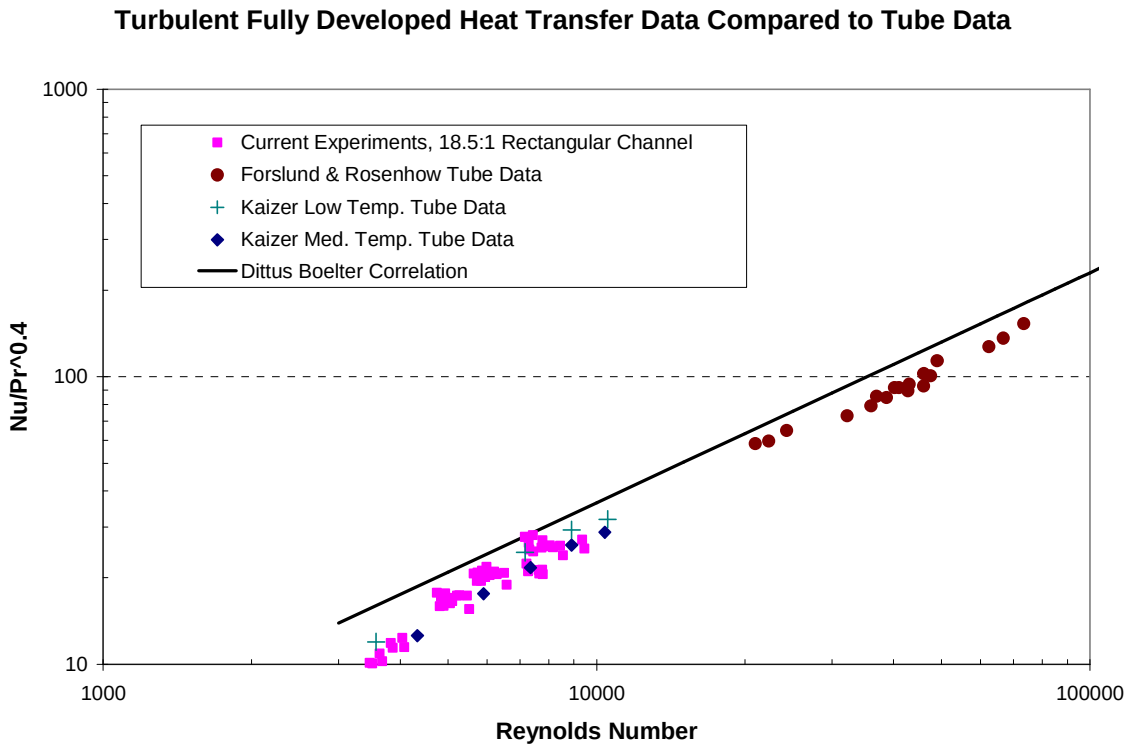

Figure **5-24**: Turbulent Fully Developed Heat Transfer Data Compared with Tube Data

Figure **5-25** gives the turbulent fully developed heat transfer data compared with rectangular data from Novotny [**16**], Sparrow [**15**], and Chin et al.[**12**].

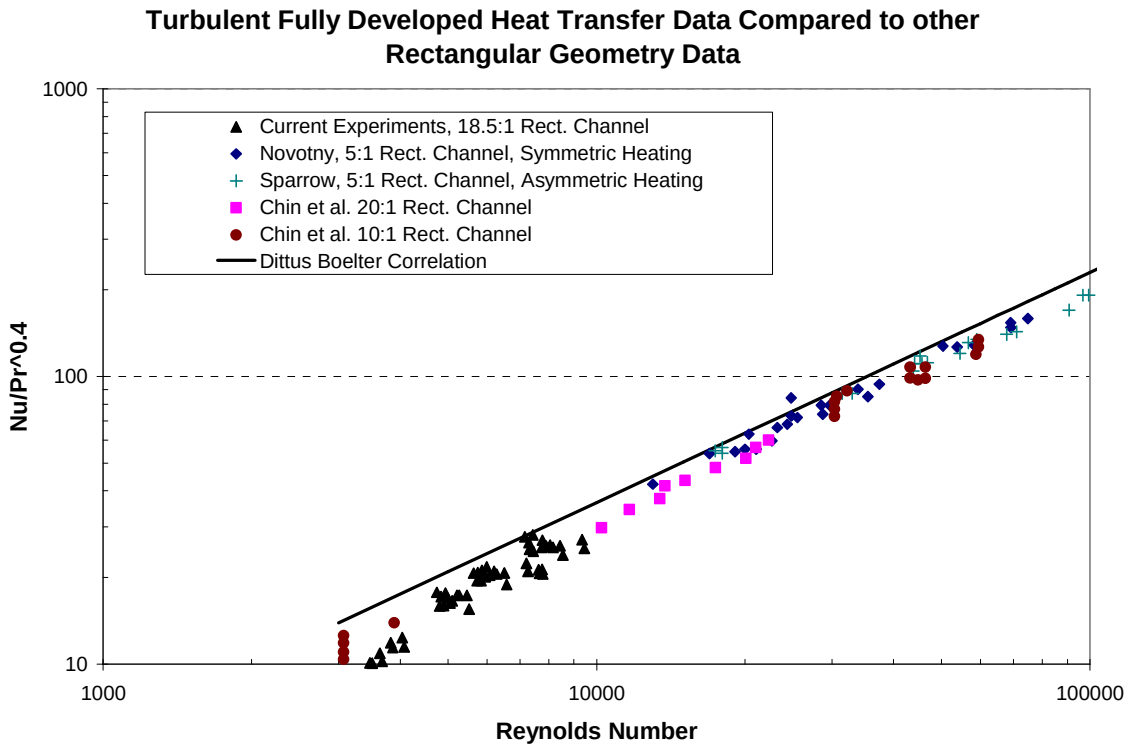

Figure **5-25**: Turbulent Fully Developed Heat Transfer Data Compared with other Rectangular Data

The current data is bracketed by the Chin data for a two different sizes of rectangular channels. Chin's data for a 20:1 channel agrees very well with a trend line from the present 18.5:1 channel as well as with Novotny's 5:1 channel data. All these data are for symmetric heating. The Sparrow data for an asymmetric heating on a 5:1 channel does show additional scatter by generally agrees with the trend of all the channel data. The data-to-data comparisons show in this figure does indicate that the experimental method and data analysis used in the present channel experiments provides results which are

comparable to other investigators. Again, all the data from the channel experiments lie below the Dittus-Boelter predictions.

Figure **5-26** gives the turbulent fully developed heat transfer data compared with all the compiled turbulent fully developed data. From, Figure **5-26** it can be seen that all the data are bracketed by the Dittus-Boelter Correlation with and uncertainty bracket of negative 25% for the turbulent region.

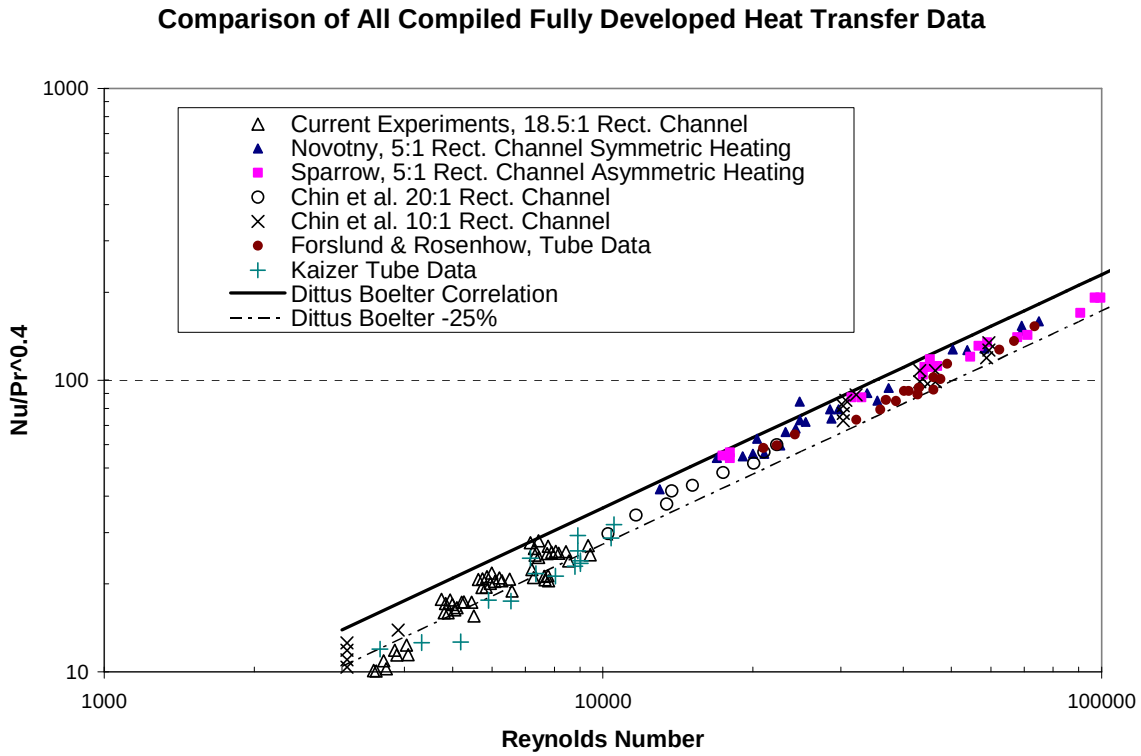

Figure **5-26**: Turbulent Fully Developed Heat Transfer Data Compared with All Compiled Data

5.7 Comparison with the Gnielinksi Correlation

The Gnielinski correlation is used for constant heat flux fully developed turbulent and transition flow heat transfer situations for tubes. The correlation is based on Re, Pr, and D/L ratio as given below in Equation **5.7** and was taken from [**20**].

$$\mathrm{Nu}_0 = \frac{\frac{\xi}{8}(\mathrm{Re}-1000)\,\mathrm{Pr}}{1+12.7\sqrt{\frac{\xi}{8}}\left(\mathrm{Pr}^{2/3}-1\right)}\left[1+\left(\frac{D}{L}\right)^{2/3}\right] \qquad (\mathbf{5.7})$$

where $\xi = \frac{1}{(1.821\log \mathrm{Re}-1.64)^2}$

To evaluate this equation, the L/D was set to 45 and the Prandtl number was held constant at 0.72. The results of this comparison are given in Figure **5-27**, and indicate that the Gnielinski correlation does agree better with the tube data by Kaizber, but over-predicts the heat transfer for the present channel data. This is also consistent with the over-prediction trend observed with the Dittus-Boelter correlation.

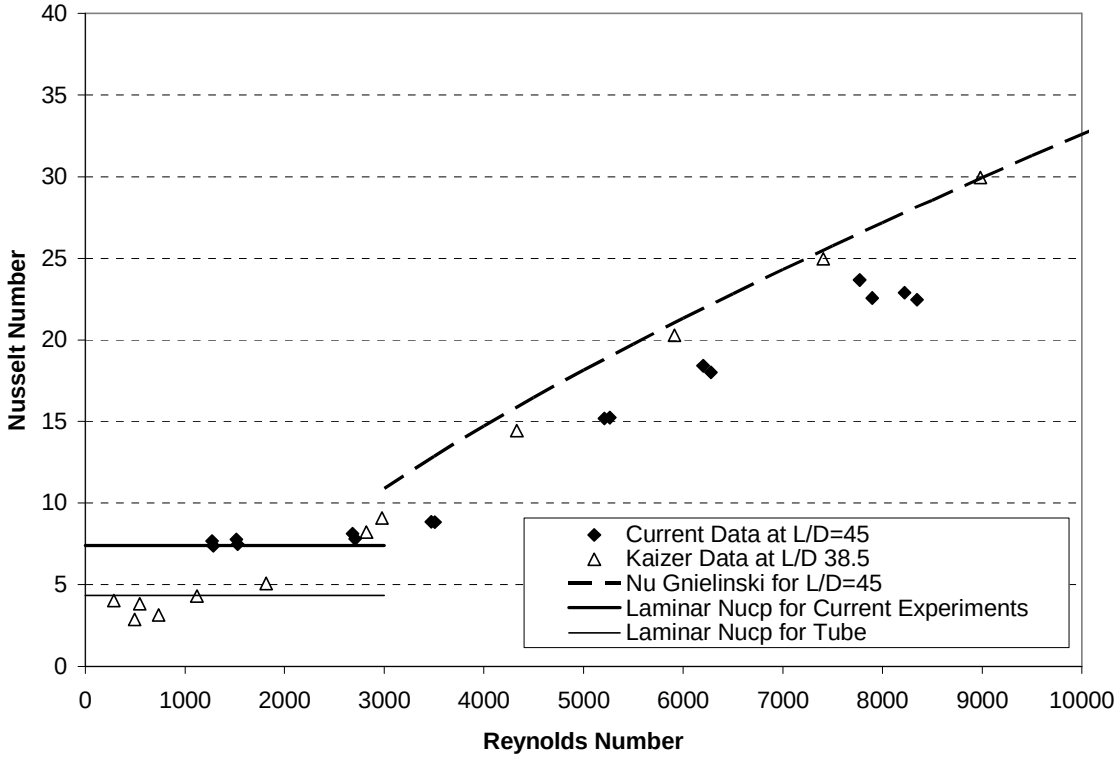

Figure **5-27**: Gnielinski Correlation compared with current experiments and data from Kaizer [**1**]

5.8 Conclusions

The data for the current experiments in the laminar regime matched well with the laminar fully developed constant property expected value of 7.397. The data showed little effect of property variation on the Nusselt number. For laminar data below a Reynolds number of ~200, the convergence of the T_{wall} and T_{bulk} made it difficult to discern an accurate heat transfer coefficient from the data. For these very low Reynolds number cases, this temperature difference was on the order of the uncertainty in the thermocouples. Great care was taken to reduce the uncertainty in the measurements as

much as possible. However, these issues are similar to what was met by Swearingen in his experiments [**5**].

Due to the strange behavior of the Nusselt number in the low Reynolds number flow regime, the presence of buoyancy was analyzed using a calculated local Grashoff number. It was discovered that the highest Grashof numbers were at the entry to the heated length but were below the threshold necessary for buoyancy to play a significant role in the heat transfer.

Turbulent data from the current experiments matched well with turbulent data found in similar literature. The current turbulent data showed little effect on the channel shape or aspect ratio, unlike the laminar regime which had an aspect ratio dependent Nu_{cp}. The current channel data as well as the data found in the literature all indicated heat transfer values below that predicted by either the Dittus-Boelter or the Gnielinski correlations.

Chapter 6

Recommended Correlations, Conclusions, and Reccomendations

The correlations and conclusions found in this chapter are based on data taken from the current experiments using a rectangular geometry test section with an aspect ratio of 18.5:1 and spanning a Reynolds number range of 150 and 10500. The current experimental data was intended to measure a constant heat flux heat transfer condition; however, axial heat losses prevented a truly constant wall heat flux. This section also includes recommendations for future work.

6.1 Turbulent Regime Conclusions

Heat transfer in the fully turbulent flow regime did not deviate much from the well known Dittus Boelter correlation. Observing the turbulent Nusselt number plots in the previous chapter shows full transition to turbulence for Reynolds numbers greater than 5000. However the current experiments show that the Dittus Boelter correlation over-predicts heat transfer for the current experimental conditions. This over-prediction is consistent with what Kaizer [**1**] saw in his turbulent tube data. To account for this over-prediction, the Dittus Boelter correlation can be adjusted to the experimental data by changing the leading coefficient. Tan and Charters [**13**] had the same approach when correlating their rectangular geometry heat transfer data, and adjusted the leading Dittus Boelter coefficient from 0.023 to 0.018. Their correlation was based on experimental

data that had only one of the parallel walls heated, although it matches very well with the current experimental data.

Figure **6-1** gives the current experimental data along with other compiled heat transfer data plotted against this modified Dittus-Boelter correlation, and indicates that modifying the lead coefficient in the Dittus-Boelter correlation will provide a better fit to the data with the majority of the data within the 25% uncertainty bands.

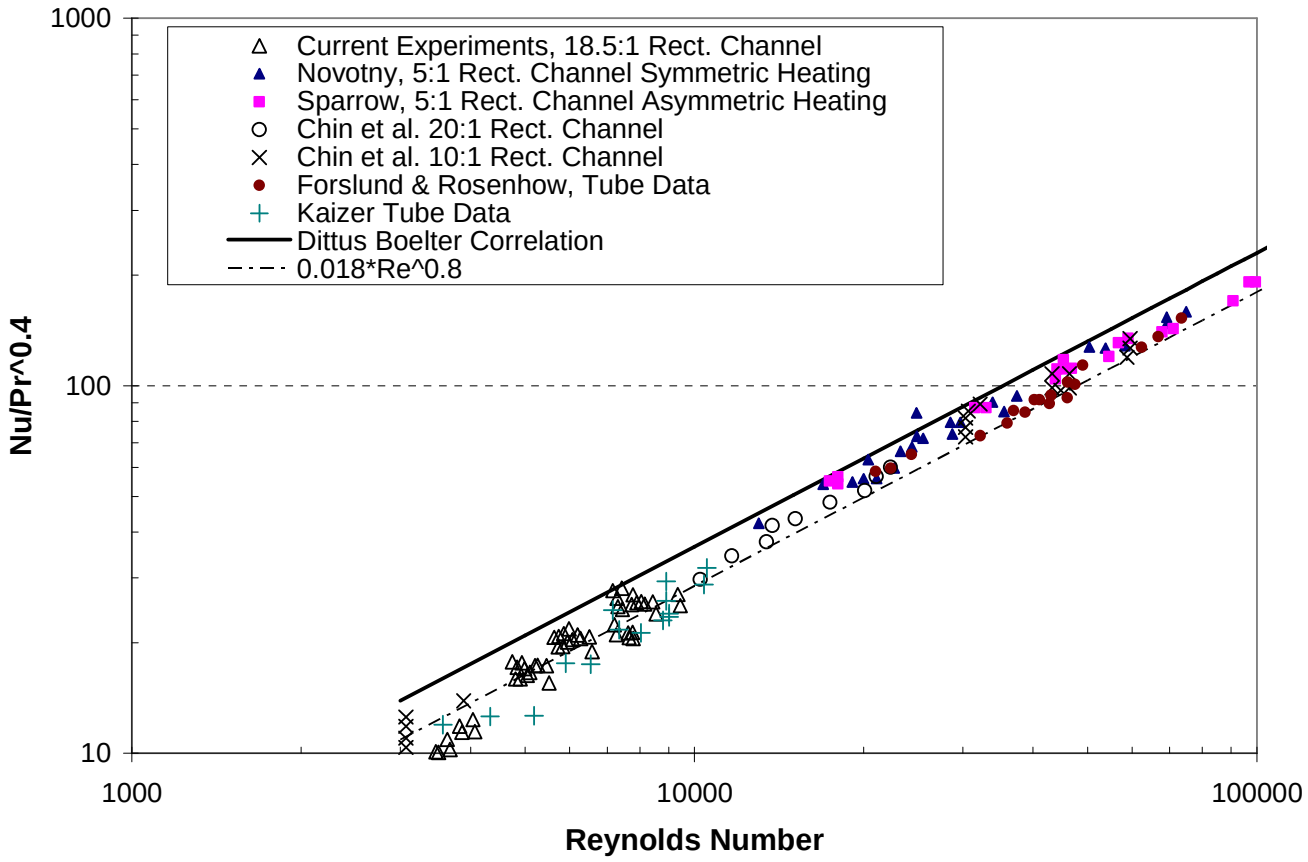

Figure **6-1**: Experimental Turbulent Heat Transfer Data with modified Dittus-Boelter Correlation

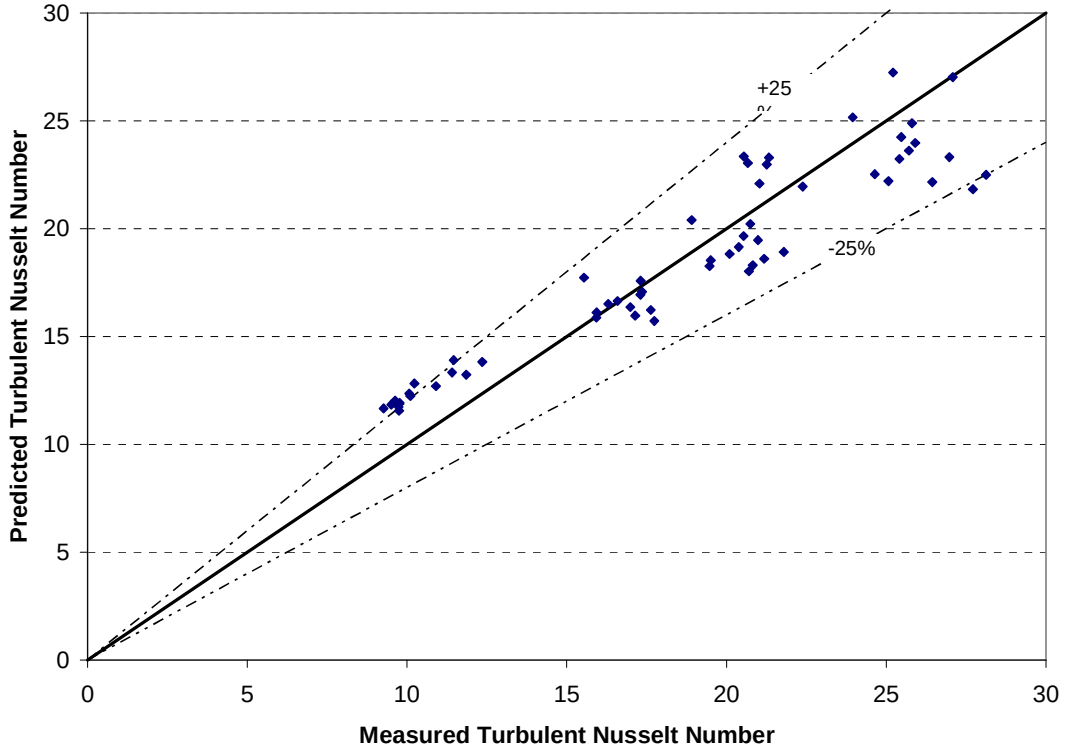

Figure **6-2**: Measured over Predicted current experimental data using a modified Dittus-Boelter correlation

6.2 Laminar Regime Conclusions

A Nusselt number correlation for the laminar regime data was much more difficult to create. Figure **6-3** gives the fully developed Reynolds number results excluding data derived from conditions below a Reynolds number of ~150. This exclusion of data is due to the T_{wall}-T_{bulk} being on the order of the δ_{Tbulk} uncertainty as seen in Appendix **F.3**.

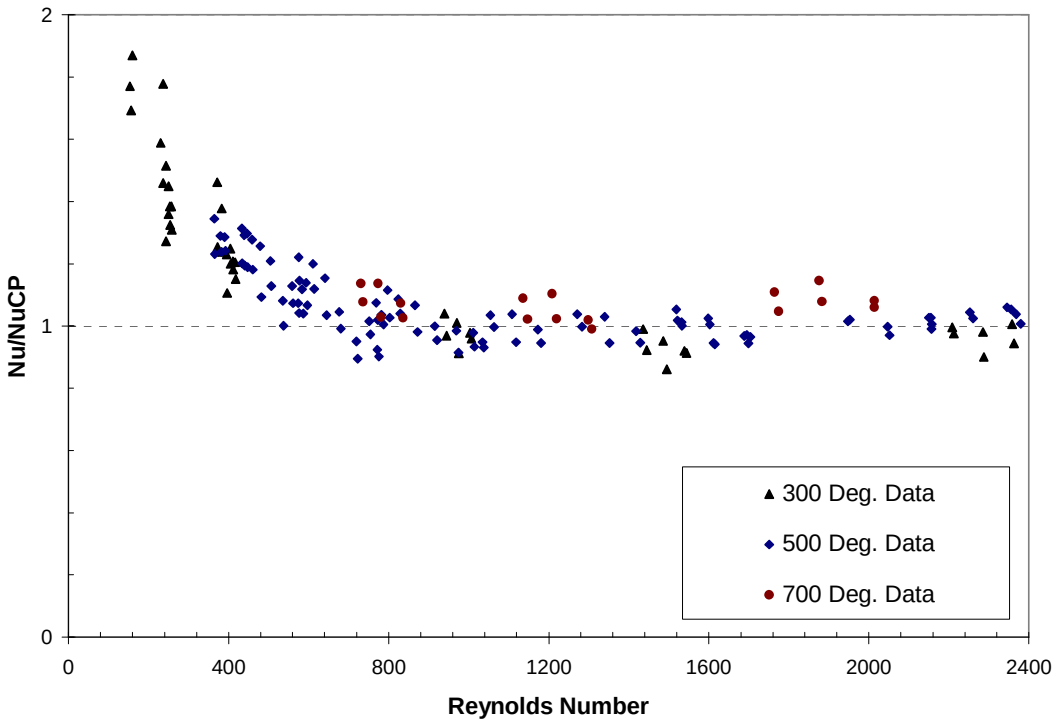

Figure **6-3**: Laminar Fully Developed Data

For Reynolds numbers above 700, the fully developed Nusselt number contains little to no Reynolds dependency and follows the laminar constant property value of 7.397. The higher temperature show slightly higher Nusselt number values than the 500 degree and 300 degree F exit temperature tests. This trend is consistent with Figure **1-1** in that the higher heat flux for the 700 degree acts to hinder the development of the heat transfer coefficient, which is a result of the continued physical property variation.

Although the data below a Reynolds number of approximately 150 has been eliminated based on the data uncertainty analysis, the data trend seen in Figure **6-3** for the data between Reynolds numbers of 150 to 700 remains difficult to explain. There is an effect of the small difference between the wall and bulk temperature which can increase

the calculated heat transfer coefficient. Great care has been used with multiple calibrations to quantify the uncertainty in the temperature measurements used for this experiment. The low Reynolds number data in which the wall to bulk temperature difference was within the data uncertainty at a 95% uncertainty limit was eliminated from Figure **6-3**. One possible explanation is that at these very low Reynolds numbers, the heat transfer is very low such that the continuing development of the flow, due to property variations, may be more significant particularly for these very low Reynolds numbers. The heat transfer rates in low Reynolds number flow are so very low such that any small mechanism, such as boundary layer re-adjustment due to heating that could enhance the flow and the resulting heat transfer behavior. Any such enhancement will have a first order effect on the resulting heat transfer. It is believed that this may be occurring in these experiments. However, since the nature of this Nusselt number increase is not fully understood, it would be conservatively recommended to use the fully developed laminar Nusselt number of 7.397.

In comparing the data from this work to other laminar flow heat transfer data on different geometries such as circular tubes and channels with different aspect ratios, normalizing the heat transfer data using the contstant property Nusselt number for that particular geometry collapses the heat transfer data and normalizes out the effects of geometry such that the data will collapse to approximately a single curve.

6.3 Correlations

This work was completed to analyze the variable property effects of heat transfer for low Reynolds number flow through a rectangular duct. The Reynolds numbers analyzed in this experimental work cover a range of 100-10500.

Turbulent data matched well with previous experimental data and correlations which were derived from the Dittus-Boelter expression. The turbulent fully developed Nusselt numbers were on average about 20% lower than what was expected for the Dittus-Boelter correlation. For this reason, the current data was correlated using a form of the Dittus-Boelter correlation, but with a multiplier of 0.018 instead of 0.023. This correlation predicted the current turbulent data with 25% error bands. The recommended turbulent flow heat transfer correlation is given below in Equation **6.1**.

$$Nu_{turb} = 0.018\,\mathrm{Re}^{0.8}\,\mathrm{Pr}^{0.4} \qquad (\mathbf{6.1})$$

The laminar data was much more difficult to understand. There were many factors which could have played a role in the results of the laminar fully developed data. They include: fluid property variation, the potential for mixed convection, bulk temperature difference uncertainties, axial heat losses, and a fully developed fluid velocity profile at the beginning of the heated length. The last factor was not analyzed and may have played a role in depressing the Nusselt number in the axial development region; however for the current experiments we are interested in the fully developed heat transfer data. With the laminar data below 700 not fully understood, it would be conservatively recommended to use the fully developed laminar Nusselt number of

7.397. The recommended laminar flow correlation for the current rectangular geometry is given below in Equation **6.2** as,

$$Nu_{lam} = 7.397 \quad (\mathbf{6.2})$$

6.4 Recommendations

If future work is to be done using this facility, a few recommendations are presented here to aid in the research:

- Additional low Reynolds number experiments should be run, possibly with another fluid, so that a greater understanding of the low Reynolds number heat transfer can be attained.
- Some natural convection tests would be helpful as well, to give greater confidence that buoyancy was not an issue for the forced laminar tests.
- For the lowest Reynolds number tests it is important to wait very long (> 4 or 5 hours) to ensure that test section is at a true steady state. There were some instances where an external door in the experimental facility was opened which resulted in noticeable changes in the steady state test section wall temperatures. This could be remedied by simply running the lowest Reynolds number tests on days when the outside air temperature is close to room temperature.

Bibliography

1. Kaizer, J.S., and Hochreiter, L.E. "Laminar Flow Heat Transfer for a Circular Geometry", Master of Science Thesis, The Pennsylvania State University, May 2006.

2. Davenport, M.E. "The Effect of Transverse Temperature Gradients on the Heat Transfer and Friction for Laminar Flow of Gases". Ph.D. Thesis, Stanford University, Mechanical Engineering, 1962.

3. Kays, W.M. and W.B. Nicoll. "Laminar Flow Heat Transfer to a Gas with Large Temperature Differences." *Journal of Heat Transfer*, vol 85, pp. 329 – 338, 1963.

4. Worsoe-Schmidt, P.M. Heat Transfer and Friction for Laminar Flow of Helium and Carbon Dioxide in a Circular Tube at a High Heating Rate. *International Journal of Heat and Mass Transfer, Vol 9, p 1291, 1966.*

5 Swearingen, T.B. "Internal Laminar Heat Transfer to a Gas with Temperature Dependent Properties". Ph.D. Thesis, University of Arizona, Mechanical Engineering, 1969.

6. Mercer, W.E. et al. Laminar Forced Convection in the Entrance Region Between Parallel Flat Plates. *Journal of Heat Transfer*. Vol. 89. Issue 3. 1967. Pages 251-257.

7. White, Frank M. *Fluid Mechanics*, 5th Ed. McGraw Hill. 2003. 866pp.

8 Rosenhow, Warren M. et al. *Handbook of Heat Transfer*. 3rd Ed. McGraw Hill. 1998. Chapter 5. Pages 5.67-5.73.

9. Hwang C.L. and Fan, T.L. Finite Difference Analysis of Forced Convection Heat Transfer in Entrance Region of a Flat Rectangular Duct. *Applied Scientific Research.* Vol. 13. Issue 6. 1964. Pages 401-422.

10. Wong, Kau-Fui Vincent. *Intermediate Heat Transfer*. Marcel Decker Publishers, New York, NY. 2003. p211-215.

11 Kreith, F. and M. Bohn, *Principles of Heat Transfer,* 4th Ed. Harper and Row Publishers, New York, NY.

12 Chin, Yun. et al. Convective Heat Transfer in Vertical Assymetrically Heated Channels. *Journal of Heat Transfer*. Vol. 124 pp.1019-1025. 2002.

13 Tan H.M. and Charters W.W.S. An Experimental Investigation of Forced Convective Heat Transfer for Fully Developed Flow in a Rectangular Duct with Assymetric Heating. *Solar Energy*, Vol. 13 pp. 121-125. 1970.

14. Burmeister, Louis C. *Convective Heat Transfer*, 2nd Ed. John Wiley and Sons. 1993. 619pp.

15 Sparrow, E.M. et al. Experiments on Turbulent Heat Transfer in an Asymmetrically Heated Rectangular Duct. *Transactions of the ASME*. May 1966. pp. 170-174.

16 Novotny, J.L. et al. Heat Transfer for Turbulent Flow in Rectangular Ducts with Two Heated and Two Unheated Walls. *A.I.Ch.E. Journal*. Vol. 10, No. 4. Pages 466-470.

17. Washington, L., and Marks, W. M., "Heat Transfer and Pressure Drop in Rectangular Air Passages," Ind. Eng. Chem., 29, 1937, pp. 337-345.

18. Wibulswas, P. "Laminar Flow Heat Transfer in Non-Circular Ducts", PhD. Thesis, University College London. May 1966.

19 Forslund, R.P. and Rosenhow, W.M. Dispersed Flow Film Boiling. Journal of Heat Transfer. November 1968. pp.399-407.

20 Website. "Correlations for Convective Heat transfer" http://www.cheresources.com/convection.shtml Accessed 1/2008

21. FT Series Turbine Flowmeters Installation, Operation and Maintenance Manual. TM-86675 Rev. W. Published by Flow Technology, Inc. January 2005

22. Nist Chemistry Webbook. http://webbook.nist.gov. Thermo-physical properties of fluid systems. Accessed for Nitrogen Property data 2/2007.

23. Dixon, Wilfred J. and Massey, Frank J. *Introduction to Statistical Analysis.* 3rd Edition. McGraw Hill. 1969.

Appendix A

Facility Photographs

This Appendix gives photographs mainly taken when the test section was being built and instrumented.

Figure **A.1**: Test section at the machine shop, held in a strong-back to protect the fragile thin wall to heated wall welds

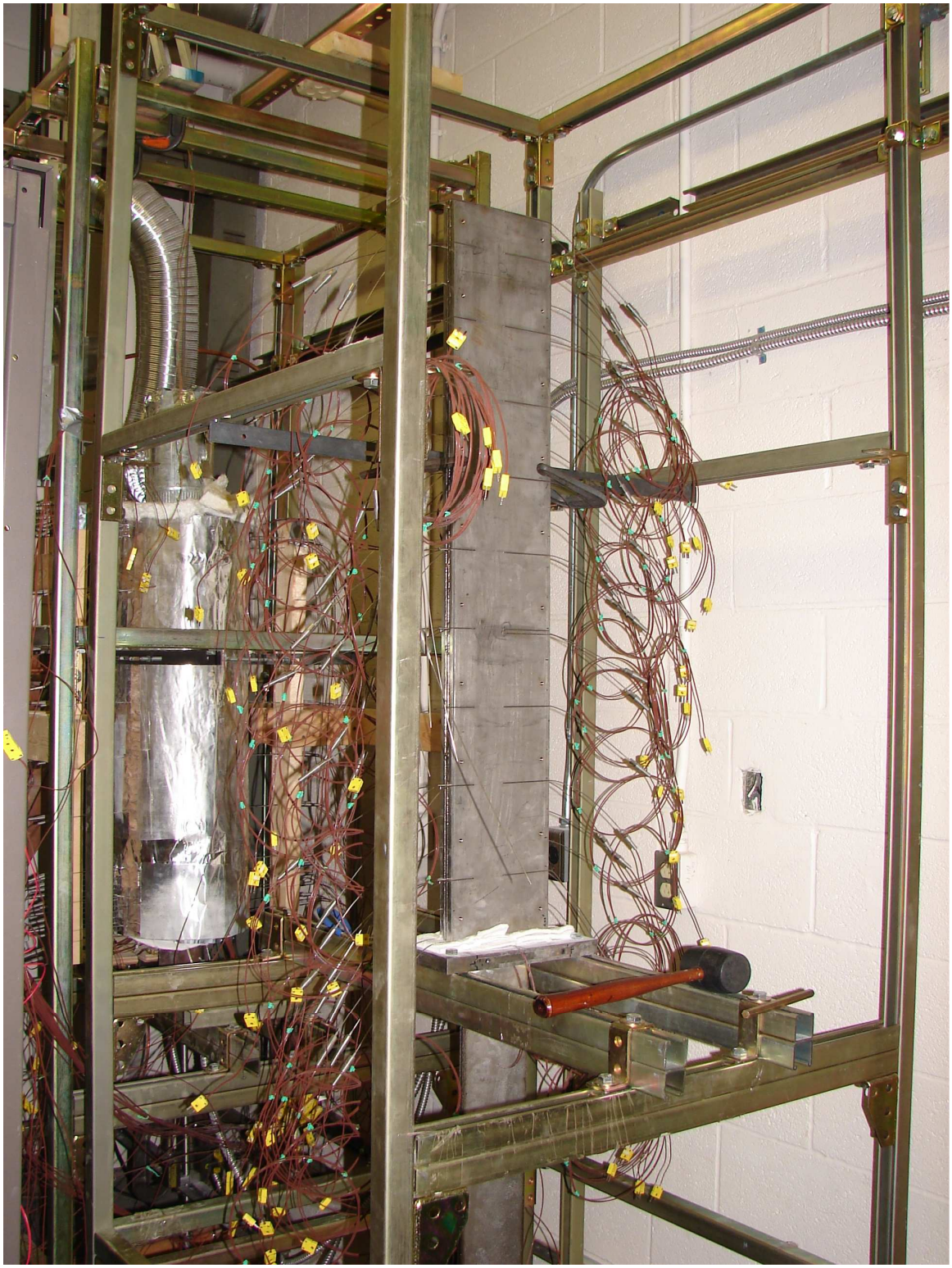

Figure **A.2**: The initial hanging and instrumentation of the test section

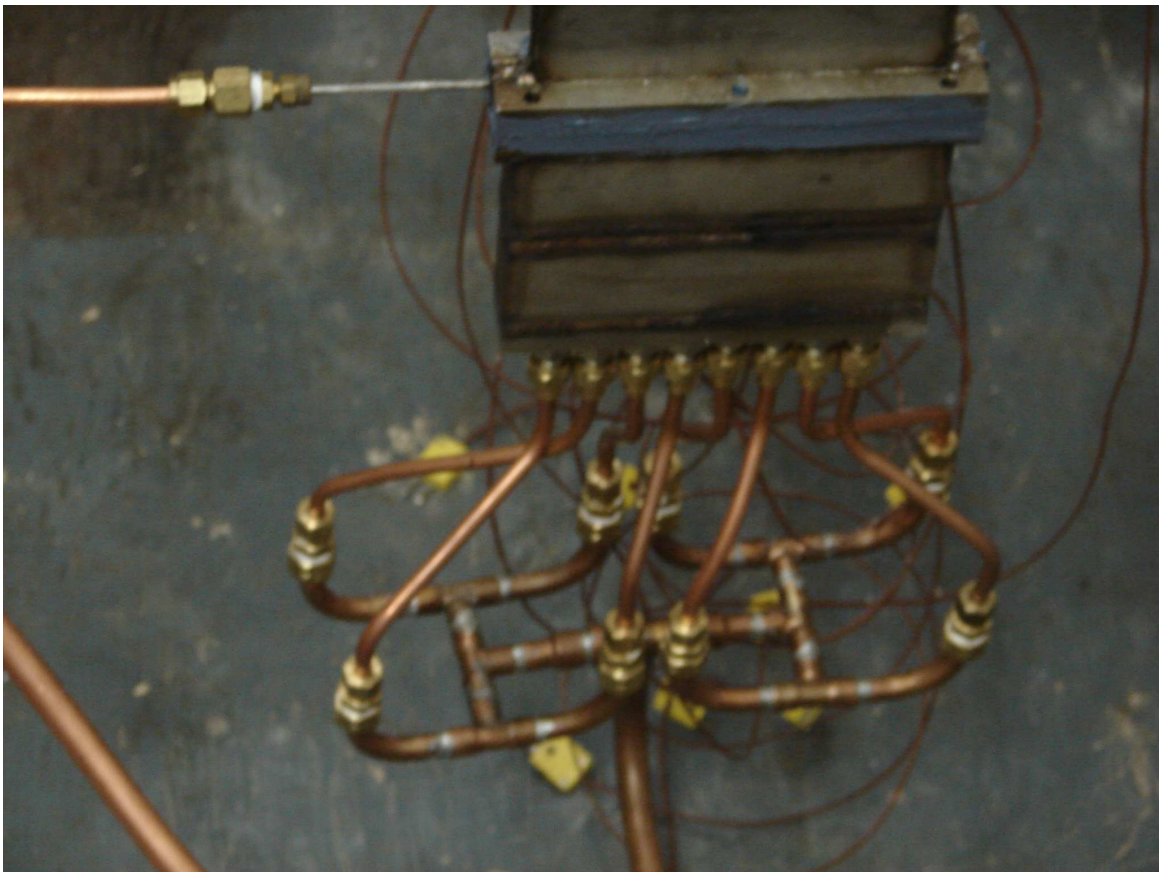

Figure **A.3**: Inlet manifold and flow straigtener, as well as the inlet pressure tap

Figure **A.4**: Ceramic Fiber Heater Attachment, also showing pressure tap and thermocouple instrumentation

Figure **A.5**: Fully instrumented with both ceramic fiber heaters attached

Appendix B

Instrumentation Information

B.1 Instrumentation Required for the Rectangular Geometry

The instrumentation used in the tube geometry tests was sufficient for most of the tests needed for the rectangular geometry. However, the rectangular geometry had a cross section much larger $1.350in^2$ compared to $0.204in^2$ that required much larger flows to achieve the required Reynolds numbers for fully turbulent flow. The tube geometry instrumentation allowed for Reynolds numbers up to around 4500. The flow was mainly hindered by the backpressure which was limited to 30psia by the previous absolute pressure transducer. To solve this issue a new absolute pressure transducer and a new higher flow turbine flow-meter were purchased. This new instrumentation allowed for the higher Reynolds number flows to be measurable in the higher Reynolds number ranges. For all other instrumentation data which was used for both test section geometries, see Appendix A in Kaizer [**1**].

B.2 0-80 PSIA Absolute Pressure Transducer

A Rosemount absolute pressure transducer was used to achieve higher measurable backpressures at the flow-meter, which allowed for higher flow-rates into the rectangular geometry test section. The transducer was scaleable between 0-150psia but calibrated from 0-80psia. The model number was 3051S ultra performance absolute pressure

transducer with 0.025% of span accuracy. Calibrated from 0-80psia, the accuracy was within 0.02psia. For more information on this pressure transducer see www.rosemount.com.

B.3 2-25 CFM Flow-Meter

A larger flow-meter was needed to attain higher flow readings needed for the Rectangular geometry. A Flow-Technology FT-12 turbine flow-meter was used to measure flow rates, and was caliberated at 20, 30, and 50psia. The different back-pressure calibrations broadened measurable range of the flow-meter. Uncertainties listed for the 20psia calibration are +/-0.2% and for the 30 and 50psia calibrations are +/-0.5%. It is recommended that the flow-meters be recalibrated on a 12 month interval.

B.4 Instrumentation Matrix & Data Channels

The instrumentation was plugged into 4 National Instrument data chasses. They are labeled SC Mod 1, SC Mod 2, SC Mod 3, and SC Mod 4 in the LabView chassis interface. Information for each instrument and instrument chassis is given in. Each Table may have complete rows empty. This means that channel in the data chasses was not used

Table **B-1**: Information for Data Chassis – SC Mod 1

Input Number	Instrument Description	Axial Location, Heated Elevation (inches)	Column in Gross Output Files	Main Use
	SC Mod 1 - Instrument Tray 1			
0	Abs Press		124	Ouput Absolute Pressure
1	Diff. Press.		129	Ouput Differential Pressure
2				
3	Center Wall 03	0.1	24	Wall Temperature
4	Center Wall 04	2	23	Wall Temperature
5	Center Wall 05	4	22	Wall Temperature
6	Center Wall 06	6	21	Wall Temperature
7	Center Wall 07	8	20	Wall Temperature
8	Center Wall 08	10	19	Wall Temperature
9	Center Wall 09	15	18	Wall Temperature
10	Center Wall 10	20	17	Wall Temperature
11	Center Wall 11	25	16	Wall Temperature
12	Center Wall 12	27.5	15	Wall Temperature
13	Center Wall 13	30	14	Wall Temperature
14	Center Wall 14	32.5	13	Wall Temperature
15	Center Wall 15	35	12	Wall Temperature
16	Center Wall 16	37.5	11	Wall Temperature
17	Center Wall 17	40	10	Wall Temperature
18	Center Wall 18	42.5	9	Wall Temperature
19	Center Wall 19	45	8	Wall Temperature
20	Center Wall 20	47.9	7	Wall Temperature
21	Side Wall 21	0.1	43	Wall Temperature
22	Side Wall 22	2	42	Wall Temperature
23	Side Wall 23	4	41	Wall Temperature
24	Side Wall 24	6	40	Wall Temperature
25	Side Wall 25	8	39	Wall Temperature
26	Side Wall 26	10	38	Wall Temperature
27	Side Wall 27	15	37	Wall Temperature
28	Side Wall 28	20	36	Wall Temperature
29	Side Wall 29	25	35	Wall Temperature
30	Side Wall 30	27.5	34	Wall Temperature
31	Side Wall 31	30	33	Wall Temperature

Table **B-2**: Information for Data Chassis – SC Mod 2

Input Number	Instrument Description	Axial Location, Heated Elevation (inches)	Column in Gross Output Files	Main Use
		SC Mod 2 - Instrument Tray 2		
32	Side Wall 32	32.5	32	Wall Temperature
33	Side Wall 33	35	31	Wall Temperature
34	Side Wall 34	37.5	30	Wall Temperature
35				
36	Side Wall 36	40	29	Wall Temperature
37	Side Wall 37	42.5	28	Wall Temperature
38	Side Wall 38	45	27	Wall Temperature
39	Side Wall 39	47.9	26	Wall Temperature
40	Center Redundant 40	0.1	55	Redun. Wall Temperature
41	Center Redundant 41	4	54	Redun. Wall Temperature
42	Center Redundant 42	10	53	Redun. Wall Temperature
43	Center Redundant 43	15	52	Redun. Wall Temperature
44	Center Redundant 44	20	51	Redun. Wall Temperature
45	Center Redundant 45	25	50	Redun. Wall Temperature
46	Center Redundant 46	30	49	Redun. Wall Temperature
47	Center Redundant 47	35	48	Redun. Wall Temperature
48	Center Redundant 48	40	47	Redun. Wall Temperature
49	Center Redundant 49	45	46	Redun. Wall Temperature
50	Center Redundant 50	47.9	45	Redun. Wall Temperature
51	Side Redundant 51	0.1	67	Redun. Wall Temperature
52	Side Redundant 52	4	66	Redun. Wall Temperature
53	Side Redundant 53	10	65	Redun. Wall Temperature
54	Side Redundant 54	15	64	Redun. Wall Temperature
55	Side Redundant 55	20	63	Redun. Wall Temperature
56	Side Redundant 56	25	62	Redun. Wall Temperature
57	Side Redundant 57	30	61	Redun. Wall Temperature
58	Side Redundant 58	35	60	Redun. Wall Temperature
59	Side Redundant 59	40	59	Redun. Wall Temperature
60	Side Redundant 60	45	58	Redun. Wall Temperature
61	Side Redundant 61	47.9	57	Redun. Wall Temperature
62	Spacer 62	0.1	79	Spacer Wall Temperature
63	Spacer 63	4	78	Spacer Wall Temperature

Table **B-3**: Information for Data Chassis – SC Mod 3

Input Number	Instrument Description	Axial Location, Heated Elevation (inches)	Column in Gross Output Files	Main Use
		SC Mod 3 - Instrument Tray 3		
64	Spacer 64	10	77	Spacer Wall Temperature
65	Spacer 65	15	76	Spacer Wall Temperature
66	Spacer 66	20	75	Spacer Wall Temperature
67	Spacer 67	25	74	Spacer Wall Temperature
68	Spacer 68	30	73	Spacer Wall Temperature
69	Spacer 69	35	72	Spacer Wall Temperature
70	Spacer 70	40	71	Spacer Wall Temperature
71	Spacer 71	45	70	Spacer Wall Temperature
72	Spacer 72	47.9	69	Spacer Wall Temperature
73	Probe1 73		81	Bulk Temperature
74	Probe1 74		82	Bulk Temperature
75	Probe1 75		83	Bulk Temperature
76	Probe2 76		84	Bulk Temperature
77	Probe2 77		85	Bulk Temperature
78	Probe2 78		86	Bulk Temperature
79				
80	Flow Inlet T		143	Inlet Temperature
81				
82				
83				
84				
85				
86				
87				
88				
89				
90				
91	Exhaust T 91			Exhaust Temperature
92				
93				
94				
95				

Table **B-4**: Information for Data Chassis – SC Mod 4

Input Number	Instrument Description	Axial Location, Heated Elevation (inches)	Column in Gross Output Files	Main Use
SC Mod 4 - Instrument Tray 4				
96	Support Plate Top		88	Calculate Support Heat Loss
97	Support Plate Bottom		89	Calculate Support Heat Loss
98	Thin Wall Section 2" from support	-2	90	Conduction Heat Loss to Unheated Length
99	Thin Wall Section 4" from support	-4	91	Conduction Heat Loss to Unheated Length
100	Thin Wall Section 6" from support	-6	92	Conduction Heat Loss to Unheated Length
101	Thin Wall Section 8" from support	-8	93	Conduction Heat Loss to Unheated Length
102	Thin Wall Section 12" from support	-12	94	Conduction Heat Loss to Unheated Length
103	Thin Wall Section 16" from support	-16	95	Conduction Heat Loss to Unheated Length
104	Thin Wall Section Side 2" from support	-2	96	Conduction Heat Loss to Unheated Length
105	Thin Wall Section Side 4" from support	-4	97	Conduction Heat Loss to Unheated Length
106	Thin Wall Section Side 6" from support	-6	98	Conduction Heat Loss to Unheated Length
107	Thin Wall Section Side 8" from support	-8	99	Conduction Heat Loss to Unheated Length
108	Heater Wall 10"	10	100	Main Lateral Heat Loss Node 1
109	Heater Wall 20"	20	101	Main Lateral Heat Loss Node 2
110	Heater Wall 30"	30	102	Main Lateral Heat Loss Node 3
111	Heater Wall 40"	40	103	Main Lateral Heat Loss Node 4
112	Outside Main Wall 10"	10	104	Main Lateral Heat Loss Node 1
113	Outside Main Wall 20"	20	105	Main Lateral Heat Loss Node 2
114	Outside Main Wall 30"	30	106	Main Lateral Heat Loss Node 3
115	Outside Main Wall 40"	40	107	Main Lateral Heat Loss Node 4
116	Side Wall In 10"	10	108	Side Lateral Heat Loss Node 1
117	Side Wall In 40"	40	109	Side Lateral Heat Loss Node 2
118	Side Out 10"	10	110	Side Lateral Heat Loss Node 1
119	Side Out 40"	40	111	Side Lateral Heat Loss Node 2
120	Top Heat Loss inner	48.25	112	Axial Heat Loss out the top of test section
121	Top Heat Loss outer	48.5	113	Axial Heat Loss out the top of test section
122				
123				
124				
125				
126	Heater 1 Power		117	Power Measurement
127	Heater 2 Power		119	Power Measurement

Appendix C

Procedures

C.1 Startup

The following procedure walks the user through the startup of the test facility from a cold condition to a point where the test section is heating and approaching steady state.

1. Turn on the power to the National Instruments data chassis (SCXI-1001)
2. Restart the computer so that it will recognize the powered up equipment.
3. Open up the LabVIEW program “Main 1-4N.vi”

4. From the front panel, adjust the run number and also ensure that the correct flow-meter and pressure settings are chosen for the particular test.
5. Run the virtual instrument.
6. Ensure that circuit breaker 1 (CB1) in on by checking the circuit box in the NW corner of the laboratory.
7. Ensure that the traversing probe is fully withdrawn.
8. Turn the Heater Panel Knob 1 to the setup position and Knob 2 to medium.
9. Adjust CNT1 and CNT2 to the power percentage desired for test section heating.
10. Turn Knob 1 to on.
11. Observe the power and temperatures from the computer screen and fine tune the power settings if necessary.
12. When the wall temperatures are nearing the desired test conditions, reduce the heater power to the expected power necessary for the given test.
13. Ensure there is enough pressure in the large red tank to drive flow at the desired pressure for the given test.

Caution: If using the FT 2-8 low flow meter do not open CV-1 more than ¼ turn before applying backpressure to the flow-meter. This may cause an expensive and time consuming over-spin to the delicate bearings in this meter.

14. Open CV-1 slightly
15. Ensure that SV-3 and SV-4 are closed and that SV-1 is open.
16. Ensure that the blue knob to the pressure regulating valve (PV-1) prior to SV-2 is fully closed.
17. Open SV-2
18. Turn on the Exhaust fan
19. Slowly open the blue knob to the pressure regulating valve, constantly watching the absolute pressure reading from the computer. Adjust the pressure until the desired flow-meter backpressure is achieved. For normal tests this is 20psia, but for the higher flow tests, 30, and 50 psia were used as well.
20. Adjust CV-1 and the blue pressure regulating valve (PV-1) until the desired flow-rate and backpressure is achieved

A flow balance must now be attained in the large red tank. This can either be done with the small high pressure nitrogen bottles or with the liquid nitrogen tank depending on the necessary flow. Enough flow must enter the red tank to maintain a near constant pressure in the tank.

21. At this point, the flow, absolute pressure, and power must be monitored and maintained while the test facility approaches steady state.
22. Take note of a set of the axial wall temperatures on 15-30 minute intervals while the test section is approaching steady state.
23. Depending on the flow, this can take anywhere from 3-8 hours. Steady state was determined to be when these temperatures were changing less than 2°F every 15 minutes.
24. When the initial steady state is attained measurements may be taken.

C.2 Taking Steady State Measurements

This procedure will walk the user through taking each steady state measurement from the differential pressure to the axial temperature profiles.

Important Note: It is advised that the "Main 1-4N.vi" be restarted after steady state is attained and prior to the steady state measurements. This will greatly reduce the file size of the unreduced output files.

C.2.1 Differential Pressure Measurements

The differential pressure manifold was redesigned for the rectangular geometry tests because of the added pressure inputs. This section is meant to replace the differential pressure measurement section of the procedures by Kaizer [**1**]. To begin, make sure the differential pressure manifold valves are in the positions given in Table **C-1** which also serves as an inventory of all the pressure manifold valves.

Table **C-1**: Pressure Manifold valves and Initial Positions

Valve	Purpose	Beginning Position
A.P. Input	Separates absolute pressure signal from the entire manifold	Open
A.P. Shutoff	Separates absolute pressure transducer from the entire manifold	Open
Separate D.P-A.P.	Separates the absolute and differential pressure lines	Closed
Purge	Allows for a line purge when different gasses are used	Closed
H.L.S.	Separates the high and low differential pressure signals	Open
D.P.H.	Separates the differential pressure transducer high side from the manifold	Open
D.P.L.	Separates the differential pressure transducer low side from the manifold	Open
I.U.	Unheated entrance pressure input	Closed
I.1	First heated pressure input @ 0.5"	Closed
I.2	Second heated pressure input @ 12"	Closed
I.3	Third heated pressure input @ 24"	Closed
I.4	Fourth heated pressure input @ 36"	Closed
I.5	Fifth heated pressure input @ 47.5"	Closed
S.U.1	Separates I.U pressure signal as high and I.1 as low	Open
S.1.2	Separates I.1 pressure signal as high and I.2 as low	Open
S.2.3	Separates I.2 pressure signal as high and I.3 as low	Open
S.3.4	Separates I.3 pressure signal as high and I.4 as low	Open
S.4.5	Separates I.4 pressure signal as high and I.5 as low	Open

The following procedure will walk the user through taking differential pressure measurements the same way they were taken for all the rectangular geometry tests.

Caution: Always make sure the LabVIEW data marker is in the correct position for the reading about to be taken. However, if a mistake is made, the data point can and should be retaken because the data reduction program will always look for the last data point taken for a given data marker.

To obtain the pressure drop between pressure tap U and pressure tap 1:

1. Open I.U
2. Open I.1
3. Close S.U.1
4. Close H.L.S
5. Wait for reading to steady
6. Turn on 30 second timer in LabVIEW
7. Make sure data marker is set to take U-1 measurement
8. Wait for timer to light up, then Flag the measurement
9. Open H.L.S
10. Open S.U.1
11. Close I.U
12. Close I.1

To obtain the pressure drop between pressure tap 1 and pressure tap 2:

1. Open I.1
2. Open I.2
3. Close S.1.2
4. Close H.L.S
5. Wait for reading to steady
6. Turn on 30 second timer in LabVIEW
7. Make sure data marker is set to take 1-2 measurement
8. Wait for timer to light up, then Flag the measurement
9. Open H.L.S
10. Open S.1.2
11. Close I.1
12. Close I.2

To obtain the pressure drop between pressure tap 2 and pressure tap 3:

1. Open I.2
2. Open I.3
3. Close S.2.3
4. Close H.L.S
5. Wait for reading to steady
6. Turn on 30 second timer in LabVIEW
7. Make sure data marker is set to take 2-3 measurement
8. Wait for timer to light up, then Flag the measurement
9. Open H.L.S
10. Open S.2.3
11. Close I.2
12. Close I.3

To obtain the pressure drop between pressure tap 3 and pressure tap 4:

1. Open I.3
2. Open I.4
3. Close S.3.4
4. Close H.L.S
5. Wait for reading to steady
6. Turn on 30 second timer in LabVIEW
7. Make sure data marker is set to take 3-4 measurement
8. Wait for timer to light up, then Flag the measurement
9. Open H.L.S
10. Open S.3.4
11. Close I.3
12. Close I.4

Differential pressure measurements were not taken between pressure taps 4 and 5 during heated tests because of interference with the thermocouple probes. However, the procedure is still provided. To obtain the pressure drop between pressure tap 4 and pressure tap 5:

1. Open I.4
2. Open I.5
3. Close S.4.5
4. Close H.L.S
5. Wait for reading to steady
6. Turn on 30 second timer in LabVIEW
7. Make sure data marker is set to take 4-5 measurement
8. Wait for timer to light up, then Flag the measurement
9. Open H.L.S
10. Open S.4.5
11. Close I.4
12. Close I.5

C.2.2 Axial Fluid Temperature Profile Measurement

This procedure walks the user through taking the steady state temperature profile at each axial location. When this procedure is complete, all steady state measurements are completed and cool-down may begin unless another test is to be run.

Caution: The dimensions are very close between the probe thermocouple spacer width and the width of the test section channel. Due to thermal expansion and slight imperfections in the manufacture of the test apparatus, the probe spacer tends to get stuck occasionally. It is very important to watch the probes carefully any time they are moving axially. If the probe spacer does get stuck, it can be freed by gently shaking the probes or by moving the probe axially up and down slightly. This phenomenon almost always happened when lower flow tests were being performed.

1. Move the data marker on the front panel to represent the desired thermocouple probe axial position.

2. Rotate the traversing probe rod screw until the traversing probe reaches the desired height. The numbers in parentheses on the front panel data marker represent the expected axial position on the measuring stick. These are based upon a 22" offset between the reading on the measuring stick and the actual axial position of the thermocouple probe with respect to the heated length. For reference, the rod screw has a pitch of 5 turns per inch, but for each measurement it is advised to visually check the axial location using the pointer on the traversing assembly.

3. Wait until the probe temperatures have stabilized

4. Turn on the 30 second timer switch on the Main 1-4N front panel

5. When the green light turns on, it is ok to flag the measurement

6. Turn off the 30 second timer switch

Caution: The -3.0 inch axial location represented on the front panel of the virtual instrument is physically unattainable with the current probe configuration. Data for this marker is still collected; however it is just taken as a repeat of the prior -0.95 inch measurement.

7. Repeat steps 1-6 until all axial fluid temperature measurements are taken

8. Click the ‘Stop’ button on the front panel to stop the test when it is complete.

C.3 Cooldown

This procedure walks the user through the test section cool-down. This procedure is only necessary when all tests for a single day have been taken, or any time the hot test section will be left unattended for a long period of time.

1. Turn Knob 1 on the Heater Panel to the off position.

2. Turn CB-1 in the circuit breaker box to the off position.

3. Turn the blue knob to the pressure control valve (PV-1) completely off, this will shutoff the flow momentarily while the cool-down valve positions are set.

4. Close CV-1 and SV-2

5. Open SV-4, which will bypass the flow-meter

6. Turn the blue pressure regulating valve (PV-1) on until flow returns to the test section.

7. Wait until every measurable temperature reads below 200°F

8. Shut flow off to the test section by closing PV-1

9. Close off the main source valves on the high pressure nitrogen bottles, or if using liquid nitrogen, turn off the liquid flow to the red tank.

C.4 Use of Liquid Nitrogen

Liquid nitrogen was used to provide flow for the high Reynolds number tests. A copper line from the liquid side of the liquid nitrogen tank is connected to the large red tank in the laboratory. This large red tank acts as a heat exchanger and vaporizer for the nitrogen. This red tank was the limiting factor for the highest Reynolds number achievable because any higher flows would literally freeze the tank and lower the inlet nitrogen temperature unreasonably. If higher flows were necessary, strip heaters could be used to help heat the nitrogen to room temperature more efficiently.

Safety is always a concern when working with liquid nitrogen and the following safety precautions should be employed at all times.

1. Wear gloves when adjusting the needle valves on the liquid nitrogen tank.
2. Always wear long sleeves when working with liquid nitrogen.
3. Never replace any of the provided valves on the liquid nitrogen tank.
4. Always remember to close all valves on the liquid nitrogen tank before leaving the laboratory. Especially the pressure building (P.B.) valve, which will just waste nitrogen as excess pressure will be purged from the pressure release valve.

Appendix D

MatLab Data Reduction

D.1 Data Reduction Code Files

The data reduction code is broken up into 4 files, each with a specific purpose. The file names are as follows: reduce_all.m, bulktemp.m, getnusselt.m, and getnusselt_fits.m. The function, inputs, and outputs of each file are described in this section.

D.1.1 reduce_all.m

Reduce_all is the main program and all other program files are called within it. The function of reduce_all is to complete the initial reduction of the LabView output by time averaging the data into the format seen in Section **E.4** . This program receives the data from LabView in a binary format and subsequently reduces and outputs the gross reduced data file seen in Table **E-14** thru Table **E-22**. This reduced matrix of data variable is named the 'B' matrix in the actual source code.

Reduce_all has many other functions as well. It prepares smaller data matrixes to be sent to the bulktemp.m and getnusselt.m programs. These smaller data matrixes include the bulk temperature profiles at each axial node center, the wall temperature data matrixes, defined axial node location arrays, and the inlet conditions

based on the inlet flow-rate and inlet temperature. Reduce_all also calculates all the heat loss and pressure drop results.

D.1.2 Bulktemp.m

Bulktemp is a program function designed to calculate the fluid bulk temperature at each axial node center location. It does this by integrating laterally across the temperature and velocity profiles. Bulktemp accepts fluid temperature profiles, inlet conditions, and node locations from reduce_all.m. It also reads in the specified velocity profile from file. It uses all this data to calculate the bulk fluid temperatures axially, then returns a data matrix back to reduce_all called 'Bulk_Temp_Data'. 'Bulk_Temp_Data' includes the axial bulk temperature calculations, as well as fluid property conditions at the axial node centers.

D.1.3 getnusselt.m

Getnusselt is a program function designed to calculate the heat transfer parameters at each axial node center location. It receives data from reduce_all including the axial bulk fluid temperatures, the wall temperatures, inlet conditions, and node locations. It uses this data to calculate the heat transfer coefficient and Nusselt numbers at the specified axial locations. Getnusselt returns a data matrix back to reduce_all called 'NusseltDATA'. 'NusseltDATA' includes the calculated heat transfer areas, T_{wall}-T_{bulk}, heat flux, heat transfer coefficients, and Nusselt numbers for each axial node center.

D.1.4 getnusselt_fits.m

Getnusselt_fits is virtually the same program as getnusselt, only it attempts to fit the bulk fluid temperatures and the wall temperatures to a specified line. By altering the code slightly, the fits can be linear, polynomial, or spline fits. The code then uses these fits to calculate the heat transfer parameters at 45 axial locations. This program does not return a data matrix to reduce all because data from this program was not used in the final analysis.

D.2 Hand Calculations

Hand calculations are performed here to demonstrate the method that the data reduction code takes to get from the temperature and velocity profile data to the axial node center Nusselt numbers. Columns of data will be referenced according to the already time averaged data matrix seen in Table **E-14** thru Table **E-22**. Calculations are performed on the node centers of each axial node. These axial locations are listed in the first column of Table **E-23.** The hand calculations for the bulk temperature were performed on test 901, however, the rest of the hand calculations are performed on test 913, so that the Tables in Section **E.4** thru Section **E.6** can be referenced.

D.2.1 Bulk Temperature Calculation

To obtain the bulk temperatures at each axial node center location, the velocity and temperature profiles were integrated across the lateral 0.27" channel width according to Equation **4.1**. The lateral nodes were 0.01" wide and their data were derived by spline interpolating the lateral bulk fluid temperature profiles at each axial location. Fluid properties at the lateral nodes were based on these interpolated temperatures. Table **D-1** gives an Excel spreadsheet which calculates the bulk temperature at an axial location of 38.75 inches for test 901. Run 901 was reduced using an offset of 6 degrees F between the wall and bulk fluid temperatures. The temperature adjustment column is due to the 6 degree offset between the wall and bulk fluid temperature measurements. A rectangular integration scheme was used to integrate the numerator and denominator of Equation **4.1**. The bulk temperature at this location calculated by the MatLab data reduction code is very close to the hand calculation. After this accurate comparison between the two bulk temperature calculations, it can be assumed that the MatLab code is correctly calculating the bulk temperatures.

Table **D-1**: Bulk Temperature Spreadsheet for Test 901 at an axial location of 38.75 inches

Lateral Distance (in)	Fluid Temp (degF)	Adjusted Fluid Temp (degF)	Vel. (ft/s)	Cp (Btu/lbm-R)	Density (lbm/ft^3)	Lateral Midpoint (x)	Temperature and Velocity Integral @x	Velocity Integral @x
0.00	531.28	525.28	0.00000	0.25457	0.03686			
0.01	478.24	472.24	0.25808	0.25330	0.03895	0.005	6.195E-03	1.242E-05
0.02	443.78	437.78	0.51616	0.25256	0.04044	0.015	1.768E-02	3.886E-05
0.03	424.22	418.22	0.74091	0.25216	0.04133	0.025	2.775E-02	6.485E-05
0.04	415.90	409.90	0.88785	0.25200	0.04172	0.035	3.530E-02	8.525E-05
0.05	415.17	409.17	1.03479	0.25198	0.04176	0.045	4.141E-02	1.011E-04
0.06	418.35	412.35	1.17718	0.25205	0.04161	0.055	4.772E-02	1.162E-04
0.07	421.78	415.78	1.31653	0.25211	0.04144	0.065	5.404E-02	1.305E-04
0.08	422.58	416.58	1.45588	0.25213	0.04141	0.075	6.025E-02	1.448E-04
0.09	420.96	414.96	1.55147	0.25210	0.04148	0.085	6.532E-02	1.571E-04
0.10	417.91	411.91	1.64219	0.25204	0.04163	0.095	6.915E-02	1.673E-04
0.11	414.42	408.42	1.72092	0.25197	0.04179	0.105	7.250E-02	1.768E-04
0.12	411.49	405.49	1.75169	0.25191	0.04193	0.115	7.453E-02	1.831E-04
0.13	409.94	403.94	1.78245	0.25189	0.04201	0.125	7.561E-02	1.868E-04
0.14	409.94	403.94	1.78246	0.25189	0.04201	0.135	7.619E-02	1.886E-04
0.15	411.49	405.49	1.75171	0.25191	0.04193	0.145	7.561E-02	1.868E-04
0.16	414.42	408.42	1.72097	0.25197	0.04179	0.155	7.453E-02	1.831E-04
0.17	417.91	411.91	1.64225	0.25204	0.04163	0.165	7.250E-02	1.768E-04
0.18	420.96	414.96	1.55153	0.25210	0.04148	0.175	6.915E-02	1.673E-04
0.19	422.58	416.58	1.45595	0.25213	0.04141	0.185	6.533E-02	1.571E-04
0.20	421.78	415.78	1.31660	0.25211	0.04144	0.195	6.026E-02	1.448E-04
0.21	418.35	412.35	1.17724	0.25205	0.04161	0.205	5.405E-02	1.305E-04
0.22	415.17	409.17	1.03485	0.25198	0.04176	0.215	4.772E-02	1.162E-04
0.23	415.90	409.90	0.88790	0.25200	0.04172	0.225	4.141E-02	1.011E-04
0.24	424.22	418.22	0.74095	0.25216	0.04133	0.235	3.530E-02	8.525E-05
0.25	443.78	437.78	0.51619	0.25256	0.04044	0.245	2.776E-02	6.485E-05
0.26	478.24	472.24	0.25810	0.25330	0.03895	0.255	1.768E-02	3.887E-05
0.27	531.28	525.28	0.00000	0.25457	0.03686	0.265	6.196E-03	1.242E-05
						Sum =	1.371E+00	3.319E-03

Bulk temp =	413.15	at 38.75in
MatLab	413.06	At 38.75in

D.2.2 Heat Addition to the Fluid Calculation

Equation **4.2** gives the formula for calculating the heat flux to the fluid at each axial node. Figure **D-1** gives the hand calculation of the heat flux for run 913 at the fully developed axial location of 22.5" into the heated length.

$$q''_{22.5} = \frac{\dot{m} \cdot Cp_{22.5}}{(2L + 2W)} \left(\frac{dT_{bulk}}{dz} \right)_{22.5}$$

$$q''_{22.5} = \frac{CFM_{@\,20\,psi} \left(\frac{20\,psi}{14\,psi} \right) \cdot \rho_{inlet} Cp_{22.5}}{(2 \cdot 5.0in + 2 \cdot 0.27in)} \left[\frac{T_{bulk\,@\,22.5} - T_{bulk\,@\,17.5}}{22.5in - 17.5in} \right]$$

$$q''_{22.5} = \frac{1.83 \frac{ft^3}{\min} \left(\frac{20\,psi}{14\,psi} \right) \left(\frac{60\min}{1hr} \right) \cdot 0.07 \frac{lbm}{ft^3} 0.2501 \frac{Btu}{lbm - °F}}{(2 \cdot 0.4167\,ft + 2 \cdot 0.0225\,ft)} \left[\frac{291.1°F - 237.1°F}{1.8750\,ft - 1.4583\,ft} \right]$$

$$q''_{22.5} = 405.13 \frac{Btu}{hr - ft^2}$$

$$q_{22.5} = q''_{22.5} \cdot A_{22.5}$$

$$q_{22.5} = q''_{22.5} \cdot (2 \cdot L + 2 \cdot W) \cdot L_{axial-node}$$

$$q_{22.5} = q''_{22.5} \cdot (2 \cdot 5.0in + 2 \cdot 0.27in) \cdot 5.0in \cdot \left(\frac{1\,ft^2}{144in^2} \right)$$

$$\boxed{q_{22.5} = 148.27 \frac{Btu}{hr}}$$

Matlab Calculates 144.8 Btu/hr, See Table **E-24** , Row 8, Column 11 for Comparison

Figure **D-1**: Hand Calculation of the heat flux to the fluid at an axial location of 22.5"

D.2.3 Heat Transfer Coefficient Calculation

The heat transfer coefficient is calculated using Equation **4.3**. Figure **D-2** demonstrates this calculation for test 913 at an axial node center location of 22.5".

From Figure **D-1** ,

$$q''_{22.5} = 405.13 \frac{Btu}{hr - ft^2}$$

$$h_{22.5} = \frac{q''_{22.5}}{T_{wall,22.5} - T_{bulk,22.5}}$$

$$h_{22.5} = \frac{405.13 \frac{Btu}{hr - ft^2}}{417.0°F - 291.1°F}$$

$$\boxed{h_{22.5} = 3.218 \frac{Btu}{hr - ft^2 - °F}}$$

MatLab Calculates 3.14 Btu/hr-ft^2-°F, See Table **E-25 ,** Row 8, Column 1for Comparison

Figure **D-2**: Hand Calculation of the heat flux to the fluid at an axial location of 22.5"

D.2.4 Nusselt Number Calculation

The Nusselt Number is calculated using Equation **4.4** Figure **D-3** demonstrates this calculation for test 913 at an axial node center location of 22.5".

From Figure **D-2** ,

$$h_{22.5} = 3.218 \frac{Btu}{hr - ft^2 - °F}$$

$$Nu_{22.5} = \frac{h_{22.5} \cdot D_h}{k_{22.5}}$$

$$Nu_{22.5} = \frac{3.218 \frac{Btu}{hr - ft^2 - °F} \cdot 0.0425\, ft}{0.01921 \frac{Btu}{hr - ft - °F}}$$

$$\boxed{Nu_{22.5} = 7.12}$$

MatLab Calculates 6.95, See Table **E-25 ,** Row 8, Column 3for Comparison

Figure **D-3**: Hand Calculation of the Nusselt Number at an axial location of 22.5"

Appendix E

Run Matrix and Output Files for a Selected Test

E.1 Run Matrix

Table **E-1** and Table **E-2** below gives the run matrix with data pertaining to each of the completed test runs. The inlet Reynolds numbers were estimates based upon the expected flow-rate for each test. The heater power was the actual power seen for each test to attain steady state. After the first several runs, it became a nuisance to re-zero the differential pressure reading as it required a Hart Communicator from Rosemount, which had to be borrowed from another lab. The slightly non-zero reading was accounted for in the data reduction, and can be found in the 'Comments' column of Table **E-1.**

Table **E-1**: Run Matrix Data 1 of 2

Date	Run #	Meter CFM	Meter Pressure (psi)	Comments
2/15/2007	903	4.50	20.00	
2/19/2007	904	5.70	20.00	Pressure Drop Bad
2/19/2007	905	6.50	20.00	Pressure Drop Bad
2/21/2007	906	7.35	20.00	
2/21/2007	907	5.00	20.00	
2/21/2007	908	4.15	20.00	
2/21/2007	909	3.30	20.00	
3/1/2007	910	3.30	20.00	Differential pressure was reading 0.001 low
3/1/2007	911	2.80	20.00	Differential pressure was reading 0.001 low
3/1/2007	912	2.30	20.00	Differential pressure was reading 0.001 low
3/1/2007	913	1.80	20.00	Differential pressure was reading 0.001 low
3/5/2007	914	1.40	20.00	Differential pressure was reading 0.00175 low
3/5/2007	915	1.05	20.00	Differential pressure was reading 0.0011 low
3/5/2007	916	0.73	20.00	Differential pressure was reading 0.0012 low
3/7/2007	917	1.80	20.00	Differential pressure was reading 0.002 low
3/7/2007	918	2.80	20.00	Differential pressure was reading 0.0018 low
3/7/2007	919	4.15	20.00	Differential pressure was reading 0.0014 low
4/2/2007	920	0.40	20.00	Differential pressure was reading 0.0001 low
4/4/2007	921	7.50	30.00	Differential pressure was reading 0.0008 low
4/4/2007	922	8.50	30.00	Differential pressure was reading 0.0000 low
4/6/2007	923	6.50	50.00	Differential pressure was reading 0.0000 low
4/10/2007	924	6.50	50.00	Differential pressure was reading 0.0000 low
4/10/2007	925	0.24	20.00	Differential pressure was reading 0.0000 low
4/11/2007	926	0.37	20.00	Differential pressure was reading -0.0002 low
4/13/2007	927	0.54	20.00	Differential pressure was reading 0.0000 low
4/16/2007	928	1.80	20.00	Differential pressure was reading -0.0002 low
4/16/2007	929	2.80	20.00	Differential pressure was reading 0.0016 low
4/16/2007	930	4.20	20.00	Differential pressure was reading -0.0001 low
4/27/2007	931	0.28	20.00	Differential pressure was reading -0.00075 low
4/27/2007	932	0.45	20.00	Differential pressure was reading -0.00075 low
4/27/2007	933	0.73	20.00	Differential pressure was reading -0.0010 low
5/2/2007	934	0.28	20.00	Differential pressure was reading -0.0012 low

Table **E-2**: Run Matrix Data 2 of 2

Date	Run #	Exit Temp. (degF)	Inlet Re	Total Heater Power (watts)
2/15/2007	903	500	2800	N/A
2/19/2007	904	500	3500	N/A
2/19/2007	905	500	4000	N/A
2/21/2007	906	500	4500	1800
2/21/2007	907	500	3000	1340
2/21/2007	908	500	2500	1200
2/21/2007	909	500	2000	1060
3/1/2007	910	500	2000	1020
3/1/2007	911	500	1700	880
3/1/2007	912	500	1400	790
3/1/2007	913	500	1100	690
3/5/2007	914	500	850	520
3/5/2007	915	500	650	450
3/5/2007	916	500	400	410
3/7/2007	917	700	1100	950
3/7/2007	918	700	1700	1300
3/7/2007	919	700	2500	1700
4/2/2007	920	500	215	275
4/4/2007	921	500	6600	2500
4/4/2007	922	500	8000	2850
4/6/2007	923	500	10000	3650
4/10/2007	924	500	10000	3650
4/10/2007	925	500	150	260
4/11/2007	926	500	300	300
4/13/2007	927	500	400	310
4/16/2007	928	300	1100	320
4/16/2007	929	300	1700	500
4/16/2007	930	300	2500	700
4/27/2007	931	300	150	110
4/27/2007	932	300	250	130
4/27/2007	933	300	400	150
5/2/2007	934	180	150	50

E.2 LabVeiw Text and Binary Output Files

The output files from the LabView data acquisition software were very large because they wrote data to file every second, so even a short 1 hour test would have an output file with 3600 rows of data. Therefore, only a portion of the full output file will be shown here. Table **E-3** gives a 30 second portion of selected test 913. This 30 second excerpt was chosen when the LabView main screen looked as it does in Figure **E-1** , with the Measurement Flag set on 18. Once the data was steady for a 30 second period, the Flag Measurement button was pressed which places the '18' in the last row in column 139 of the output matrix as seen highlighted in Table **E-11**.

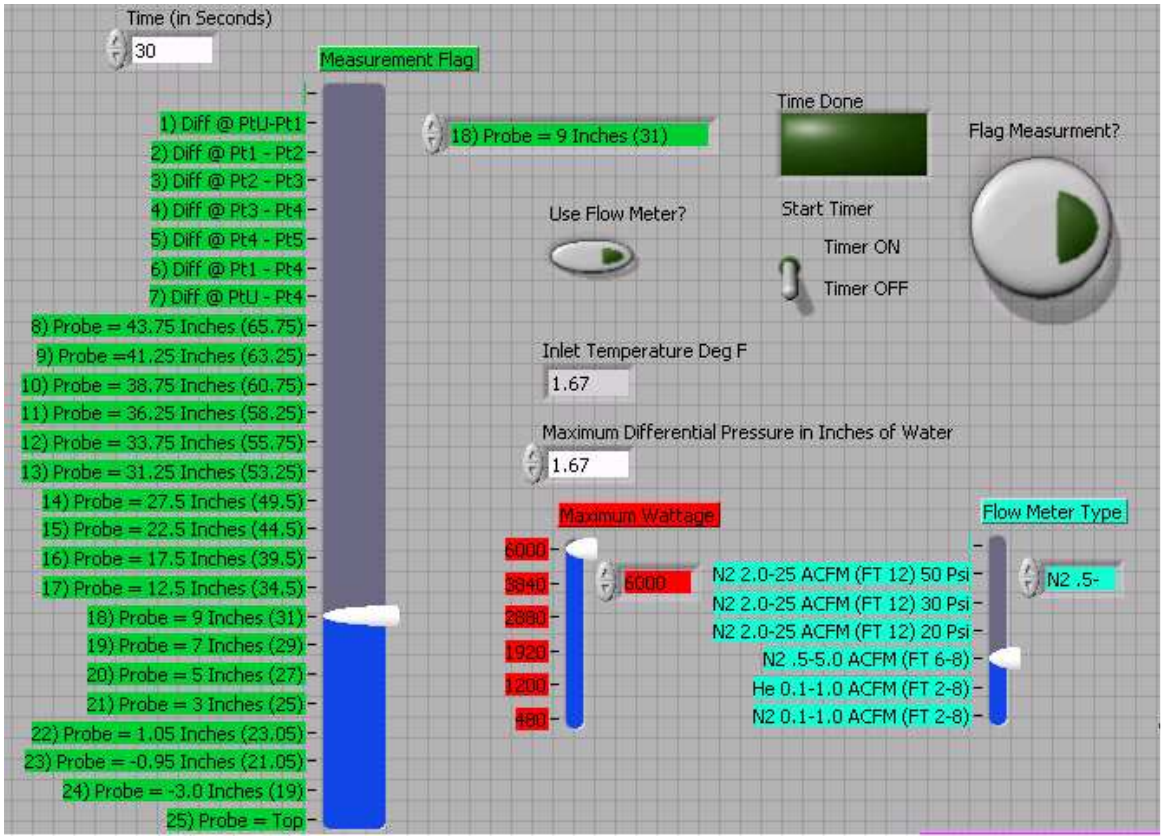

Figure **E-1**: LabView excerpt showing the measurement flag set at '18' where the probe is set at 9 inches into the heated length.

Figure **E-1** also shows the other measurement flags from 1-25 which were taken, including the axial location of the probe when the data was taken. These axial locations of the probe made up the axial node centers for later data reduction. Please note that data markers 5 and 24 are not used in the data reduction. Marker 5 was not used because the differential pressure between 4 and 5 was disrupted because the thermocouple probe could not be fully withdrawn. Marker 24 was not used because the thermocouple probe was physically not able to be lowered to -3". In both these cases, data markers are still taken, but at the previous data markers test conditions.

Table **E-3**: Test 913, 30 seconds to Steady State Output for data marker '18', Probe at 9" into the Heated Length

Column #	1	2	3	4	5	6	7	8	9	10	11	12	13	14
							CW = center Wall							
	Version		Time		Time SS		47.9	45	42.5	40	37.5	35	32.5	30
							CW 20	CW 19	CW 18	CW 17	CW 16	CW 15	CW 14	CW 13
	1.4	-99999	6384	-99999	30	-99999	535.413	549.408	551.969	547.056	535.555	521.056	504.288	486.192
	1.4	-99999	6385	-99999	30	-99999	535.463	549.387	551.948	547.106	535.605	520.965	504.267	486.171
	1.4	-99999	6386	-99999	30	-99999	535.474	549.327	551.888	547.117	535.615	521.046	504.348	486.181
	1.4	-99999	6387	-99999	30	-99999	535.474	549.398	552.029	547.117	535.544	521.046	504.277	486.253
	1.4	-99999	6388	-99999	30	-99999	535.413	549.408	551.969	547.056	535.696	521.056	504.288	486.192
	1.4	-99999	6389	-99999	30	-99999	535.474	549.398	552.029	547.187	535.615	520.975	504.206	486.253
	1.4	-99999	6390	-99999	30	-99999	535.332	549.398	551.958	547.117	535.615	521.046	504.277	486.253
	1.4	-99999	6391	-99999	30	-99999	535.474	549.468	551.888	547.046	535.686	521.117	504.277	486.181
	1.4	-99999	6392	-99999	30	-99999	535.463	549.387	551.877	547.177	535.605	521.107	504.267	486.243
	1.4	-99999	6393	-99999	30	-99999	535.463	549.317	552.018	547.106	535.746	520.965	504.267	486.243
	1.4	-99999	6394	-99999	30	-99999	535.484	549.408	551.969	547.127	535.696	521.056	504.288	486.192
	1.4	-99999	6395	-99999	30	-99999	535.403	549.398	551.958	547.187	535.615	521.117	504.277	486.253
	1.4	-99999	6396	-99999	30	-99999	535.484	549.479	551.969	547.198	535.625	521.127	504.288	486.263
	1.4	-99999	6397	-99999	30	-99999	535.463	549.529	552.018	547.106	535.605	520.965	504.338	486.171
	1.4	-99999	6398	-99999	30	-99999	535.403	549.398	552.029	547.187	535.615	521.046	504.348	486.181
	1.4	-99999	6399	-99999	30	-99999	535.474	549.468	551.958	547.258	535.615	521.046	504.42	486.253
	1.4	-99999	6400	-99999	30	-99999	535.453	549.377	552.008	547.167	535.594	521.096	504.256	486.161
	1.4	-99999	6401	-99999	30	-99999	535.474	549.398	551.958	547.187	535.615	521.046	504.348	486.181
	1.4	-99999	6402	-99999	30	-99999	535.392	549.387	551.948	547.106	535.605	521.036	504.267	486.243
	1.4	-99999	6403	-99999	30	-99999	535.474	549.468	551.888	547.117	535.544	521.046	504.277	486.181
	1.4	-99999	6404	-99999	30	-99999	535.474	549.398	551.958	547.187	535.686	521.117	504.348	486.253
	1.4	-99999	6405	-99999	30	-99999	535.403	549.468	551.958	547.187	535.615	521.117	504.277	486.253
	1.4	-99999	6406	-99999	30	-99999	535.555	549.479	552.039	547.127	535.696	521.127	504.288	486.263
	1.4	-99999	6407	-99999	30	-99999	535.474	549.398	551.958	547.046	535.686	521.117	504.277	486.253
	1.4	-99999	6408	-99999	30	-99999	535.474	549.398	551.958	547.117	535.615	521.188	504.348	486.181
	1.4	-99999	6409	-99999	30	-99999	535.605	549.387	552.018	547.106	535.675	521.107	504.267	486.314
	1.4	-99999	6410	-99999	30	-99999	535.626	549.408	551.969	547.127	535.696	521.127	504.359	486.263
	1.4	-99999	6411	-99999	30	-99999	535.605	549.458	551.948	547.177	535.675	521.107	504.267	486.243
	1.4	-99999	6412	-99999	30	-99999	535.484	549.408	551.898	547.198	535.696	521.198	504.288	486.263
	1.4	-99999	6413	-99999	30	-99999	535.494	549.348	551.979	547.208	535.707	521.138	504.298	486.346

Table **E-4**: Test 913, 30 seconds to Steady State Output for data marker '18', Probe at 9" into the Heated Length, Continued

15	16	17	18	19	20	21	22	23	24	25	26	27	28	29	30
											SW = Side Wall				
27.5	25	20	15	10	8	6	4	2	0.1		47.9	45	42.5	40	37.5
CW 12	CW 11	CW 10	CW 09	CW 08	CW 07	CW 06	CW 05	CW 04	CW 03		SW 39	SW 38	SW 37	SW 36	SW 34
466.372	444.903	397.623	347.21	297.24	272.922	248.142	222.045	195.177	169.555	-99999	540.114	548.179	549.79	544.806	533.846
466.279	444.738	397.529	347.261	297.291	272.829	248.192	221.954	195.227	169.605	-99999	540.053	548.119	549.73	544.816	533.786
466.29	444.965	397.54	347.272	297.229	272.983	248.131	221.964	195.167	169.545	-99999	540.114	548.25	549.79	544.735	533.705
466.29	444.82	397.54	347.345	297.229	272.911	248.274	221.964	195.307	169.685	-99999	540.184	548.179	549.79	544.806	533.775
466.3	444.975	397.55	347.283	297.24	272.994	248.355	221.975	195.177	169.695	-99999	540.255	548.109	549.79	544.806	533.846
466.218	444.82	397.54	347.272	297.229	272.911	248.202	221.964	195.237	169.755	-99999	540.174	548.169	549.85	544.795	533.694
466.29	444.893	397.613	347.272	297.229	272.911	248.274	222.035	195.167	169.685	-99999	540.174	548.24	549.709	544.795	533.836
466.29	445.037	397.54	347.345	297.157	272.983	248.202	221.964	195.307	169.615	-99999	540.124	548.19	549.871	544.745	533.786
466.207	444.882	397.602	347.334	297.074	272.973	248.192	221.954	195.227	169.675	-99999	540.174	548.098	549.85	544.795	533.765
466.279	444.954	397.529	347.334	297.147	272.973	248.263	221.954	195.157	169.675	-99999	540.114	548.179	549.86	544.947	533.775
466.3	444.903	397.623	347.355	297.24	272.994	248.142	221.975	195.247	169.695	-99999	540.184	548.179	549.86	544.806	533.846
466.218	444.965	397.613	347.418	297.157	272.983	248.202	222.035	195.307	169.615	-99999	540.174	548.24	549.78	544.725	533.765
466.228	444.975	397.55	347.501	297.168	272.922	248.213	221.975	195.247	169.695	-99999	540.033	548.169	549.85	544.795	533.836
466.279	444.882	397.529	347.407	297.219	272.973	248.192	221.954	195.297	169.605	-99999	540.184	548.179	549.79	544.876	533.846
466.29	445.037	397.613	347.345	297.157	272.84	248.202	221.964	195.307	169.615	-99999	540.103	548.24	549.85	544.795	533.765
466.362	444.893	397.613	347.418	297.157	272.911	248.131	221.964	195.237	169.615	-99999	540.164	548.159	549.84	544.856	533.826
466.197	444.872	397.591	347.323	297.136	272.89	248.182	221.944	195.287	169.594	-99999	540.184	548.179	549.79	544.876	533.775
466.29	445.037	397.613	347.491	297.085	272.911	248.202	221.964	195.167	169.685	-99999	540.184	548.179	549.86	544.806	533.705
466.351	444.954	397.675	347.407	297.074	272.901	248.263	221.954	195.297	169.675	-99999	540.174	548.169	549.85	544.866	533.765
466.218	444.965	397.613	347.418	297.013	272.911	248.274	221.964	195.307	169.545	-99999	540.174	548.169	549.78	544.795	533.836
466.29	444.965	397.685	347.418	297.085	272.983	248.202	221.964	195.237	169.685	-99999	540.114	548.179	549.79	544.876	533.846
466.362	444.965	397.685	347.491	297.085	272.983	248.202	222.035	195.237	169.615	-99999	540.184	548.25	549.79	544.947	533.775
466.372	444.975	397.696	347.501	297.095	272.922	248.284	221.975	195.318	169.625	-99999	540.184	548.25	549.86	544.806	533.846
466.362	444.965	397.685	347.491	297.085	272.983	248.274	221.964	195.307	169.545	-99999	540.174	548.169	549.78	544.795	533.836
466.29	444.965	397.685	347.491	297.085	272.911	248.202	221.964	195.307	169.615	-99999	540.174	548.169	549.85	544.866	533.836
466.351	444.954	397.748	347.48	297.074	272.973	248.263	221.954	195.297	169.605	-99999	540.255	548.109	549.79	544.876	533.846
466.3	444.975	397.769	347.501	297.095	272.922	248.355	222.045	195.318	169.765	-99999	540.184	548.25	549.931	544.876	533.846
466.279	445.027	397.602	347.48	297.074	272.973	248.192	221.954	195.157	169.605	-99999	540.245	548.24	549.85	544.866	533.836
466.372	444.975	397.696	347.574	297.023	272.85	248.284	221.975	195.247	169.695	-99999	540.114	548.179	549.86	544.806	533.846
466.383	445.058	397.78	347.439	297.106	272.932	248.223	221.985	195.328	169.635	-99999	540.184	548.179	549.86	544.876	533.775

Table **E-5**: Test 913, 30 seconds to Steady State Output for data marker '18', Probe at 9" into the Heated Length, Continued

31	32	33	34	35	36	37	38	39	40	41	42	43	44	45	46
													CR =	Center Redundant	
35	32.5	30	27.5	25	20	15	10	8	6	4	2	0.1			
SW 33	SW 32	SW 31	SW 30	SW 29	SW 28	SW 27	SW 26	SW 25	SW 24	SW 23	SW 22	SW 21		CR 50	CR 49
519.99	504.262	486.054	465.456	443.951	396.817	347.514	297.861	274.245	249.471	223.769	198.446	175.13	-99999	535.119	549.401
519.929	504.344	485.961	465.435	444.003	396.868	347.639	297.839	274.296	249.379	223.819	198.355	175.179	-99999	535.271	549.411
519.919	504.262	486.115	465.445	444.013	396.806	347.649	297.705	274.235	249.461	223.758	198.365	175.12	-99999	535.119	549.33
519.99	504.262	486.115	465.445	444.086	396.879	347.576	297.705	274.307	249.461	223.688	198.506	175.19	-99999	535.19	549.471
519.919	504.262	486.125	465.456	444.096	396.89	347.587	297.716	274.245	249.471	223.839	198.376	175.2	-99999	535.19	549.471
519.908	504.251	486.186	465.373	444.013	397.025	347.504	297.778	274.307	249.461	223.617	198.295	175.12	-99999	535.18	549.461
519.908	504.323	486.115	465.445	443.941	396.879	347.576	297.778	274.307	249.532	223.758	198.365	175.19	-99999	535.18	549.461
520	504.272	486.115	465.445	444.086	396.879	347.576	297.633	274.307	249.39	223.758	198.436	175.05	-99999	535.342	549.34
519.979	504.251	486.033	465.435	444.003	396.868	347.712	297.695	274.296	249.379	223.748	198.355	175.179	-99999	535.251	549.532
519.99	504.262	486.104	465.435	444.003	396.868	347.566	297.695	274.224	249.379	223.677	198.355	175.109	-99999	535.261	549.401
519.919	504.262	486.125	465.6	444.096	396.817	347.514	297.716	274.245	249.543	223.769	198.516	175.2	-99999	535.261	549.542
519.979	504.251	486.115	465.445	444.086	396.879	347.576	297.633	274.235	249.461	223.688	198.436	175.05	-99999	535.251	549.39
519.908	504.251	486.125	465.384	444.096	396.89	347.587	297.644	274.317	249.471	223.698	198.376	175.2	-99999	535.321	549.461
519.99	504.333	486.033	465.435	444.075	396.868	347.566	297.622	274.368	249.522	223.748	198.496	175.179	-99999	535.261	549.401
519.979	504.18	486.115	465.517	444.086	396.879	347.576	297.705	274.307	249.532	223.829	198.365	175.19	-99999	535.321	549.39
519.898	504.241	486.115	465.445	444.086	396.879	347.576	297.705	274.235	249.461	223.758	198.365	175.19	-99999	535.311	549.521
519.919	504.333	486.165	465.424	443.992	396.858	347.482	297.684	274.286	249.511	223.667	198.485	175.099	-99999	535.403	549.542
519.99	504.262	486.115	465.517	444.086	396.879	347.504	297.705	274.307	249.532	223.758	198.365	175.19	-99999	535.403	549.471
520.05	504.323	486.033	465.435	444.075	396.868	347.639	297.622	274.224	249.522	223.677	198.425	175.179	-99999	535.251	549.461
519.979	504.251	486.186	465.445	444.086	396.952	347.649	297.705	274.235	249.532	223.758	198.506	175.12	-99999	535.321	549.39
519.99	504.262	486.115	465.445	444.013	396.952	347.576	297.778	274.235	249.532	223.9	198.436	175.12	-99999	535.261	549.401
519.919	504.262	486.115	465.517	444.086	396.879	347.504	297.561	274.307	249.532	223.829	198.436	175.19	-99999	535.332	549.471
519.99	504.333	486.125	465.456	444.096	396.89	347.587	297.644	274.317	249.614	223.769	198.446	175.2	-99999	535.332	549.471
519.979	504.323	486.115	465.517	444.158	396.879	347.649	297.633	274.235	249.532	223.758	198.436	175.19	-99999	535.321	549.461
519.908	504.251	486.115	465.445	444.086	396.879	347.504	297.633	274.307	249.532	223.758	198.436	175.19	-99999	535.392	549.39
520.061	504.333	486.104	465.507	444.075	396.941	347.639	297.622	274.368	249.522	223.748	198.425	175.179	-99999	535.403	549.401
519.99	504.262	486.125	465.528	444.096	396.963	347.587	297.788	274.317	249.543	223.839	198.446	175.2	-99999	535.473	549.471
519.979	504.251	486.176	465.435	444.075	397.014	347.639	297.695	274.368	249.45	223.748	198.496	175.179	-99999	535.463	549.461
520.061	504.262	486.125	465.528	444.096	396.89	347.66	297.644	274.389	249.471	223.769	198.376	175.27	-99999	535.403	549.542
519.99	504.262	486.136	465.538	444.107	396.9	347.598	297.726	274.4	249.553	223.708	198.456	175.14	-99999	535.403	549.471

Table **E-6**: Test 913, 30 seconds to Steady State Output for data marker '18', Probe at 9" into the Heated Length, Continued

47	48	49	50	51	52	53	54	55	56	57	58	59	60	61	62
									SR = Side Redundant						
CR 48	CR 47	CR 46	CR 45	CR 44	CR 43	CR 42	CR 41	CR 40		SR 61	SR 60	SR 59	SR 58	SR 57	SR 56
547.368	521.313	487.55	445.152	395.959	346.467	292.001	218.319	169.601	-99999	540.104	548.824	545.566	520.933	488.075	445.298
547.449	521.323	487.561	445.09	396.043	346.477	292.084	218.4	169.611	-99999	540.114	548.834	545.435	520.802	488.157	445.309
547.368	521.384	487.622	445.08	395.886	346.467	292.146	218.389	169.601	-99999	540.104	548.895	545.566	520.933	488.218	445.226
547.298	521.313	487.55	445.007	396.032	346.613	291.929	218.319	169.671	-99999	540.174	548.895	545.637	520.791	488.075	445.226
547.298	521.384	487.622	445.152	395.886	346.54	292.001	218.389	169.671	-99999	540.104	548.824	545.566	520.862	488.003	445.154
547.287	521.373	487.54	445.141	396.021	346.529	291.991	218.379	169.661	-99999	540.093	548.814	545.556	520.852	488.136	445.215
547.428	521.373	487.54	445.141	396.021	346.456	291.991	218.309	169.801	-99999	540.164	548.814	545.414	520.852	488.136	445.288
547.378	521.323	487.561	445.162	395.97	346.477	291.939	218.329	169.681	-99999	540.185	548.905	545.506	520.944	488.157	445.236
547.287	521.302	487.683	445.141	396.021	346.529	291.991	218.309	169.661	-99999	540.164	548.743	545.414	520.923	488.279	445.143
547.368	521.455	487.55	445.08	395.959	346.54	291.929	218.389	169.671	-99999	540.174	548.824	545.495	520.862	488.218	445.154
547.298	521.313	487.693	445.152	395.959	346.467	291.929	218.319	169.601	-99999	540.174	548.754	545.566	520.933	488.218	445.298
547.287	521.373	487.54	445.141	395.948	346.456	291.991	218.45	169.661	-99999	540.164	548.814	545.556	520.923	488.136	445.215
547.358	521.373	487.611	445.141	396.021	346.602	291.991	218.309	169.661	-99999	540.235	548.814	545.556	520.852	488.136	445.288
547.439	521.384	487.622	445.152	396.032	346.54	291.929	218.389	169.671	-99999	540.104	548.824	545.637	520.862	488.147	445.226
547.428	521.373	487.54	445.141	395.948	346.602	291.918	218.45	169.731	-99999	540.306	548.814	545.556	520.852	488.136	445.215
547.277	521.292	487.529	445.131	395.938	346.446	291.908	218.369	169.721	-99999	540.154	548.874	545.475	520.913	488.197	445.349
547.368	521.384	487.55	445.224	396.105	346.54	291.857	218.389	169.671	-99999	540.174	548.754	545.495	520.862	488.29	445.298
547.439	521.384	487.693	445.152	396.032	346.613	291.784	218.389	169.671	-99999	540.245	548.824	545.495	520.933	488.147	445.226
547.358	521.444	487.611	445.069	396.021	346.602	291.918	218.379	169.661	-99999	540.093	548.814	545.485	520.852	488.136	445.288
547.358	521.444	487.611	445.141	396.021	346.602	291.846	218.379	169.591	-99999	540.093	548.814	545.556	520.852	488.136	445.288
547.368	521.313	487.622	445.152	396.032	346.686	291.929	218.389	169.741	-99999	540.174	548.895	545.495	520.862	488.147	445.226
547.439	521.313	487.55	445.152	396.105	346.613	291.929	218.46	169.671	-99999	540.174	548.895	545.566	520.933	488.147	445.298
547.368	521.313	487.55	445.152	396.032	346.686	291.929	218.319	169.671	-99999	540.104	548.824	545.495	520.933	488.147	445.298
547.428	521.373	487.54	445.214	396.094	346.602	291.918	218.45	169.591	-99999	540.164	548.814	545.485	520.852	488.279	445.288
547.358	521.373	487.54	445.214	396.021	346.602	291.846	218.379	169.591	-99999	540.235	548.814	545.556	520.923	488.136	445.288
547.368	521.455	487.622	445.152	396.105	346.686	291.784	218.46	169.671	-99999	540.174	548.895	545.566	520.933	488.075	445.298
547.368	521.313	487.693	445.152	396.032	346.758	291.857	218.389	169.741	-99999	540.174	548.895	545.354	521.004	488.075	445.226
547.428	521.444	487.611	445.141	396.167	346.748	291.918	218.309	169.731	-99999	540.235	548.814	545.556	520.923	488.136	445.288
547.368	521.384	487.693	445.224	396.032	346.686	291.857	218.389	169.601	-99999	540.174	548.824	545.566	520.862	488.218	445.226
547.368	521.313	487.693	445.224	396.178	346.686	291.857	218.46	169.671	-99999	540.245	548.895	545.566	520.933	488.147	445.226

Table **E-7**: Test 913, 30 seconds to Steady State Output for data marker '18', Probe at 9" into the Heated Length, Continued

63	64	65	66	67	68	69	70	71	72	73	74	75	76	77	78
						SP = Spacer									
SR 55	SR 54	SR 53	SR 52	SR 51		SP 72	SP 71	SP 70	SP 69	SP 68	SP 67	SP 66	SP 65	SP 64	SP 63
399.148	349.486	297.286	220.239	177.071	-99999	539.355	547.076	544.482	519.887	486.646	445.33	398.558	348.847	298.675	223.863
399.158	349.496	297.224	220.32	177.151	-99999	539.284	547.076	544.412	519.958	486.646	445.257	398.558	348.774	298.603	223.803
399.22	349.559	297.286	220.239	177.141	-99999	539.426	546.935	544.412	519.958	486.646	445.257	398.558	348.701	298.675	223.863
399.22	349.486	297.286	220.239	177.141	-99999	539.365	547.086	544.563	519.897	486.585	445.268	398.569	348.712	298.685	223.793
399.148	349.486	297.213	220.098	177.071	-99999	539.376	547.026	544.503	519.979	486.667	445.351	398.506	348.868	298.624	223.793
399.21	349.548	297.348	220.3	177.131	-99999	539.355	546.935	544.482	519.958	486.646	445.185	398.558	348.774	298.675	223.924
399.21	349.548	297.203	220.229	177.131	-99999	539.365	546.945	544.493	519.897	486.657	445.268	398.641	348.858	298.613	223.924
399.085	349.496	297.296	220.25	177.081	-99999	539.426	547.005	544.482	519.958	486.646	445.257	398.704	348.774	298.675	223.874
399.137	349.548	297.275	220.229	177.131	-99999	539.365	547.086	544.493	519.968	486.585	445.268	398.641	348.712	298.685	223.853
399.148	349.486	297.213	220.239	177.071	-99999	539.365	547.086	544.493	519.897	486.657	445.413	398.714	348.858	298.685	223.863
399.148	349.486	297.213	220.239	177.141	-99999	539.365	547.086	544.493	519.897	486.657	445.34	398.641	348.858	298.613	223.793
399.21	349.621	297.275	220.159	177.061	-99999	539.345	546.995	544.543	519.947	486.564	445.319	398.547	348.836	298.664	223.853
399.21	349.548	297.275	220.159	177.131	-99999	539.355	546.935	544.412	519.958	486.646	445.257	398.704	348.847	298.675	223.853
399.148	349.486	297.286	220.169	177.141	-99999	539.436	547.016	544.422	519.968	486.657	445.268	398.641	348.858	298.613	223.793
399.137	349.548	297.275	220.3	177.131	-99999	539.436	547.016	544.493	519.968	486.728	445.34	398.569	348.785	298.685	223.924
399.126	349.537	297.265	220.148	177.121	-99999	539.496	547.076	544.482	519.887	486.646	445.402	398.631	348.701	298.675	223.843
399.148	349.486	297.286	220.169	177.141	-99999	539.355	546.935	544.553	519.887	486.646	445.33	398.631	348.847	298.53	223.934
399.148	349.559	297.358	220.169	177.141	-99999	539.436	546.945	544.422	519.968	486.657	445.34	398.714	348.858	298.685	223.863
399.137	349.621	297.203	220.3	177.131	-99999	539.355	547.076	544.482	519.887	486.646	445.402	398.631	348.847	298.603	223.853
399.21	349.548	297.275	220.229	177.131	-99999	539.355	547.005	544.412	519.958	486.646	445.33	398.631	348.847	298.675	223.924
399.22	349.559	297.213	220.169	177.141	-99999	539.355	547.005	544.553	519.887	486.646	445.33	398.558	348.774	298.603	223.863
399.22	349.559	297.213	220.239	177.141	-99999	539.426	547.005	544.482	519.887	486.646	445.33	398.631	348.92	298.675	223.934
399.148	349.559	297.213	220.239	177.141	-99999	539.355	547.076	544.482	519.958	486.575	445.33	398.631	348.847	298.675	223.863
399.21	349.475	297.203	220.229	177.061	-99999	539.355	547.005	544.553	519.958	486.646	445.402	398.631	348.847	298.675	223.853
399.21	349.548	297.275	220.229	177.201	-99999	539.355	547.076	544.482	519.958	486.646	445.402	398.631	348.774	298.603	223.924
399.293	349.559	297.213	220.169	177.071	-99999	539.426	546.935	544.553	519.958	486.646	445.33	398.776	348.847	298.675	223.934
399.22	349.559	297.213	220.239	177.141	-99999	539.426	547.005	544.553	519.887	486.646	445.33	398.704	348.774	298.675	223.934
399.283	349.621	297.131	220.229	177.131	-99999	539.496	547.005	544.553	519.958	486.79	445.33	398.631	348.847	298.675	223.924
399.22	349.559	297.286	220.239	177.141	-99999	539.436	546.945	544.493	519.968	486.657	445.485	398.787	348.858	298.613	223.934
399.22	349.632	297.213	220.31	177.141	-99999	539.365	547.086	544.563	519.897	486.728	445.413	398.641	348.712	298.613	223.863

Table **E-8**: Test 913, 30 seconds to Steady State Output for data marker '18', Probe at 9" into the Heated Length, Continued

79	80	81	82	83	84	85	86	87	88	89	90	91	92	93	94
		PR = Probes							Insulation: TWC=Thin wall center						
SP 62		PR 1	PR 2	PR 3	PR 4	PR 5	PR 6		Support T	Support B	TWC - 2"	TWC - 4"	TWC - 6"	TWC - 8"	TWC - 12"
177.099	-99999	154.729	149.773	198.832	160.326	152.261	194.231	-99999	79.435	79.19	95.612	80.664	74.717	72.822	72.108
177.109	-99999	154.729	149.703	198.762	160.256	152.261	194.231	-99999	79.425	79.18	95.53	80.582	74.851	72.956	72.17
177.099	-99999	154.799	149.703	198.832	160.256	152.261	194.231	-99999	79.58	79.263	95.612	80.664	74.717	72.967	72.108
177.169	-99999	154.739	149.713	198.843	160.267	152.271	194.311	-99999	79.435	79.263	95.541	80.664	74.717	72.967	72.108
177.239	-99999	154.819	149.724	198.712	160.207	152.212	194.321	-99999	79.58	79.19	95.469	80.592	74.717	72.894	72.108
177.089	-99999	154.729	149.703	198.692	160.116	152.191	194.231	-99999	79.425	79.18	95.53	80.51	74.634	72.884	72.17
177.159	-99999	154.669	149.573	198.632	160.267	152.271	194.241	-99999	79.435	79.263	95.541	80.52	74.717	72.894	72.181
177.179	-99999	154.799	149.703	198.692	160.256	152.261	194.231	-99999	79.58	79.19	95.541	80.592	74.717	72.967	72.108
177.229	-99999	154.669	149.713	198.702	160.267	152.271	194.241	-99999	79.446	79.201	95.623	80.531	74.727	72.977	72.119
177.169	-99999	154.669	149.643	198.702	160.267	152.201	194.311	-99999	79.507	79.19	95.541	80.592	74.717	72.894	72.108
177.239	-99999	154.739	149.573	198.772	160.267	152.201	194.171	-99999	79.435	79.19	95.541	80.592	74.645	72.967	72.181
177.089	-99999	154.648	149.553	198.611	160.106	152.111	194.15	-99999	79.435	79.19	95.541	80.664	74.717	72.967	72.108
177.159	-99999	154.729	149.633	198.762	160.116	152.121	194.09	-99999	79.497	79.252	95.53	80.51	74.706	72.956	72.17
177.169	-99999	154.739	149.573	198.632	160.267	152.201	194.171	-99999	79.486	79.169	95.591	80.643	74.696	72.801	72.16
177.159	-99999	154.669	149.643	198.632	160.197	152.271	194.171	-99999	79.363	79.19	95.541	80.664	74.717	72.967	72.253
177.219	-99999	154.658	149.563	198.692	160.116	152.121	194.161	-99999	79.507	79.263	95.612	80.664	74.789	72.967	72.181
177.169	-99999	154.588	149.563	198.692	160.116	152.191	194.161	-99999	79.518	79.129	95.623	80.675	74.655	72.977	72.191
177.239	-99999	154.669	149.643	198.702	160.126	152.131	194.171	-99999	79.507	79.19	95.541	80.664	74.789	72.967	72.108
177.159	-99999	154.729	149.633	198.692	160.116	152.121	194.161	-99999	79.435	79.263	95.541	80.664	74.717	72.894	72.181
177.229	-99999	154.588	149.493	198.762	160.186	152.191	194.161	-99999	79.518	79.345	95.551	80.603	74.727	72.905	72.191
177.099	-99999	154.658	149.493	198.692	160.046	152.051	194.161	-99999	79.425	79.18	95.53	80.654	74.779	72.956	72.098
177.099	-99999	154.658	149.563	198.762	160.116	152.121	194.231	-99999	79.353	79.108	95.53	80.582	74.634	72.956	72.098
177.169	-99999	154.729	149.633	198.692	159.976	152.121	194.231	-99999	79.497	79.18	95.53	80.582	74.706	72.884	72.17
177.229	-99999	154.658	149.563	198.762	160.046	152.191	194.231	-99999	79.518	79.201	95.623	80.531	74.8	72.977	72.119
177.229	-99999	154.588	149.563	198.692	160.046	152.051	194.161	-99999	79.435	79.19	95.612	80.592	74.717	72.967	72.181
177.169	-99999	154.588	149.563	198.762	160.046	152.191	194.161	-99999	79.569	79.18	95.53	80.582	74.706	72.884	72.17
177.239	-99999	154.588	149.633	198.832	160.116	151.981	194.231	-99999	79.435	79.19	95.612	80.664	74.717	72.967	72.108
177.089	-99999	154.588	149.493	198.762	160.046	152.121	194.231	-99999	79.435	79.19	95.541	80.52	74.717	72.894	72.181
177.239	-99999	154.599	149.573	198.561	159.986	152.061	194.171	-99999	79.435	79.263	95.541	80.592	74.572	72.894	72.108
177.169	-99999	154.669	149.573	198.843	160.056	152.061	194.171	-99999	79.497	79.18	95.53	80.654	74.706	72.956	72.243

Table **E-9**: Test 913, 30 seconds to Steady State Output for data marker '18', Probe at 9" into the Heated Length, Continued

95	96	97	98	99	100	101	102	103	104	105	106	107	108	109	110
	TWS=Thin Wall Side				HW=Heater wall				OUT=main wall outer insulation				Side in=buried side insulation		
TWC - 16"	TWS - 2"	TWS - 4"	TWS - 6"	TWS - 8"	HW 10"	HW 20"	HW 30"	HW 40"	OUT 10"	OUT 20"	OUT 30"	OUT 40"	SIDE IN 10"	SIDE IN 40"	SIDE OUT 10"
72.078	95.678	80.92	75.228	72.894	396.965	484.927	513.971	535.439	332.779	393.643	386.018	440.204	176.374	351.26	134.285
72.14	95.596	80.838	75.218	72.811	397.028	484.916	513.89	535.287	332.695	393.632	386.008	440.121	176.294	351.177	134.275
72.151	95.607	80.776	75.156	72.822	397.038	484.927	514.042	535.439	332.706	393.643	385.945	440.132	176.304	351.187	134.285
72.078	95.607	80.776	75.156	72.822	397.111	484.927	514.042	535.368	332.779	393.57	386.018	440.132	176.304	351.26	134.215
72.223	95.607	80.848	75.084	72.894	397.111	484.927	513.9	535.368	332.706	393.57	386.018	440.06	176.374	351.26	134.285
72.068	95.596	80.766	75.146	72.811	397.028	484.916	513.961	535.358	332.695	393.632	386.08	440.194	176.294	351.177	134.205
72.151	95.607	80.776	75.156	72.894	397.111	484.998	514.042	535.439	332.706	393.643	386.018	440.204	176.374	351.26	134.215
72.078	95.607	80.776	75.156	72.894	397.111	484.927	513.971	535.51	332.633	393.643	386.164	440.132	176.304	351.26	134.215
72.089	95.689	80.859	75.167	72.905	397.049	484.937	513.981	535.52	332.789	393.653	386.029	440.215	176.314	351.271	134.296
72.151	95.607	80.776	75.084	72.894	397.038	484.927	514.042	535.439	332.779	393.643	385.945	440.204	176.304	351.333	134.285
72.151	95.607	80.848	75.228	72.894	397.184	484.998	514.113	535.439	332.852	393.57	386.091	440.132	176.374	351.333	134.215
72.078	95.678	80.848	75.228	72.894	397.184	484.927	513.971	535.439	332.779	393.643	386.091	440.204	176.374	351.333	134.285
72.212	95.668	80.91	75.073	72.884	397.1	484.845	513.961	535.429	332.695	393.632	386.008	440.194	176.294	351.177	134.275
72.129	95.657	80.755	75.135	72.873	397.09	484.906	513.95	535.418	332.758	393.694	385.997	440.111	176.284	351.239	134.265
72.151	95.678	80.92	75.301	72.894	397.111	484.927	514.042	535.368	332.852	393.643	386.018	440.277	176.234	351.187	134.215
72.151	95.607	80.776	75.156	72.894	397.111	484.998	514.113	535.439	332.779	393.715	386.091	440.204	176.374	351.26	134.215
72.161	95.617	80.859	75.167	72.905	397.122	485.08	514.124	535.449	332.789	393.653	386.175	440.287	176.314	351.344	134.225
72.151	95.678	80.776	75.228	72.894	397.184	485.07	514.042	535.439	332.852	393.643	386.091	440.204	176.304	351.26	134.215
72.223	95.607	80.848	75.156	72.822	397.184	485.07	514.113	535.439	332.852	393.715	386.091	440.132	176.374	351.187	134.215
72.089	95.617	80.859	75.167	72.832	397.267	484.937	514.124	535.52	332.789	393.653	386.029	440.215	176.314	351.271	134.225
72.068	95.596	80.838	75.218	72.884	397.173	485.059	514.103	535.5	332.768	393.632	386.008	440.194	176.224	351.25	134.205
72.068	95.668	80.838	75.146	72.811	397.1	484.988	514.032	535.429	332.768	393.632	386.008	440.121	176.294	351.323	134.134
72.14	95.525	80.838	75.146	72.811	397.173	484.988	514.032	535.429	332.768	393.632	386.008	440.194	176.364	351.323	134.205
72.089	95.689	80.931	75.167	72.905	397.195	485.009	514.124	535.591	332.935	393.726	386.029	440.215	176.314	351.198	134.155
72.151	95.678	80.776	75.084	72.822	397.257	484.998	514.113	535.581	332.852	393.788	386.091	440.204	176.304	351.333	134.215
72.14	95.596	80.838	75.146	72.956	397.173	484.916	514.174	535.5	332.841	393.632	386.08	440.121	176.294	351.25	134.205
72.151	95.75	80.92	75.156	72.967	397.257	484.927	514.042	535.51	332.852	393.643	386.091	440.349	176.444	351.187	134.285
72.223	95.678	80.848	75.156	72.749	397.33	485.07	514.113	535.51	332.852	393.788	386.091	440.204	176.304	351.333	134.215
72.151	95.678	80.776	75.156	72.894	397.257	484.998	514.184	535.581	332.924	393.715	386.018	440.204	176.304	351.333	134.145
72.212	95.668	80.766	75.146	72.956	397.246	485.059	514.103	535.5	332.841	393.632	386.08	440.194	176.294	351.25	134.205

Table **E-10**: Test 913, 30 seconds to Steady State Output for data marker '18', Probe at 9" into the Heated Length, Continued

111	112	113	114	115	116	117	118	119	120	121	122	123	124	125	126
Side out=outer side insulation				Heater Output						Absolute Pressure					
SIDE OUT 40"	Top Inner HL	Top Outer HL		Max Watts	H1 Volts	H1 Watts	H2 Volts	H2 Watts		Location	Max Psi	Abs P Volts	Abs P Psi		Location
294.851	209.288	93.121	-99999	6000	0.577	346.399	0.574	344.164	-99999	0	30	6.656	20.05	-99999	0
294.913	209.207	93.11	-99999	6000	0.577	346.399	0.574	344.164	-99999	0	30	6.656	20.051	-99999	0
294.923	209.076	93.049	-99999	6000	0.577	346.399	0.574	344.359	-99999	0	30	6.656	20.05	-99999	0
294.996	209.217	93.121	-99999	6000	0.58	347.956	0.574	344.359	-99999	0	30	6.656	20.051	-99999	0
295.068	209.217	93.049	-99999	6000	0.578	346.788	0.573	343.97	-99999	0	30	6.657	20.052	-99999	0
294.985	209.348	93.11	-99999	6000	0.577	346.204	0.574	344.359	-99999	0	30	6.656	20.051	-99999	0
294.923	209.358	93.121	-99999	6000	0.577	346.399	0.574	344.359	-99999	0	30	6.656	20.05	-99999	0
294.851	209.358	93.049	-99999	6000	0.577	346.399	0.573	343.97	-99999	0	30	6.656	20.051	-99999	0
294.934	209.228	92.988	-99999	6000	0.58	347.956	0.573	343.97	-99999	0	30	6.657	20.052	-99999	0
294.923	209.217	93.049	-99999	6000	0.577	346.399	0.573	343.97	-99999	0	30	6.657	20.052	-99999	0
294.996	209.217	93.049	-99999	6000	0.577	346.399	0.574	344.164	-99999	0	30	6.656	20.05	-99999	0
295.068	209.288	92.977	-99999	6000	0.579	347.372	0.574	344.164	-99999	0	30	6.657	20.052	-99999	0
294.913	209.207	93.11	-99999	6000	0.58	347.956	0.576	345.528	-99999	0	30	6.656	20.051	-99999	0
294.902	209.197	92.957	-99999	6000	0.58	347.956	0.577	345.917	-99999	0	30	6.656	20.05	-99999	0
294.923	209.288	92.906	-99999	6000	0.58	347.762	0.576	345.528	-99999	0	30	6.656	20.05	-99999	0
294.996	209.217	92.977	-99999	6000	0.58	348.151	0.574	344.359	-99999	0	30	6.657	20.052	-99999	0
294.934	209.298	92.988	-99999	6000	0.58	348.151	0.574	344.164	-99999	0	30	6.656	20.05	-99999	0
294.923	209.358	92.906	-99999	6000	0.58	348.151	0.577	345.917	-99999	0	30	6.656	20.051	-99999	0
294.996	209.358	92.977	-99999	6000	0.58	348.151	0.577	346.112	-99999	0	30	6.656	20.051	-99999	0
295.006	209.368	92.845	-99999	6000	0.581	348.54	0.576	345.722	-99999	0	30	6.657	20.052	-99999	0
294.913	209.207	92.824	-99999	6000	0.58	347.956	0.576	345.722	-99999	0	30	6.656	20.051	-99999	0
294.841	209.207	92.895	-99999	6000	0.58	347.956	0.576	345.528	-99999	0	30	6.656	20.051	-99999	0
294.913	209.207	92.824	-99999	6000	0.578	346.593	0.574	344.359	-99999	0	30	6.657	20.052	-99999	0
294.934	209.298	92.845	-99999	6000	0.577	346.399	0.574	344.164	-99999	0	30	6.656	20.051	-99999	0
295.068	209.358	92.763	-99999	6000	0.58	347.956	0.574	344.359	-99999	0	30	6.656	20.051	-99999	0
294.913	209.489	92.824	-99999	6000	0.58	348.151	0.574	344.164	-99999	0	30	6.656	20.051	-99999	0
294.923	209.358	92.834	-99999	6000	0.58	347.956	0.574	344.359	-99999	0	30	6.656	20.051	-99999	0
294.923	209.358	92.763	-99999	6000	0.577	346.399	0.574	344.164	-99999	0	30	6.656	20.051	-99999	0
294.923	209.288	92.834	-99999	6000	0.577	346.399	0.574	344.164	-99999	0	30	6.656	20.051	-99999	0
294.841	209.277	92.824	-99999	6000	0.578	346.593	0.574	344.164	-99999	0	30	6.657	20.051	-99999	0

Table **E-11**: Test 913, 30 seconds to Steady State Output for data marker '18', Probe at 9" into the Heated Length, Continued

127	128	129	130	131	132	133	134	135	136	137	138	139	140	141	142	143
Delta Pressure					Flow Meter											
Max inches H2O	DP Volts	DP Inches	DP Cell		Frequency			Flow ACFM	Interp.Err.			Data Point		Elevation		Inlet Temp (F)
1.67	1.808	-0.001	2	-99999	991.117	-99999	0	1.823	0	2	-99999	0	-99999	0	-99999	72.816
1.67	1.808	-0.001	2	-99999	1001.515	-99999	0	1.842	0	2	-99999	0	-99999	0	-99999	72.889
1.67	1.808	-0.001	2	-99999	1005.404	-99999	0	1.849	0	2	-99999	0	-99999	0	-99999	72.744
1.67	1.808	-0.001	2	-99999	1005.568	-99999	0	1.849	0	2	-99999	0	-99999	0	-99999	72.899
1.67	1.808	-0.001	2	-99999	1007.468	-99999	0	1.853	0	2	-99999	0	-99999	0	-99999	72.91
1.67	1.808	-0.001	2	-99999	1007.62	-99999	0	1.853	0	2	-99999	0	-99999	0	-99999	72.889
1.67	1.808	-0.001	2	-99999	990.7	-99999	0	1.822	0	2	-99999	0	-99999	0	-99999	72.827
1.67	1.808	-0.001	2	-99999	992.1	-99999	0	1.825	0	2	-99999	0	-99999	0	-99999	72.889
1.67	1.809	-0.001	2	-99999	1005.379	-99999	0	1.849	0	2	-99999	0	-99999	0	-99999	72.899
1.67	1.809	-0.001	2	-99999	996.239	-99999	0	1.832	0	2	-99999	0	-99999	0	-99999	72.899
1.67	1.808	-0.001	2	-99999	993.456	-99999	0	1.827	0	2	-99999	0	-99999	0	-99999	72.899
1.67	1.808	-0.001	2	-99999	992.002	-99999	0	1.824	0	2	-99999	0	-99999	0	-99999	72.806
1.67	1.809	-0.001	2	-99999	1006.859	-99999	0	1.852	0	2	-99999	0	-99999	0	-99999	72.816
1.67	1.808	-0.001	2	-99999	991.056	-99999	0	1.823	0	2	-99999	0	-99999	0	-99999	72.827
1.67	1.808	-0.001	2	-99999	1005.556	-99999	0	1.849	0	2	-99999	0	-99999	0	-99999	72.899
1.67	1.808	-0.001	2	-99999	1005.202	-99999	0	1.849	0	2	-99999	0	-99999	0	-99999	72.816
1.67	1.808	-0.001	2	-99999	992.63	-99999	0	1.826	0	2	-99999	0	-99999	0	-99999	72.889
1.67	1.808	-0.001	2	-99999	995.062	-99999	0	1.83	0	2	-99999	0	-99999	0	-99999	72.827
1.67	1.808	-0.001	2	-99999	996.872	-99999	0	1.833	0	2	-99999	0	-99999	0	-99999	72.816
1.67	1.809	-0.001	2	-99999	993.739	-99999	0	1.828	0	2	-99999	0	-99999	0	-99999	72.816
1.67	1.808	-0.001	2	-99999	999.813	-99999	0	1.839	0	2	-99999	0	-99999	0	-99999	72.889
1.67	1.808	-0.001	2	-99999	1005.088	-99999	0	1.848	0	2	-99999	0	-99999	0	-99999	72.816
1.67	1.808	-0.001	2	-99999	995.136	-99999	0	1.83	0	2	-99999	0	-99999	0	-99999	72.889
1.67	1.808	-0.001	2	-99999	990.271	-99999	0	1.821	0	2	-99999	0	-99999	0	-99999	72.816
1.67	1.808	-0.001	2	-99999	994.58	-99999	0	1.829	0	2	-99999	0	-99999	0	-99999	72.816
1.67	1.808	-0.001	2	-99999	1005.366	-99999	0	1.849	0	2	-99999	0	-99999	0	-99999	72.816
1.67	1.808	-0.001	2	-99999	992.063	-99999	0	1.825	0	2	-99999	0	-99999	0	-99999	72.816
1.67	1.808	-0.001	2	-99999	998.739	-99999	0	1.837	0	2	-99999	0	-99999	0	-99999	72.816
1.67	1.808	-0.001	2	-99999	999.55	-99999	0	1.838	0	2	-99999	0	-99999	0	-99999	72.827
1.67	1.808	-0.001	2	-99999	995.26	-99999	0	1.83	0	2	-99999	**18**	-99999	0	-99999	72.827

E.3 MatLab Input Files

The MatLab data reduction code required 3 input files: the binary run file with data taken every second, a velocity profile input file, and a fluid properties input file.

The binary input was described in the last section. The velocity profile data file from Fluent was formatted as an Excel file and input into the data reduction code. A sample from the test 913 velocity profile input file is given in Table **E-12**. The left-hand column represents the lateral position in meters. The right-hand column represents the fluid velocity in meters/second. The velocity profiles were calculated at all the same axial locations as the wall thermocouple placements.

The fluid property input file was also formatted as an Excel file. Nitrogen data from the NIST Chemistry Web-Book (http://webbook.nist.gov/chemistry/fluid/) was used. The pressure was held constant at 14.0 psia which is the nominal atmospheric pressure for the laboratory location in State College, PA. The fluid property input file is given in Table **E-13**. All fluid property data was spline interpolated by temperature to attain the values used in the data analysis.

Table **E-12**: Velocity Profile Input File for Test Run 913, at an Axial Position of 45 inches into the Heated Length

(title "Velocity Magnitude")
(labels "Position" "Velocity Magnitude")

((xy/key/label "aa-forty-five")		
0.009398	0	
0.009144	0.499278	
0.00889	0.959754	
0.008636	1.38169	
0.008382	1.76501	
0.008128	2.1097	
0.007874	2.41579	
0.00762	2.68334	
0.007366	2.91242	
0.007112	3.10313	
0.006858	3.25556	
0.006604	3.36979	
0.00635	3.44591	
0.006096	3.48396	
0.005842	3.48396	
0.005588	3.44591	
0.005334	3.36979	
0.00508	3.25556	
0.004826	3.10313	
0.004572	2.91242	
0.004318	2.68334	
0.004064	2.41579	
0.00381	2.1097	
0.003556	1.76501	
0.003302	1.38169	
0.003048	0.959753	
0.002794	0.499279	
0.00254	0	

Table **E-13**: Nitrogen Property Data Input File @ 14.0 psia

Temperature (F)	Pressure (psia)	Density (lbm/ft3)	Volume (ft3/lbm)	Internal Energy (Btu/lbm)	Enthalpy (Btu/lbm)	Entropy (Btu/lbm*R)	Cv (Btu/lbm*R)	Cp (Btu/lbm*R)	Sound Spd. (ft/s)	Joule-Thomson (F/psia)	Viscosity (lbm/ft*s)	Therm. Cond. (W/m*K)	Phase
40	14.0	0.07317	13.667	88.42	123.85	1.6193	0.1776	0.2489	1114.5	0.03105	1.13E-05	0.02434	vapor
100	14.0	0.06530	15.313	99.08	138.78	1.6476	0.1777	0.2489	1179.5	0.02429	1.24E-05	0.02658	vapor
160	14.0	0.05897	16.958	109.75	153.72	1.6729	0.1779	0.2491	1241.0	0.01905	1.34E-05	0.02874	vapor
220	14.0	0.05376	18.602	120.44	168.67	1.6960	0.1783	0.2494	1299.3	0.01488	1.43E-05	0.03083	vapor
280	14.0	0.04939	20.246	131.16	183.65	1.7171	0.1789	0.2500	1354.9	0.01148	1.52E-05	0.03287	vapor
340	14.0	0.04569	21.889	141.92	198.67	1.7366	0.1797	0.2507	1407.9	0.00867	1.61E-05	0.03486	vapor
400	14.0	0.04250	23.532	152.73	213.74	1.7548	0.1807	0.2517	1458.6	0.00631	1.70E-05	0.03683	vapor
460	14.0	0.03972	25.175	163.61	228.88	1.7718	0.1819	0.2529	1507.2	0.00432	1.78E-05	0.03878	vapor
520	14.0	0.03729	26.818	174.57	244.09	1.7878	0.1833	0.2543	1553.9	0.00261	1.86E-05	0.04071	vapor
580	14.0	0.03514	28.461	185.61	259.39	1.8030	0.1848	0.2558	1598.8	0.00114	1.94E-05	0.04263	vapor
640	14.0	0.03322	30.103	196.75	274.79	1.8174	0.1865	0.2575	1642.2	-0.00013	2.01E-05	0.04454	vapor
700	14.0	0.03150	31.745	208.00	290.30	1.8311	0.1883	0.2593	1684.2	-0.00123	2.09E-05	0.04644	vapor
760	14.0	0.02995	33.388	219.36	305.91	1.8442	0.1902	0.2612	1724.8	-0.00220	2.16E-05	0.04834	vapor
820	14.0	0.02855	35.030	230.83	321.64	1.8568	0.1921	0.2631	1764.3	-0.00305	2.23E-05	0.05022	vapor
880	14.0	0.02727	36.672	242.41	337.48	1.8689	0.1940	0.2650	1802.8	-0.00379	2.30E-05	0.05209	vapor
940	14.0	0.02610	38.315	254.11	353.44	1.8806	0.1960	0.2669	1840.2	-0.00445	2.37E-05	0.05395	vapor
1000	14.0	0.02503	39.957	265.93	369.51	1.8918	0.1979	0.2689	1876.8	-0.00504	2.44E-05	0.05580	vapor
1060	14.0	0.02404	41.599	277.86	385.70	1.9027	0.1998	0.2708	1912.6	-0.00556	2.50E-05	0.05763	vapor

E.4 MatLab Gross Reduced Output Files (a.k.a. Time Averaged Output)

The gross reduced output files from MatLab contain the time averaged data for each data marker. Looking back to Table **E-3** thru Table **E-11**, which contain the 30 seconds of data at data marker 18, the gross reduced output file time averages the 30 rows prior to the '18' data marker row, into a single row. This means that the entire output file for a test is reduced to a total of 25 time averaged rows, each representing a data marker. Table **E-14** thru **E-22** gives the gross reduced output file for test 913.

Table **E-14**: Time Averaged Output File for Test 913

Column #	1	2	3	4	5	6	7	8	9	10	11	12	13	14
							CW = center Wall							
	Version		Time		Time SS		47.9	45	42.5	40	37.5	35	32.5	30
							CW 20	CW 19	CW 18	CW 17	CW 16	CW 15	CW 14	CW 13
	1.4	-99999	3909.5	-99999	30	-99999	532.75	545.05	546.49	541.06	529.53	515.16	498.2	479.78
	1.4	-99999	3978.5	-99999	30	-99999	532.94	545.15	546.6	541.15	529.63	515.28	498.32	479.9
	1.4	-99999	4051.5	-99999	30	-99999	533.07	545.28	546.72	541.28	529.75	515.37	498.43	480.02
	1.4	-99999	4112.5	-99999	30	-99999	533.18	545.4	546.81	541.38	529.87	515.47	498.53	480.11
	1.4	-99999	4175.5	-99999	30	-99999	533.33	545.52	546.92	541.51	529.99	515.6	498.63	480.24
	1.4	-99999	4253.5	-99999	30	-99999	533.52	545.67	547.05	541.66	530.12	515.73	498.78	480.4
	1.4	-99999	4352.5	-99999	30	-99999	533.71	545.82	547.24	541.83	530.3	515.92	498.95	480.59
	1.4	-99999	4596.5	-99999	30	-99999	536.47	545.64	547.61	542.28	530.74	516.36	499.37	481.03
	1.4	-99999	4740.5	-99999	30	-99999	537.19	546.25	546.92	542.45	530.96	516.61	499.64	481.3
	1.4	-99999	4940.5	-99999	30	-99999	538.41	547.3	547.53	541.4	531.29	517.01	500.05	481.74
	1.4	-99999	5090.5	-99999	30	-99999	539.05	548.08	548.16	542.07	530.31	517.25	500.39	482.05
	1.4	-99999	5281.5	-99999	30	-99999	539.7	548.84	549.22	543.15	530.87	515.99	500.64	482.44
	1.4	-99999	5415.5	-99999	30	-99999	539.92	549.41	549.81	543.93	531.5	516.51	499.7	482.67
	1.4	-99999	5582.5	-99999	30	-99999	537.73	549.87	550.48	544.71	532.66	517.62	500.46	479.8
	1.4	-99999	5761.5	-99999	30	-99999	535.76	549.86	551.01	545.38	533.5	518.83	501.69	483.12
	1.4	-99999	6042.5	-99999	30	-99999	534.55	549.53	551.34	546.09	534.5	519.94	503.04	484.82
	1.4	-99999	6217.5	-99999	30	-99999	535.34	549.52	551.75	546.65	534.94	520.59	503.81	485.57
	1.4	-99999	6397.5	-99999	30	-99999	535.47	549.41	551.96	547.14	535.63	521.07	504.3	486.22
	1.4	-99999	6599.5	-99999	30	-99999	534.99	550.04	551.86	547.49	536.15	521.83	504.72	486.68
	1.4	-99999	6798.5	-99999	30	-99999	535.81	550.39	552.74	547.04	536.53	522.32	505.56	487.18
	1.4	-99999	6968.5	-99999	30	-99999	536.23	550.83	553.17	548.06	536.26	522.71	505.95	487.72
	1.4	-99999	7153.5	-99999	30	-99999	536.47	551.31	553.74	548.75	537.01	522.62	506.31	488.17
	1.4	-99999	7307.5	-99999	30	-99999	537.15	551.62	554.15	549.31	537.69	522.87	506.41	488.5
	1.4	-99999	7314.5	-99999	30	-99999	537.18	551.62	554.17	549.33	537.72	522.87	506.41	488.5
	1.4	-99999	7690.5	-99999	30	-99999	536.03	551.23	553.6	548.59	536.93	522.51	505.88	487.85

Table **E-15**: Gross Reduced Output File for Test 913, Continued

15	16	17	18	19	20	21	22	23	24	25	26	27	28	29	30
											SW = Side Wall				
27.5	25	20	15	10	8	6	4	2	0.1		47.9	45	42.5	40	37.5
CW 12	CW 11	CW 10	CW 09	CW 08	CW 07	CW 06	CW 05	CW 04	CW 03		SW 39	SW 38	SW 37	SW 36	SW 34
459.83	438.73	392.59	343.35	292.03	267.13	242.82	217.6	192.19	167.72	-99999	536.24	544.62	546.25	541.26	530.28
459.93	438.84	392.69	343.41	292.22	267.32	242.99	217.71	192.24	167.71	-99999	536.28	544.64	546.29	541.31	530.31
460.07	438.93	392.81	343.51	292.43	267.49	243.19	217.86	192.31	167.71	-99999	536.33	544.7	546.33	541.35	530.38
460.17	439.03	392.89	343.61	292.62	267.66	243.33	217.95	192.34	167.72	-99999	536.41	544.75	546.38	541.37	530.42
460.27	439.12	393.01	343.7	292.82	267.83	243.46	218.07	192.4	167.74	-99999	536.47	544.79	546.45	541.47	530.49
460.42	439.29	393.14	343.83	293.08	268.04	243.65	218.23	192.48	167.78	-99999	536.56	544.9	546.53	541.53	530.57
460.6	439.46	393.31	343.99	293.36	268.31	243.9	218.38	192.6	167.82	-99999	536.67	545.01	546.63	541.66	530.71
461.06	439.92	393.77	344.41	294.07	268.93	244.48	218.85	192.87	167.95	-99999	537.39	545.09	546.94	541.98	531.03
461.35	440.2	394.04	344.6	294.46	269.31	244.81	219.1	193.05	168.07	-99999	537.84	545.13	546.87	542.15	531.23
461.76	440.61	394.46	345.05	295	269.82	245.25	219.47	193.3	168.24	-99999	538.55	545.67	546.66	541.93	531.5
462.11	440.91	394.76	345.36	295.39	270.18	245.58	219.76	193.52	168.36	-99999	539.06	546.13	546.94	541.68	531.31
462.5	441.37	395.18	345.8	295.88	270.63	246.01	220.08	193.76	168.54	-99999	539.66	546.68	547.57	542.06	530.87
462.78	441.68	395.51	346.08	296.23	270.94	246.3	220.33	193.95	168.68	-99999	540.03	547.07	547.97	542.53	531.11
462.82	442.01	395.89	346.46	296.65	271.35	246.66	220.66	194.19	168.85	-99999	540.33	547.47	548.41	543.03	531.7
463.62	438.57	396.25	346.86	297.06	271.74	247.02	220.96	194.45	169.01	-99999	540.37	547.8	548.81	543.47	532.24
464.77	443.2	391.08	347.38	297.66	272.29	247.56	221.4	194.79	169.3	-99999	540.19	548	549.33	544.09	532.94
465.57	444.22	396.03	343.46	298.05	272.67	247.89	221.68	195.04	169.47	-99999	540.11	548.09	549.6	544.47	533.35
466.3	444.94	397.61	347.39	297.14	272.94	248.22	221.98	195.25	169.64	-99999	540.16	548.18	549.82	544.83	533.8
466.91	445.62	398.66	348.64	294.27	271.62	248.42	222.29	195.53	169.84	-99999	540.21	548.33	550.09	545.19	534.25
467.4	446.24	399.46	349.48	297.41	269.05	247.11	222.43	195.75	170.03	-99999	540.37	548.56	550.33	545.48	534.67
467.82	446.71	400.04	350.04	298.35	271.82	245.04	221.43	195.84	170.19	-99999	540.63	548.8	550.61	545.73	534.93
468.32	447.19	400.6	350.56	299.27	272.96	247.39	218.53	194.81	170.18	-99999	540.89	549.08	550.94	546.09	535.2
468.63	447.61	401.12	351.02	299.88	273.7	248.13	221.14	192.11	168.99	-99999	541.11	549.35	551.25	546.4	535.49
468.64	447.61	401.14	351.04	299.9	273.72	248.17	221.19	192.05	168.91	-99999	541.12	549.36	551.26	546.43	535.51
468.03	446.95	400.77	350.92	300.12	274.14	248.75	222	195	169.32	-99999	541.65	550.3	552.29	547.44	536.5

Table **E-16**: Gross Reduced Output File for Test 913, Continued

31	32	33	34	35	36	37	38	39	40	41	42	43	44	45	46
														CR = Center Redundant	
35	32.5	30	27.5	25	20	15	10	8	6	4	2	0.1			
SW 33	SW 32	SW 31	SW 30	SW 29	SW 28	SW 27	SW 26	SW 25	SW 24	SW 23	SW 22	SW 21		CR 50	CR 49
516.54	500.75	482.31	461.57	440.26	393.82	344.79	293.11	269.29	244.81	219.96	195.87	173.52	-99999	530.47	545.24
516.57	500.76	482.34	461.59	440.27	393.81	344.79	293.15	269.35	244.88	220.02	195.86	173.49	-99999	530.58	545.33
516.61	500.8	482.39	461.65	440.31	393.85	344.79	293.23	269.45	244.99	220.07	195.88	173.46	-99999	530.7	545.44
516.67	500.87	482.44	461.68	440.35	393.91	344.82	293.28	269.53	245.06	220.12	195.88	173.44	-99999	530.74	545.52
516.7	500.93	482.5	461.76	440.42	393.93	344.83	293.38	269.64	245.17	220.19	195.91	173.43	-99999	530.85	545.6
516.81	500.99	482.59	461.84	440.5	394.03	344.88	293.5	269.78	245.3	220.28	195.93	173.42	-99999	530.97	545.72
516.91	501.1	482.71	461.97	440.63	394.14	344.99	293.68	269.97	245.47	220.41	196.03	173.42	-99999	531.1	545.87
517.23	501.45	483.06	462.33	440.97	394.45	345.29	294.16	270.42	245.92	220.77	196.2	173.5	-99999	534.44	545.61
517.46	501.68	483.3	462.56	441.23	394.7	345.52	294.46	270.73	246.21	220.99	196.35	173.58	-99999	535.14	545.94
517.77	502.02	483.68	462.94	441.57	395.08	345.88	294.9	271.2	246.6	221.33	196.56	173.73	-99999	536.12	546.98
517.99	502.27	483.94	463.23	441.87	395.37	346.15	295.25	271.54	246.93	221.58	196.74	173.84	-99999	536.35	547.72
517.66	502.55	484.29	463.6	442.25	395.76	346.57	295.71	271.99	247.31	221.92	196.98	174	-99999	537	548.48
517.28	502.36	484.53	463.89	442.56	396.04	346.84	296.03	272.29	247.61	222.15	197.16	174.16	-99999	537.28	549.02
517.66	501.98	483.73	464.12	442.92	396.39	347.22	296.41	272.65	247.96	222.45	197.38	174.34	-99999	535.82	549.61
518.28	502.52	484.26	463.84	441.93	396.73	347.58	296.79	273.04	248.32	222.74	197.62	174.5	-99999	534.33	549.33
519.08	503.35	485.17	464.48	442.92	395.45	348.12	297.42	273.64	248.84	223.21	197.99	174.81	-99999	534.99	549.58
519.53	503.83	485.67	464.97	443.54	396.1	347.23	297.75	273.98	249.16	223.48	198.18	174.96	-99999	529.78	549.77
519.96	504.27	486.1	465.46	444.06	396.89	347.58	297.7	274.29	249.49	223.76	198.42	175.17	-99999	535.29	549.45
520.48	504.75	486.61	465.98	444.59	397.64	348.18	296.57	274.02	249.73	224.05	198.69	175.37	-99999	536.6	550.39
520.95	505.22	487.07	466.48	445.12	398.28	348.79	296.94	272.88	249.45	224.26	198.9	175.57	-99999	537.08	551.04
521.31	505.66	487.48	466.88	445.54	398.77	349.31	297.39	273.13	248.42	224.02	199.03	175.71	-99999	537.16	551.49
521.61	506.08	487.92	467.33	446.01	399.28	349.81	297.99	273.63	248.59	222.94	198.74	175.75	-99999	537.25	551.78
521.82	506.33	488.26	467.69	446.39	399.69	350.19	298.49	274.16	248.92	223.05	197.82	175.26	-99999	537.38	552.07
521.84	506.35	488.28	467.71	446.4	399.71	350.21	298.51	274.17	248.94	223.06	197.79	175.22	-99999	537.37	552.09
522.73	507.18	489.09	468.53	447.27	400.73	351.18	299.6	275.34	250.05	223.98	198.47	175.17	-99999	534.29	551.45

Table **E-17**: Gross Reduced Output File for Test 913, Continued

47	48	49	50	51	52	53	54	55	56	57	58	59	60	61	62
									SR = Side Redundant						
CR 48	CR 47	CR 46	CR 45	CR 44	CR 43	CR 42	CR 41	CR 40		SR 61	SR 60	SR 59	SR 58	SR 57	SR 56
541.84	515.95	481.63	439.61	391.42	342.74	288.06	214.51	167.95	-99999	536.8	545.62	542.22	517.72	484.58	441.5
541.93	516.03	481.72	439.7	391.51	342.82	288.16	214.6	167.92	-99999	536.81	545.61	542.21	517.7	484.59	441.5
542.06	516.11	481.81	439.77	391.62	342.89	288.26	214.7	167.92	-99999	536.85	545.63	542.25	517.72	484.62	441.52
542.14	516.2	481.9	439.88	391.72	342.98	288.37	214.8	167.93	-99999	536.88	545.65	542.31	517.75	484.66	441.57
542.24	516.28	481.98	439.97	391.83	343.06	288.48	214.9	167.93	-99999	536.93	545.7	542.34	517.81	484.73	441.63
542.38	516.41	482.13	440.09	391.97	343.2	288.63	215.02	167.97	-99999	537	545.77	542.43	517.86	484.79	441.72
542.53	516.56	482.27	440.24	392.14	343.35	288.82	215.17	167.96	-99999	537.09	545.88	542.54	517.97	484.89	441.83
542.93	516.96	482.68	440.62	392.57	343.75	289.27	215.54	168.08	-99999	537.67	545.91	542.82	518.26	485.22	442.18
543.15	517.18	482.95	440.92	392.82	344.02	289.6	215.77	168.16	-99999	538.1	545.93	543.02	518.46	485.46	442.39
542.1	517.54	483.33	441.3	393.26	344.44	290.04	216.08	168.31	-99999	538.76	546.47	542.77	518.79	485.8	442.77
542.54	517.76	483.64	441.65	393.58	344.74	290.38	216.33	168.42	-99999	539.22	546.87	542.68	518.97	486.07	443.04
543.68	516.42	484	442.04	394	345.16	290.81	216.63	168.56	-99999	539.7	547.36	543.23	518.66	486.42	443.44
544.39	516.87	484.23	442.31	394.31	345.42	291.13	216.81	168.7	-99999	540.1	547.73	543.59	518.43	486.65	443.71
544.99	517.8	480.56	442.69	394.68	345.79	291.5	217.11	168.87	-99999	540.55	548.13	543.95	518.88	485.95	444.04
545.87	518.99	484.21	439.58	395.03	346.17	291.9	217.38	169.05	-99999	540.48	548.38	544.25	519.33	486.63	443.2
546.67	520.55	485.93	443.56	391.15	346.74	292.5	217.82	169.31	-99999	540.24	548.59	544.89	520.01	487.33	444.5
546.81	521.14	486.85	444.44	394.62	343.55	292.82	218.11	169.49	-99999	540.02	548.81	545.24	520.47	487.72	444.89
547.37	521.37	487.59	445.14	396.01	346.57	291.94	218.38	169.66	-99999	540.16	548.83	545.52	520.89	488.15	445.25
547.94	521.61	488.15	446.03	396.88	347.68	289.84	218.68	169.84	-99999	540.7	549.11	545.91	521.27	488.66	445.68
546.77	522.11	488.42	446.73	397.62	348.39	292.35	218.8	170.05	-99999	541.08	549.45	546.22	521.66	489.12	446.22
548.73	522.76	488.48	447.08	398.22	348.92	293.09	217.73	170.17	-99999	541.34	549.75	546.48	522.03	489.46	446.65
549.47	522.9	488.73	447.3	398.97	349.41	293.84	215.97	170.13	-99999	541.58	550.07	546.9	522.38	489.8	447.08
549.99	523.18	489.26	447.35	399.46	349.8	294.35	217.53	169.11	-99999	541.82	550.31	547.23	522.64	490.1	447.41
550.01	523.18	489.27	447.36	399.48	349.82	294.37	217.57	169.05	-99999	541.82	550.32	547.25	522.64	490.12	447.42
549.16	522.83	489.07	447.31	399.38	350.02	294.74	218.39	169.38	-99999	541.68	551.14	548.27	523.6	491.05	448.28

Table **E-18**: Gross Reduced Output File for Test 913, Continued

63	64	65	66	67	68	69	70	71	72	73	74	75	76	77	78
						SP = Spacer									
SR 55	SR 54	SR 53	SR 52	SR 51		SP 72	SP 71	SP 70	SP 69	SP 68	SP 67	SP 66	SP 65	SP 64	SP 63
395.81	346.07	292.91	216.75	175.6	-99999	535.65	543.87	541.46	517	483.36	442.02	395.84	345.98	294.48	220.46
395.82	346.05	292.93	216.78	175.53	-99999	535.58	543.81	541.43	516.96	483.36	441.96	395.79	345.91	294.46	220.47
395.86	346.08	292.99	216.84	175.5	-99999	535.57	543.79	541.42	516.96	483.33	441.97	395.79	345.86	294.46	220.49
395.87	346.1	293.02	216.9	175.46	-99999	535.57	543.79	541.44	516.97	483.38	441.97	395.78	345.87	294.49	220.53
395.91	346.15	293.12	216.97	175.46	-99999	535.6	543.83	541.46	517.01	483.4	442.01	395.79	345.88	294.55	220.57
396	346.21	293.21	217.05	175.45	-99999	535.62	543.87	541.51	517.04	483.44	442.05	395.85	345.91	294.62	220.62
396.1	346.3	293.36	217.15	175.44	-99999	535.71	543.93	541.59	517.13	483.56	442.15	395.91	345.96	294.75	220.74
396.47	346.63	293.79	217.46	175.52	-99999	536.26	544.03	541.87	517.41	483.87	442.45	396.2	346.22	295.12	221.03
396.69	346.85	294.06	217.67	175.59	-99999	536.57	544.04	542.02	517.61	484.09	442.67	396.43	346.43	295.37	221.23
397.05	347.22	294.49	217.94	175.72	-99999	537.14	544.41	541.99	517.91	484.39	443.02	396.76	346.75	295.77	221.54
397.34	347.49	294.8	218.16	175.81	-99999	537.55	544.74	541.85	518.09	484.67	443.3	397.03	347.01	296.09	221.78
397.73	347.91	295.25	218.47	175.99	-99999	538.12	545.22	542.11	517.98	485	443.66	397.4	347.4	296.51	222.06
398.01	348.18	295.55	218.7	176.11	-99999	538.47	545.56	542.35	517.77	485.22	443.92	397.67	347.67	296.79	222.28
398.36	348.55	295.93	219	176.29	-99999	538.89	545.98	542.73	517.97	484.25	444.25	398.02	348.02	297.2	222.6
398.73	348.92	296.33	219.26	176.47	-99999	539.19	546.37	543.14	518.37	485.21	443.31	398.35	348.41	297.58	222.89
397.52	349.46	296.95	219.71	176.74	-99999	539.3	546.75	543.78	519.03	485.79	444.48	396.74	348.94	298.19	223.32
398.62	348.61	297.27	219.95	176.93	-99999	539.34	546.94	544.16	519.49	486.2	444.91	398.18	347.85	298.55	223.58
399.18	349.54	297.25	220.22	177.12	-99999	539.39	547.01	544.49	519.94	486.65	445.32	398.63	348.82	298.65	223.88
399.69	350.07	296.41	220.54	177.32	-99999	539.53	547.2	544.85	520.39	487.13	445.78	399.18	349.19	297.71	224.16
400.23	350.49	297.15	220.72	177.52	-99999	539.73	547.45	545.18	520.82	487.6	446.29	399.73	349.63	298.27	224.37
400.66	350.8	297.52	220.5	177.67	-99999	539.96	547.68	545.45	521.17	487.97	446.74	400.21	350.04	298.55	224.28
401.19	351.21	297.96	219.61	177.67	-99999	540.23	547.96	545.78	521.52	488.39	447.2	400.72	350.51	298.93	223.31
401.61	351.54	298.28	219.94	177.24	-99999	540.43	548.22	546.1	521.78	488.68	447.58	401.14	350.89	299.33	223.62
401.63	351.56	298.3	219.95	177.21	-99999	540.45	548.23	546.12	521.79	488.71	447.59	401.16	350.91	299.34	223.62
402.66	352.45	299.08	220.53	177.15	-99999	540.65	549	547.04	522.65	489.57	448.47	402.19	351.86	300.3	224.19

Table **E-19**: Gross Reduced Output File for Test 913, Continued

79	80	81	82	83	84	85	86	87	88	89	90	91	92	93	94
		PR = Probes							Insulation: TWC=Thin wall center						
SP 62		PR 1	PR 2	PR 3	PR 4	PR 5	PR 6		Support T	Support B	TWC - 2"	TWC - 4"	TWC - 6"	TWC - 8"	TWC - 12"
175.71	-99999	501.23	496.56	502.07	507.47	501.75	505.89	-99999	79.583	79.3	95.666	80.908	75.007	73.156	72.378
175.63	-99999	501.25	496.54	502.07	507.51	501.77	505.9	-99999	79.586	79.293	95.667	80.889	75.015	73.154	72.359
175.58	-99999	501.37	496.65	502.15	507.52	501.77	505.9	-99999	79.568	79.275	95.646	80.895	75.011	73.165	72.386
175.55	-99999	501.44	496.7	502.22	507.52	501.75	505.91	-99999	79.564	79.28	95.649	80.884	75.002	73.18	72.353
175.51	-99999	501.5	496.76	502.28	507.55	501.78	505.94	-99999	79.558	79.277	95.617	80.868	75.001	73.162	72.362
175.48	-99999	501.6	496.87	502.38	507.64	501.86	506.02	-99999	79.567	79.272	95.598	80.856	74.998	73.154	72.39
175.5	-99999	501.75	497	502.52	507.75	501.97	506.1	-99999	79.562	79.254	95.58	80.86	75.002	73.178	72.368
175.55	-99999	497.81	490.95	494.65	503.7	496.66	499.25	-99999	79.562	79.26	95.49	80.75	74.921	73.101	72.318
175.62	-99999	479.34	473.27	486.05	486.73	478.99	490.5	-99999	79.515	79.227	95.456	80.722	74.898	73.064	72.288
175.75	-99999	459.5	453.7	473.2	468.29	460.23	475.58	-99999	79.5	79.214	95.467	80.724	74.902	73.101	72.33
175.84	-99999	436.79	432	459.55	446.39	438.44	460.17	-99999	79.496	79.193	95.47	80.693	74.869	73.061	72.294
176.03	-99999	412.84	408.77	442.19	422.98	415.25	444.27	-99999	79.496	79.213	95.508	80.729	74.898	73.09	72.314
176.15	-99999	388.86	384.48	420.28	400.07	392.02	420.68	-99999	79.48	79.192	95.552	80.726	74.892	73.101	72.313
176.35	-99999	349.42	345.45	388.76	359.92	351.77	387.3	-99999	79.456	79.163	95.588	80.755	74.921	73.115	72.337
176.52	-99999	294.87	289.8	337.63	304.75	296.41	338.19	-99999	79.431	79.141	95.658	80.806	74.958	73.148	72.379
176.82	-99999	241.17	235.31	284.77	248.99	240.2	283.31	-99999	79.443	79.143	95.61	80.722	74.862	73.056	72.29
177	-99999	188.99	183.35	232.97	195.97	187.22	230.72	-99999	79.431	79.148	95.606	80.684	74.824	72.991	72.235
177.17	-99999	154.68	149.62	198.72	160.16	152.18	194.21	-99999	79.47	79.208	95.558	80.607	74.715	72.931	72.15
177.38	-99999	135.95	132.07	178.92	141.35	133.76	172.8	-99999	79.454	79.168	95.595	80.618	74.726	72.896	72.137
177.56	-99999	119.25	115.77	158.88	123.99	117.22	153.78	-99999	79.513	79.184	95.563	80.562	74.679	72.835	72.076
177.7	-99999	104.48	102.28	140.37	108.29	103.22	134.74	-99999	79.458	79.193	95.594	80.542	74.66	72.842	72.08
177.76	-99999	93.474	91.801	118.61	94.737	92.185	115.07	-99999	79.475	79.161	95.576	80.509	74.617	72.794	72.045
177.44	-99999	84.948	84.443	106.11	84.465	84.059	101.69	-99999	79.468	79.166	95.442	80.471	74.576	72.746	72.016
177.41	-99999	84.918	84.406	106.17	84.415	84.019	101.75	-99999	79.472	79.172	95.441	80.472	74.577	72.745	72.02
177.31	-99999	507.12	502.35	508.3	515.16	509.34	512.5	-99999	79.372	79.089	95.642	80.709	74.836	73.014	72.262

Table **E-20**: Gross Reduced Output File for Test 913, Continued

95	96	97	98	99	100	101	102	103	104	105	106	107	108	109	110
	TWS=Thin Wall Side				HW=Heater wall				OUT=main wall outer insulation				Side in=buried side insulation		
TWC -16"	TWS -2"	TWS -4"	TWS -6"	TWS -8"	HW 10"	HW 20"	HW 30"	HW 40"	OUT 10"	OUT 20"	OUT 30"	OUT 40"	SIDE IN 10"	SIDE IN 40"	SIDE OUT 10"
72.2	95.787	81.162	75.459	73.084	374.03	460.84	492.94	514.84	323.47	381.89	384.43	427.79	178.72	353.09	136.47
72.194	95.763	81.148	75.452	73.079	374.25	461.31	493.42	515.45	322.94	381.55	383.96	427.72	178.28	352.8	136.13
72.18	95.743	81.156	75.443	73.073	374.64	461.93	494	516.16	322.5	381.32	383.55	427.77	178.04	352.53	135.94
72.195	95.734	81.154	75.446	73.095	374.99	462.47	494.54	516.75	322.24	381.22	383.29	427.88	177.78	352.34	135.67
72.201	95.712	81.11	75.455	73.099	375.45	463.13	495.11	517.39	322.06	381.21	383.05	428.03	177.5	352.15	135.45
72.177	95.69	81.119	75.438	73.089	376.13	463.96	495.92	518.21	321.95	381.3	382.81	428.35	177.53	351.98	135.64
72.188	95.667	81.095	75.434	73.112	377.04	465.06	496.94	519.26	321.95	381.54	382.61	428.81	177.69	351.73	135.66
72.184	95.599	80.992	75.353	73.036	379.62	468	499.57	521.89	322.51	382.59	382.45	430.21	177.22	351.4	135.17
72.182	95.562	80.959	75.33	73.03	381.19	469.71	501.09	523.38	323.12	383.4	382.52	431.15	176.13	351.28	133.9
72.177	95.554	80.978	75.356	73.029	383.43	472	503.12	525.33	324.15	384.66	382.73	432.42	175.93	351.14	133.86
72.182	95.554	80.966	75.323	73.001	385.11	473.68	504.57	526.71	325.04	385.66	383.01	433.46	176.34	351.06	134.15
72.194	95.595	80.971	75.332	73.013	387.18	475.69	506.31	528.35	326.21	386.98	383.4	434.64	176.3	351.03	134.07
72.186	95.613	80.966	75.341	73.041	388.6	477.05	507.47	529.41	327.05	387.86	383.71	435.43	176.02	350.98	133.66
72.176	95.644	80.989	75.377	73.033	390.26	478.64	508.82	530.64	328.08	388.95	384.09	436.37	176.01	350.96	133.38
72.163	95.714	81.036	75.388	73.056	392	480.27	510.14	531.88	329.18	390.12	384.56	437.33	176.2	350.98	133.92
72.144	95.693	80.962	75.306	73.003	394.45	482.51	512.04	533.6	330.87	391.8	385.22	438.69	176.27	351.05	134.4
72.139	95.674	80.912	75.227	72.929	395.82	483.76	513.05	534.54	331.84	392.74	385.63	439.44	176.17	351.13	134.01
72.134	95.638	80.83	75.164	72.868	397.14	484.97	514.04	535.45	332.79	393.65	386.05	440.18	176.33	351.26	134.23
72.133	95.656	80.833	75.163	72.862	398.54	486.22	515.06	536.42	333.78	394.63	386.46	440.89	176.46	351.4	134.16
72.113	95.636	80.775	75.087	72.813	399.82	487.36	516.01	537.29	334.71	395.5	386.94	441.59	176.51	351.5	134.03
72.108	95.66	80.763	75.092	72.791	400.82	488.25	516.79	537.98	335.5	396.21	387.28	442.13	176.59	351.67	134.13
72.089	95.61	80.742	75.054	72.751	401.89	489.23	517.57	538.71	336.26	396.92	387.66	442.67	177.08	351.83	134.69
72.082	95.472	80.658	75.001	72.693	402.67	489.95	518.2	539.26	336.84	397.48	387.97	443.11	176.78	351.94	134.03
72.078	95.469	80.649	75	72.699	402.72	489.99	518.23	539.28	336.86	397.51	387.98	443.13	176.77	351.94	134.01
72.125	95.72	80.946	75.285	72.956	404.48	491.64	519.6	540.52	338.25	398.8	388.68	444.09	177.09	352.31	134.42

Table **E-21**: Gross Reduced Output File for Test 913, Continued

111	112	113	114	115	116	117	118	119	120	121	122	123	124	125	126
Side out=outer side insulation				Heater Output						Absolute Pressure					
SIDE OUT 40"	Top Inner HL	Top Outer HL		Max Watts	H1 Volts	H1 Watts	H2 Volts	H2 Watts		Location	Max Psi	Abs P Volts	Abs P Psi		Location
297.11	204.32	90.346	-99999	6000	0.572	343.22	0.56974	341.85	-99999	0	30	6.6449	20.004	-99999	0
296.81	205.46	90.289	-99999	6000	0.5741	344.47	0.57122	342.73	-99999	0	30	6.6466	20.011	-99999	0
296.56	206.09	90.271	-99999	6000	0.5774	346.44	0.57351	344.11	-99999	0	30	6.6482	20.017	-99999	0
296.35	206.28	90.285	-99999	6000	0.5744	344.66	0.57096	342.57	-99999	0	30	6.6494	20.022	-99999	0
296.16	205.69	89.214	-99999	6000	0.5747	344.79	0.57074	342.44	-99999	0	30	6.6505	20.027	-99999	0
295.98	205.61	89.314	-99999	6000	0.5734	344.04	0.57045	342.27	-99999	0	30	6.6517	20.032	-99999	0
295.72	206.07	89.308	-99999	6000	0.5717	343	0.56818	340.91	-99999	0	30	6.653	20.037	-99999	0
295.43	207.47	89.225	-99999	6000	0.5743	344.59	0.57087	342.52	-99999	0	30	6.6557	20.048	-99999	0
295.26	209.56	89.061	-99999	6000	0.5754	345.22	0.57152	342.91	-99999	0	30	6.657	20.054	-99999	0
295.07	212.81	90.272	-99999	6000	0.5783	346.98	0.57367	344.2	-99999	0	30	6.6575	20.056	-99999	0
294.99	212.88	90.008	-99999	6000	0.5799	347.91	0.57592	345.55	-99999	0	30	6.6581	20.058	-99999	0
294.94	212.81	89.797	-99999	6000	0.5795	347.72	0.57515	345.09	-99999	0	30	6.6586	20.06	-99999	0
294.85	213.26	90.826	-99999	6000	0.5787	347.21	0.57414	344.48	-99999	0	30	6.6586	20.06	-99999	0
294.8	208.65	92.893	-99999	6000	0.5728	343.69	0.57059	342.35	-99999	0	30	6.6584	20.06	-99999	0
294.8	209.93	92.658	-99999	6000	0.5691	341.49	0.56617	339.7	-99999	0	30	6.6582	20.059	-99999	0
294.88	209.91	92.799	-99999	6000	0.5786	347.13	0.57408	344.45	-99999	0	30	6.6573	20.055	-99999	0
294.86	210.44	92.606	-99999	6000	0.579	347.41	0.57456	344.74	-99999	0	30	6.6568	20.053	-99999	0
294.94	209.28	92.968	-99999	6000	0.5788	347.27	0.57434	344.61	-99999	0	30	6.6563	20.051	-99999	0
295.09	209.2	92.803	-99999	6000	0.5765	345.92	0.57262	343.57	-99999	0	30	6.6561	20.05	-99999	0
295.13	209.75	92.411	-99999	6000	0.5785	347.11	0.57443	344.66	-99999	0	30	6.6556	20.048	-99999	0
295.28	210.4	91.985	-99999	6000	0.5776	346.57	0.57385	344.31	-99999	0	30	6.6548	20.045	-99999	0
295.38	210.84	91.984	-99999	6000	0.5795	347.7	0.57522	345.13	-99999	0	30	6.6536	20.04	-99999	0
295.49	211.86	92.418	-99999	6000	0.5827	349.64	0.57856	347.14	-99999	0	30	6.6529	20.037	-99999	0
295.49	211.75	92.336	-99999	6000	0.5829	349.71	0.57865	347.19	-99999	0	30	6.6529	20.037	-99999	0
295.75	208.51	91.229	-99999	6000	0.5821	349.24	0.57748	346.49	-99999	0	30	6.6518	20.032	-99999	0

Table **E-22**: Gross Reduced Output File for Test 913, Continued

127	128	129	130	131	132	133	134	135	136	137	138	139	140	141	142	143
Delta Pressure					Flow Meter											
Max inches H2O	DP Volts	DP Inches	DP Cell		Frequency			Flow ACFM	Interp. Err.			Data Point		Elevation		Inlet Temp (F)
1.67	1.9232	0.025614	2	-99999	993.31	-99999	0	1.8269	0.0002051	2	-99999	0	-99999	0	-99999	72.822
1.67	1.8477	0.008224	2	-99999	994.26	-99999	0	1.8286	0.0002058	2	-99999	0	-99999	0	-99999	72.831
1.67	1.8591	0.010848	2	-99999	993.26	-99999	0	1.8268	0.000204	2	-99999	0	-99999	0	-99999	72.792
1.67	1.8705	0.013472	2	-99999	993.86	-99999	0	1.8279	0.000206	2	-99999	0	-99999	0	-99999	72.799
1.67	1.9365	0.028679	2	-99999	993.93	-99999	0	1.828	0.0002062	2	-99999	0	-99999	0	-99999	72.805
1.67	1.9629	0.034765	2	-99999	993.25	-99999	0	1.8268	0.0002054	2	-99999	0.2	-99999	0	-99999	72.822
1.67	2.0794	0.061619	2	-99999	995.07	-99999	0	1.8301	0.0002067	2	-99999	0	-99999	0	-99999	72.835
1.67	1.8078	-0.00096	2	-99999	996.68	-99999	0	1.833	0.000209	2	-99999	0	-99999	0	-99999	72.847
1.67	1.808	-0.00093	2	-99999	995.74	-99999	0	1.8313	0.0002092	2	-99999	0	-99999	0	-99999	72.836
1.67	1.8079	-0.00094	2	-99999	998.02	-99999	0	1.8355	0.0002092	2	-99999	0	-99999	0	-99999	72.806
1.67	1.808	-0.00093	2	-99999	993.39	-99999	0	1.827	0.0002052	2	-99999	0	-99999	0	-99999	72.844
1.67	1.8077	-0.00099	2	-99999	995.59	-99999	0	1.831	0.0002078	2	-99999	0.4	-99999	0	-99999	72.836
1.67	1.8078	-0.00097	2	-99999	994.94	-99999	0	1.8298	0.000207	2	-99999	0	-99999	0	-99999	72.843
1.67	1.8079	-0.00093	2	-99999	997.66	-99999	0	1.8348	0.0002099	2	-99999	0	-99999	0	-99999	72.871
1.67	1.8082	-0.00088	2	-99999	998.12	-99999	0	1.8356	0.0002106	2	-99999	0.5	-99999	0	-99999	72.856
1.67	1.8084	-0.00084	2	-99999	998.97	-99999	0	1.8372	0.0002096	2	-99999	0.53333	-99999	0	-99999	72.844
1.67	1.8081	-0.00089	2	-99999	994.34	-99999	0	1.8287	0.0002071	2	-99999	0.56667	-99999	0	-99999	72.819
1.67	1.8081	-0.00089	2	-99999	998.38	-99999	0	1.8361	0.0002099	2	-99999	0	-99999	0	-99999	72.847
1.67	1.8083	-0.00086	2	-99999	995.48	-99999	0	1.8308	0.000208	2	-99999	0.63333	-99999	0	-99999	72.878
1.67	1.8082	-0.00087	2	-99999	994.58	-99999	0	1.8292	0.0002072	2	-99999	0.66667	-99999	0	-99999	72.88
1.67	1.8082	-0.00088	2	-99999	994.84	-99999	0	1.8297	0.0002081	2	-99999	0	-99999	0	-99999	72.862
1.67	1.808	-0.00093	2	-99999	997.47	-99999	0	1.8345	0.0002094	2	-99999	0	-99999	0	-99999	72.837
1.67	1.8079	-0.00094	2	-99999	997.38	-99999	0	1.8343	0.0002099	2	-99999	0	-99999	0	-99999	72.857
1.67	1.808	-0.00093	2	-99999	996.46	-99999	0	1.8326	0.0002099	2	-99999	1.5667	-99999	0	-99999	72.851
1.67	1.8079	-0.00094	2	-99999	997.68	-99999	0	1.8348	0.0002094	2	-99999	0	-99999	0	-99999	72.9

E.5 Processed Axial Output Files

With the data in a time averaged format as given in Table **E-14** thru Table **E-22** above, the data is then processed using the velocity profile input file and the fluid property data input file. Processed output is given in Table **E-23** thru Table **E-25** for test 913. Each row now represents the center of each axial node along the heated test section length. This is the same axial location where the bulk fluid temperature profiles were taken. However, the wall temperatures and the velocity profiles are axially located at the node ends. Because of this, the wall temperatures and the velocity profiles had to be interpolated to match the axial location of the bulk temperature measurement before the heat transfer calculations could be made. Also, the last four columns of Table **E-23** thru Table **E-25** are post processing done in Excel and would not normally appear in the MatLab output.

Table **E-23**: Processed Axial Output File for Test 913

Node Center (in)	Density1 (ft3/lbm)	Density2 (ft3/lbm)	μ1 (lbm/ft-s)	μ2 (lbm/ft-s)	Cp 1 (Btu/lbm-F)	Cp 2 (Btu/lbm-F)	K1 (Btu/hr-ft-F)	K2 (Btu/hr-ft-F)	bulktemps1	bulktemps2
1.05	0.0666056	0.0665867	1.2177E-05	1.2179E-05	0.248875548	0.248875719	0.015133356	0.015136661	89.1034101	89.25831366
3	0.0651643	0.0650151	1.2382E-05	1.2404E-05	0.248891886	0.248893975	0.015390292	0.015417419	101.1959666	102.4784638
5	0.0635088	0.0632868	1.2628E-05	1.2661E-05	0.248919697	0.248924245	0.015697255	0.015739437	115.7711922	117.7847325
7	0.0616957	0.0614593	1.2908E-05	1.2946E-05	0.248963185	0.248969989	0.016049191	0.016096378	132.6478162	134.9236819
9	0.0598456	0.0595609	1.3209E-05	1.3256E-05	0.249024276	0.249035378	0.016426733	0.016486571	150.9406991	153.8571822
12.5	0.0566852	0.0562945	1.3757E-05	1.3828E-05	0.249178106	0.249202552	0.017118802	0.017208848	184.9452097	189.4125524
17.5	0.0524403	0.0520384	1.4573E-05	1.4656E-05	0.249534633	0.24958073	0.018157677	0.018263492	237.0560379	242.4308609
22.5	0.048664	0.0481939	1.539E-05	1.5499E-05	0.250073988	0.250159774	0.019211517	0.019352814	291.0716407	298.3894712
27.5	0.0453568	0.044957	1.6193E-05	1.6296E-05	0.250795418	0.250904224	0.020261096	0.020397388	345.7841961	352.9428416
31.25	0.0432967	0.0428781	1.674E-05	1.6856E-05	0.251415833	0.251561014	0.020987974	0.021143486	384.087853	392.3209432
33.75	0.0421033	0.0417396	1.7076E-05	1.7181E-05	0.251848285	0.251991789	0.021438891	0.021581035	407.9946791	415.552034
36.25	0.041024	0.0406997	1.7392E-05	1.749E-05	0.252291395	0.252435023	0.021867591	0.022000521	430.8157617	437.9086743
38.75	0.0400739	0.0397675	1.7682E-05	1.7778E-05	0.252726937	0.252877269	0.022262781	0.022394046	451.9237709	458.9485072
41.25	0.0392615	0.0389948	1.7938E-05	1.8024E-05	0.253136562	0.253279012	0.02261497	0.022733626	470.7854929	477.1499707
43.75	0.0385604	0.038329	1.8166E-05	1.8243E-05	0.253519729	0.253652517	0.02293016	0.02303659	487.7019112	493.4212683

Table **E-24**: Processed Axial Output File for Test 913, Continued

RE1	RE2	PR1	PR2	Axial Spacing (in)	incremental area (ft2)	center wall temps	side wall temps	Tbulk1-Twall 1	Tbulk2-Twall 2	Q1 (Btu/hr)	Q2 (Btu/hr)
1108.7	1108.5	0.720903	0.720902	0.95	0.069534722	180.2758112	184.68471	91.1724	95.4264	43.39292935	43.80628
1090.3	1088.4	0.720885	0.720883	1.95	0.142729167	205.4927883	208.11333	104.2968	105.6349	32.26814594	35.27735
1069.2	1066.3	0.720871	0.720869	2	0.146388889	231.2770746	232.93838	115.5059	115.1537	38.89732135	40.84902
1045.9	1042.9	0.720863	0.720862	2	0.146388889	256.0856881	257.7986	123.4379	122.8749	45.04699802	45.74845
1022.1	1018.5	0.720862	0.720862	2	0.146388889	280.9715104	282.0125	130.0308	128.1553	48.83924995	50.55186
981.38	976.34	0.720877	0.720881	3.5	0.256180556	320.151244	320.30368	135.206	130.8911	90.84301841	94.99546
926.43	921.21	0.720975	0.720992	5	0.365972222	368.5413936	369.65623	131.4854	127.2254	139.413218	141.8672
877.22	871.07	0.721206	0.721247	5	0.365972222	417.0032912	417.84637	125.9317	119.4569	**144.8214509**	150.0823
833.76	828.48	0.721568	0.721626	5	0.365972222	460.7287118	462.37127	114.9445	109.4284	147.1132344	146.7489
806.5	800.94	0.721904	0.721983	3.75	0.274479167	489.9289281	492.20848	105.8411	99.88754	103.247135	106.2046
790.64	785.8	0.722139	0.722217	2.5	0.182986111	507.6935922	509.30218	99.69891	93.75015	64.55145968	62.76263
776.25	771.91	0.722378	0.722456	2.5	0.182986111	523.4240377	524.05055	92.60828	86.14188	61.72823068	60.5064
763.53	759.42	0.722614	0.722696	2.5	0.182986111	536.6144135	536.74023	84.69064	77.79173	57.19314213	57.04233
752.63	749.04	0.722837	0.722916	2.5	0.182986111	545.3987235	544.98368	74.61323	67.83371	51.18955608	49.42545
743.19	740.07	0.723048	0.723121	2.5	0.182986111	547.3671207	546.63297	59.66521	53.2117	45.97961421	44.24931

Table **E-25**: Processed Axial Output File for Test 913, Continued

h1 (Btu/hr-ft2-F)	h2 (Btu/hr-ft2-F)	nu1	nu2	Post Center Wall Temps	Post Side Wall Temps	gr*	Ra*	Ra*(dh/L)	gr*/Re^2
6.844691091	6.601857437	19.22	18.54	182.1823	186.70483	2.18E+05	1.57E+05	1.67E+03	1.77E-01
2.167655232	2.339784792	5.986	6.45	208.47887	211.10901	6.97E+04	5.02E+04	5.34E+02	5.86E-02
2.300421819	2.423236798	6.228	6.543	235.5358	237.04043	7.10E+04	5.12E+04	5.44E+02	6.21E-02
2.492925583	2.543343363	6.602	6.715	261.43518	262.79864	7.03E+04	5.07E+04	5.39E+02	6.43E-02
2.565751543	2.694587819	6.638	6.946	287.29947	287.69358	6.48E+04	4.67E+04	4.96E+02	6.20E-02
2.622704238	2.83299923	6.511	6.997	327.20865	326.45668	5.19E+04	3.74E+04	3.97E+02	5.38E-02
2.897199779	3.046914199	6.781	7.09	375.68137	376.02948	3.74E+04	2.70E+04	2.87E+02	4.36E-02
3.142316138	3.432971349	**6.951**	7.539	424.55019	424.51645	2.66E+04	1.92E+04	2.04E+02	3.45E-02
3.497158901	3.664345557	7.336	7.635	468.14228	468.93189	1.89E+04	1.37E+04	1.45E+02	2.73E-02
3.553975095	3.873669445	7.197	7.786	497.04465	498.44478	1.40E+04	1.01E+04	1.08E+02	2.16E-02
3.53832333	3.658567426	7.014	7.205	514.42586	515.22679	1.14E+04	8.27E+03	8.79E+01	1.83E-02
3.642637063	3.838564512	7.08	7.415	529.98063	529.84002	9.62E+03	6.95E+03	7.38E+01	1.60E-02
3.69054412	4.007243045	7.045	7.605	543.33749	542.53395	7.94E+03	5.74E+03	6.10E+01	1.36E-02
3.749275825	3.981868891	7.046	7.444	552.04275	550.71923	6.43E+03	4.65E+03	4.94E+01	1.14E-02
4.211395467	4.544449263	7.806	8.384	553.3161	552.14673	5.31E+03	3.84E+03	4.08E+01	9.61E-03

E.6 Heat Loss and Friction Factor Output

The heat loss and friction factor were output in a separate output file. These heat losses were calculated using the thermocouples outlined in Section **3.2.2.3**. The heat losses calculated from these heat loss thermocouples were not used in calculating any heat transfer parameter other than for use in heat balance comparisons made in Section **5.2**. The friction factors were calculated using Equation **4.15** using adjusted pressure drops accounting for acceleration (Equation **4.12**) and head pressure (Equation **5.4**). Table **E-26** gives the heat loss and friction factor output file for test 913.

Table **E-26**: Heat Loss and Friction Factor Output File for Test 913

Friction Length	**Delta P (in Water)**
Unheated Length	0.085053
0-12"	0.084411
12-24"	0.096723
24-36"	0.108143
0-12"	0.083867
12-24"	0.096152
24-36"	0.107643
Re Inlet	1099.378
Re 0-12"	1048.821
Re 12-24"	915.4236
Re 24-36"	810.8447
Re 0-12"	1045.918
Re 12-24"	910.2157
Re 24-36"	805.3728
Heat Loss (W)	187.208
Heater Power (W)	686.7841
Nodal Energy Addition (W)	333.7772

Appendix F

Uncertainty Analysis

F.1 Pressure Uncertainty

The uncertainty in the absolute pressure transducer was +/- 0.025% of the current span (20-50 psia) or +/- 0.0050-0.0125 psia. The uncertainty in the differential pressure transducer was +/- 0.09% of the current span (1.67 inches of water) or +/- 0.001503 inches of water $\left(5.43 \cdot 10^{-5}\ psi\right)$.

F.2 Flow Uncertainty

Three uncertainties were applied to each flow-meter; each of the three uncertainties was given by the supplier. First, an uncertainty in the accuracy of the calibration device was applied as +/- 0.2% of reading. Second, an uncertainty in the repeatability of the reading was applied as +/- 0.1% of reading. Third, an uncertainty in the non-linearity between the each calibration point was applied as +/- 0.1% of reading. (Normally a 1% uncertainty would be applied to the linearity, however the setup of the flow meter was consistent with linearizing electronics and a 0.1% uncertainty could be applied instead). Using the square root sum of the squares, these three uncertainties resulted in a final flow uncertainty of 0.245% of reading. Installation effects were considered negligible as the inlet geometry recommended by the vendor (Flow

Technology) was used. However, there was a slight difference between the temperature and pressure that the flow meter was calibrated at and the temperature and pressure during the experiment. This variance is described below and the method for calculating this uncertainty was reviewed by an Application Engineer at Flow Technology.

From page 10 of the flow meter manual [**21**], the equation for converting Actual Cubic Feet to Standard Cubic Feet per minute was calculated from Equation **F.1** as,

$$Q_S = Q_A\left(\frac{P_A}{P_S}\right)\left(\frac{T_S}{T_A}\right) \qquad (\mathbf{F.1})$$

Where:

Q_S = Standard flow rate in SCFM.

Q_A = Actual measured flow rate in ACFM.

P_S = Standard pressure (14.7 psia).

P_A = Actual measured pressure at pressure tap on meter (psia).

T_S = Standard temperature (540°R).

T_A = Actual measured temperature down stream of meter (°R).

Equation **F.1** was used to obtain an uncertainty in the flow rate by adapting the above variables. Standard conditions were considered those conditions the flow meter was under during calibration and actual were those the flow meter was under during testing. The percent uncertainty was obtained from Equation **F.2** as,

$$\delta_{Flow} = \frac{Q_{Measured} - Q_{Actual}}{Q_{Actual}} = \frac{Q_A - Q_S}{Q_S} = \frac{Q_A}{Q_S} - 1 = \left(\frac{P_A}{P_S}\right)\left(\frac{T_S}{T_A}\right) - 1 \qquad (\mathbf{F.2})$$

It is important to note that the deviations in pressure and temperature will be offsetting uncertainties. Therefore, the temperature and pressure deviations were considered separately when examining the uncertainty which will maximize the total flow uncertainty. The uncertainty for the temperature deviations was calculated from Equation **F.3** as,

$$\delta_{Flow,Temperature} = \left(\frac{T_S}{T_A}\right) - 1 \qquad \textbf{(F.3)}$$

The uncertainty for the pressure deviations was calculated from Equation **F.4**

$$\delta_{Flow,Temperature} = \left(\frac{P_A}{P_S}\right) - 1 \qquad \textbf{(F.4)}$$

The values of conditions of the flow meter during calibration and during experimentation can be seen in Table **F-1**.

Table **F-1**: Flow meter Calibration and Test Parameters

Flow Meter	P_S (psia) (max)	P_S (psia) (min)	P_A (psia) (max)	P_A (psia) (min)	T_S (F) (max)	T_S (F) (min)	T_A (F) (max)	T_A (F) (min)	$\delta_{Flow,Temp.}$	$\delta_{Flow,Press.}$
Low Nitrogen	20.09	20.01	20.1	19.99	80.7	78.7	69.6	68.5	**2.31E-02**	**4.50E-03**
Mid Nitrogen	20.07	20.01	20.1	19.99	78.8	77.9	74.1	70.1	**1.64E-02**	**4.50E-03**
High Nitrogen (20psia)	20.09	19.99	20.1	19.99	74.3	72.6	78.1	68.3	**1.14E-02**	**5.50E-03**
High Nitrogen (30psia)	30.34	30.07	30.3	29.99	72.1	71.7	67.2	63.2	**1.70E-02**	**7.65E-03**
High Nitrogen (50psia)	51.38	49.38	50.5	49.99	75.1	70.4	52.7	44.4	**6.09E-02**	**2.27E-02**

The variables P_S, T_S were the pressures and temperatures during the calibration of the specific flow meter. The variables P_A, T_A are the pressures and temperatures during

Penn State experiments. For the flow temperature uncertainty, the maximum T_S was used with the minimum T_A, thus maximizing the uncertainty. For the flow pressure uncertainty, the maximum P_A was used with the minimum P_S, thus maximizing the uncertainty. The total uncertainty for each flow measurement is given in Table **F-2**.

Table **F-2**: Flow Meter Uncertainties

Flow Meter	Calibration	Repeatability	Non-linearity	Flow Temp.	Flow Press.	Total Maximum Uncertainty
	%	%	%	%	%	**%**
Low Nitrogen	0.10%	0.20%	0.10%	1.64%	0.45%	**1.72%**
Mid Nitrogen	0.10%	0.20%	0.10%	1.79%	0.50%	**1.88%**
High Nitrogen (20psi)	0.10%	0.20%	0.10%	1.14%	0.55%	**1.29%**
High Nitrogen (30psi)	0.10%	0.20%	0.10%	1.70%	0.76%	**1.88%**
High Nitrogen (50psi)	0.10%	0.20%	0.10%	6.09%	2.27%	**6.50%**

The uncertainty for the High Nitrogen (50psi) flow meter is much higher than the rest because of the disparity between the calibration conditions and the test conditions for the high pressure runs. The inlet flow was unable to be kept near room temperature for these runs because the high flow rates of liquid nitrogen were unable to be warmed efficiently by the inlet piping.

F.3 Fluid Property Uncertainty

The uncertainty of the fluid properties is 0.02% as given on the NIST website [**22**] which included the specific heat, density, and viscosity. The fluid thermal conductivity uncertainty was given as 2.0%.

F.4 Thermocouple Uncertainty

Sample thermocouples were sent to Delta M Corporation to obtain the uncertainty in the measurement of the bulk fluid and wall temperatures. The thermocouples were calibrated to a reference Type S thermocouple for temperatures of 32, 67, and 212 degrees Fahrenheit. The thermocouple probe that was sent to Delta M for calibration is the actual probe used in the heat transfer experiments for this research. The wall thermocouple that was sent to Delta M for calibration was a spare thermocouple from the same lot as the thermocouples embedded in the walls of the rectangular test section. Figure **F-1** shows the probe thermocouples as well as the wall and Type-S thermocouples, bound and ready for calibration.

Figure **F-1**: Thermocouple Calibration Setup

Figure **F-2** shows the thermocouples being calibrated at 32°F in an ice bath.

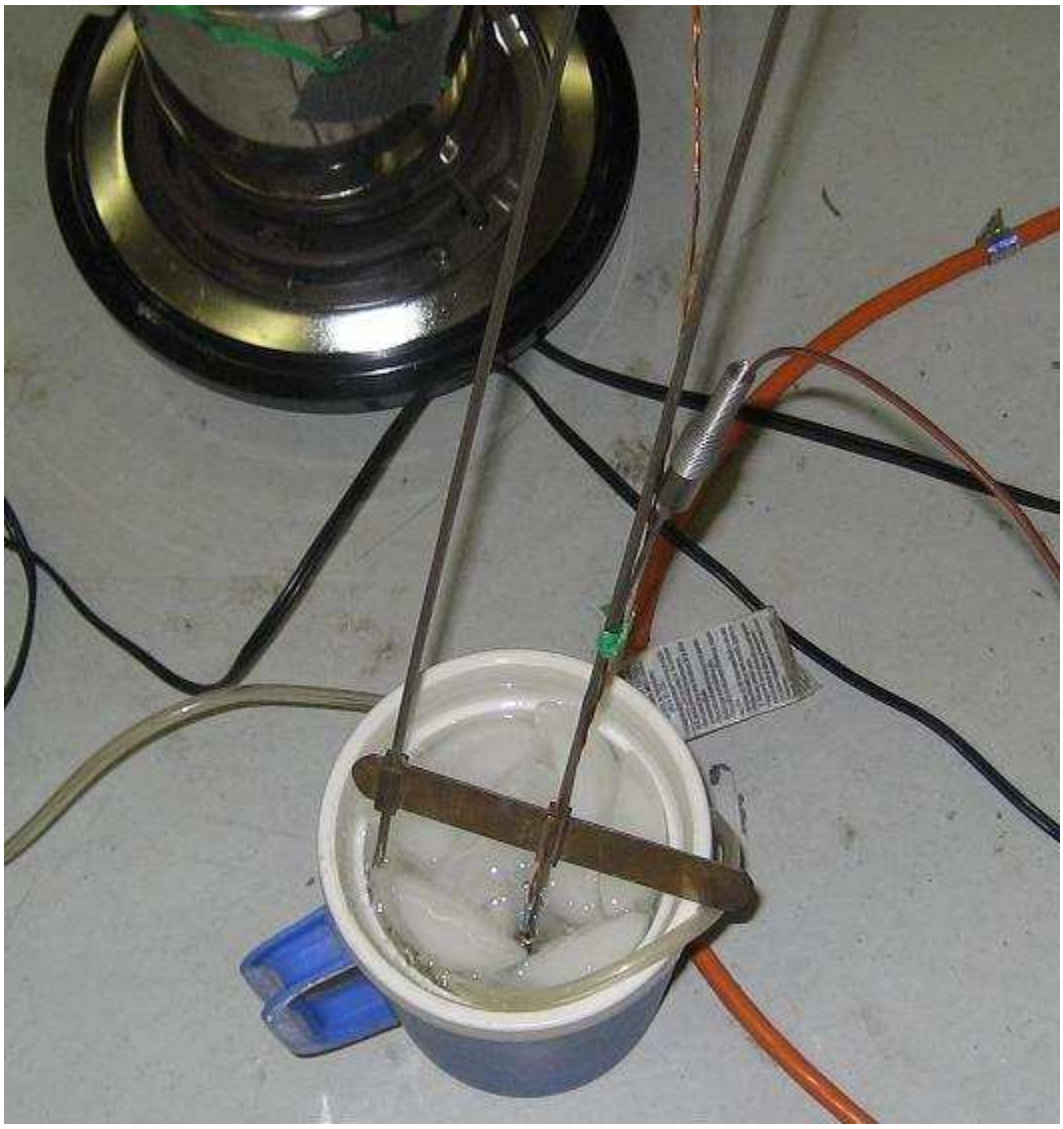

Figure **F-2**: Thermocouples Being Calibrated in an Ice Bath

The result of the Delta-M calibration for all three thermocouples on the thermocouple probe is shown below in Figure **F-3**. The standard deviation for the three thermocouples and three calibration temperatures was found to be 0.33 degrees F.

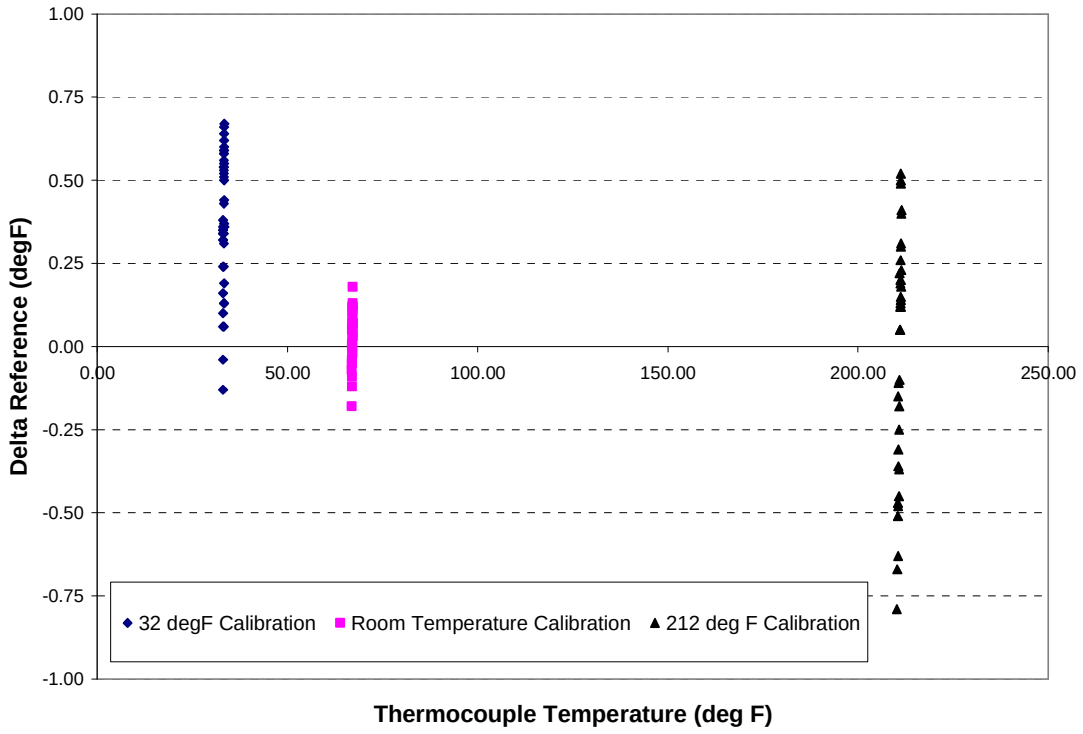

Figure **F-3**: Thermocouple Probe Calibration data

Figure **F-4** gives similar calibration data for the wall thermocouples. The wall thermocouple which was sent to Delta M for calibration was from the same lot as the wall thermocouples in the test section. The standard deviation of the uncertainty for this wall thermocouple from the reference thermocouple was 0.33 degrees F.

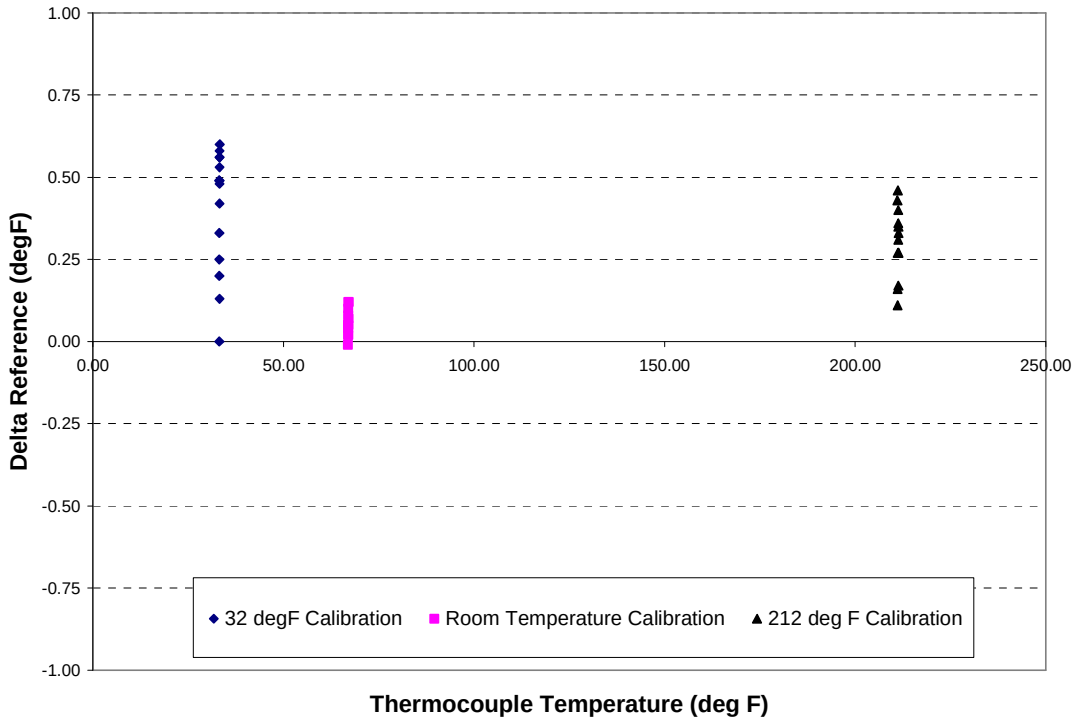

Figure **F-4**: Wall thermocouple calibration data

In order to get these temperature deviations in terms of an absolute percentage, Equation **F.5** was used. Using this equation, the percentage deviation for the probe thermocouple was calculated as 0.8035% and the deviation for the wall thermocouple was calculated as 0.8238%.

$$\delta_{TC} = \sqrt{\frac{\sum_{n}\left(\frac{T_{measured} - T_{reference}}{T_{reference}}\right)^2}{n}} \times 100\% \qquad \text{(F.5)}$$

F.5 Heat Transfer Parameters

This section calculates the uncertainty in the heat transfer parameters using the square root sum of squares method. These parameters include the bulk temperature, heat rate to the fluid, and Nusselt number. The equation for the bulk temperature uncertainty is given below in Equation **F.6** as,

$$\delta_{Tbulk} = \left[\delta_{TCprobe}^2 + \delta_{flow}^2 + \delta_{density}^2 + \delta_{Cp}^2\right]^{0.5} \quad \textbf{(F.6)}$$

The bulk temperature uncertainty is solved as follows,

$$\delta_{Tbulk} = \sqrt{0.8035^2 + 1.88^2 + 0.02^2 + 0.02^2} = 2.045\%$$

which uses a flow uncertainty of 1.88% that bounds all the cases except the two runs over a Reynolds number of 10,000.

The equation for heat added to the fluid is given by Equation **F.7** as,

$$\dot{q} = \dot{m}_{fluid} c_p \frac{dT_{bulk}}{dx} \quad \textbf{(F.7)}$$

The uncertainty in the heat added to the fluid is given by Equation **F.8** as,

$$\delta_q = \left[\delta_{\dot{m}}{}^2 + \delta_{cp}{}^2 + \delta_{Tbulk}{}^2\right]^{0.5} \quad \textbf{(F.8)}$$

Using values already presented, the heat rate uncertainty is given as,

$$\delta_q = \left[1.88^2 + 0.02^2 + 2.045^2\right]^{0.5} = 2.778\%$$

The equation for the heat transfer coefficient is given by Equation **F.9** as,

$$h = \frac{\dot{q}}{A(T_{wall} - T_{bulk})} \quad \textbf{(F.9)}$$

The uncertainty for the heat transfer rate is given by Equation **F.10** as,

$$\delta_h = \left[\delta_q{}^2 + \delta_{Twall}{}^2 + \delta_{Tbulk}{}^2\right]^{0.5} \qquad \textbf{(F.10)}$$

Using values already presented, the heat transfer coefficient uncertainty is given as,

$$\delta_h = \sqrt{2.778^2 + 0.8238^2 + 0.8035^2} = 3.007\%$$

The equation for the Nusselt number is given by Equation **F.11** below as,

$$Nu = \frac{hD_h}{k_f} \qquad \textbf{(F.11)}$$

and the uncertainty for the Nusselt number is given by Equation **F.12** below as,

$$\delta_{Nu} = \left[\delta_h^2 + \delta_{Dh}^2 + \delta_k^2\right]^{0.5} \qquad \textbf{(F.12)}$$

The uncertainty for the Nusselt number is then solved as,

$$\boxed{\delta_{Nu} = \sqrt{3.007^2 + 2.0^2} = 3.61\%}$$

There is still an uncertainty issue that was unique to this experiment because of the nature of low Reynolds number heat transfer; the wall and bulk temperatures converged to a point where the difference between them was on the order of the uncertainty of the wall and fluid thermocouples. Therefore, at points below this threshold Reynolds number the data should not be used since the temperature difference is the uncertainty. This criterion that must be satisfied is given below as,

$T_{wall} - T_{bulk} \geq \delta_{Twall} + \delta_{Tbulk}$ and is dependent on the minimum fully developed bulk temperature difference at a given Reynolds number.

In order to quantify this uncertainty in terms of a temperature difference, we must convert the uncertainty of the bulk temperature to a degrees F scale. This is done by

taking the ratio of the bulk temperature uncertainty to the probe temperature uncertainty as,

$$\frac{\delta_{Tbulk}(\%)}{\delta_{Tprobe}(\%)} = \frac{\delta_{Tbulk}(^{\circ}F)}{\delta_{Tprobe}(^{\circ}F)} \rightarrow \frac{2.045\%}{0.8035\%} = \frac{\delta_{Tbulk}(^{\circ}F)}{0.33^{\circ}F}$$

Solving for the bulk temperature uncertainty, $\boxed{\delta_{Tbulk}(^{\circ}F) = 0.85^{\circ}F}$

Summing this with the wall temperature uncertainty of 0.33°F gives a wall to bulk temperature uncertainty of 1.17°F. Using a 95th percentile multiplier of 1.645 [**23**] this uncertainty becomes 1.93°F. Using this methodology, experimental data that contains a Nusselt number derived from a wall to bulk temperature difference less than 1.93°F would be excluded due to the increased combined uncertainty. Table **F-3** below gives the relevant low Reynolds number bulk temperature difference data.

Table **F-3**: Bulk Temperature Difference Data

Run #	~Texit (degF)	Fully Developed Values @45L/D		
		Local Reynolds Number	Nusselt Number	Twall-Tbulk (degF)
910	500	1612	6.99	214.03
911	500	1352	6.99	191.72
912	500	1119	7.02	156.71
913	500	872.2	7.26	119.94
914	500	644.5	7.65	88.99
915	500	481.8	8.08	59.09
916	500	364.3	10.00	31.11
933	300	372.2	9.27	19.51
932	300	230.1	11.80	9.14
931	300	138.6	70.60	0.81

Using the above justifications, run 931 seen in Table **F-3** would be excluded because it has a fully developed wall to bulk temperature difference below 1.93°F.